Poly(ethylene glycol) Hydrogels Crosslinked via the Strain-Promoted Alkyne-Azide Cycloaddition

POLY(ETHYLENE GLYCOL) HYDROGELS CROSSLINKED VIA THE STRAIN-PROMOTED ALKYNE-AZIDE CYCLOADDITION

BY

SABRINA M. HODGSON, B.Sc.

A THESIS
SUBMITTED TO THE SCHOOL OF GRADUATE STUDIES
OF MCMASTER UNIVERSITY
IN PARTIAL FULFILMENT OF THE REQUIREMENTS
FOR THE DEGREE OF
DOCTOR OF PHILOSOPHY
IN CHEMISTRY

PhD of Chemistry (2017) McMaster University
(Chemistry and Chemical Biology) Hamilton, Ontario, Canada

TITLE: Poly(ethylene glycol) Hydrogels Crosslinked via the Strain-Promoted Alkyne-Azide Cycloaddition

AUTHOR: Sabrina M. Hodgson
B.Sc. (Chemistry)
McMaster University, Hamilton, Canada

SUPERVISOR: Professor Alex Adronov

NUMBER OF PAGES: xxii, 151

Abstract

Hydrogels are promising materials for a number of biomedical applications, including tissue engineering, controlled drug delivery, and wound healing. Due to the semi-permeable nature of the water-swollen crosslinked polymer network, hydrogels have the unique ability to encapsulate materials, while allowing passage of any necessary resources, such as the import of oxygen or nutrients and the export of waste or therapeutic agents. Hydrogel properties vary greatly depending on the polymer material and crosslinking chemistry chosen, all of which can be tuned for a particular application. Current hydrogel systems typically involve either natural or synthetic polymers. Synthetic polymers afford more structural control to the resulting hydrogel, however the employed crosslinking chemistry is often non-ideal, due to the high temperatures required or the presence of cytotoxic catalysts. Click chemistry, particularly the strain-promoted alkyne-azide cycloaddition (SPAAC), is ideal for hydrogel crosslinking as it is fast at physiological temperatures, bio-orthogonal, doesn't produce any byproducts, and doesn't require a catalyst or external stimuli. For the hydrogel material, synthetic poly(ethylene glycol) (PEG) is most appealing since it is non-toxic, easy to functionalize, and physiologically stable. At the time of this thesis, there were few examples of PEG hydrogels prepared via SPAAC, with limited characterization of the physical properties of these gels and the parameters that dictate their gelation behavior.

The work presented in this thesis involved the optimized synthesis of a cyclooctyne derivative, aza-dibenzocyclooctyne (DIBAC), which was subsequently used for the preparation and characterization of a series of PEG hydrogels crosslinked via SPAAC. We showed that the PEG chain length and number of crosslinking groups had a significant effect on the swelling,

degradation time and stiffness of the resulting hydrogels. Additionally, there was very little protein adsorption on the surface of the hydrogels, and the polymer components proved non-cytotoxic.

A second objective of this work was to investigate reproducible hydrogels. We created novel, SPAAC crosslinked PEG hydrogels that contained well-defined dendritic crosslinking groups, making them more reproducible than the previous linear analogs. These hydrogels have short gelation times at low polymer concentration, minimal swelling at physiological temperatures, and kept human mesenchymal stem cells (hMSCs) viable for over 15 days.

Acknowledgements

The past 6 years of my PhD have been some of the most exciting and rewarding, albeit stressful, years of my life. I've learned so much, and I have so many people to thank for helping me through this journey.

First and foremost, I want to thank my supervisor, Dr. Alex Adronov. Alex, none of this would have been possible without your constant support and guidance. You have taught me so much, for which I am extremely grateful. I couldn't have asked for a better mentor throughout my graduate (and undergraduate!) studies. Your passion for research and tremendous drive has inspired me since 3LA3, 8 years ago. Thank you for all the kind words and wisdom since that day, for always being reliable and quick to respond to emails, and for being the perfect combination of tough, yet invaluably benevolent and helpful.

Thank you to my committee members, Dr. Todd Hoare and Dr. Harald Stöver for your time, resources, and brilliant ideas that cultivated this project and fostered so many wonderful collaborations. A huge thank you also to the NSERC CREATE-IDEM program, which ultimately gave me opportunities that I wouldn't have otherwise experienced, and to all of the participating research groups for their knowledge, suggestions, and collaborations. In particular, thank you to Dr. Kari Dalnoki-Veress for your mechanical tester.

I must also thank Dr. Kristi Anseth for hosting me in her research lab for 2 months. I had such a wonderful experience and learned so much during my time there; I only wish I could have stayed longer!

Thank you to all of my collaborators, including Emilia Paron, Dr. Ryan Chadwick, Stuart McNelles, Leonora Abdullahu, Ian Marozas, and Alison Stewart. I am so grateful for the skills I learned from each of you, and for the valuable conversations. To Emilia, a thousand thank you's for guiding me into the world of hydrogels and teaching me everything I needed to know. Thank

you for the writing parties, Starbucks dates (with Steph and Maddi!), and for keeping me sane throughout these last few years.

Thank you to all my friends at McMaster, especially everyone in the Adronov group, past and present. You have all made this a beautiful journey. Lukas Sadowski and Victoria Laval, I couldn't have asked for two better people to be there when I started grad school, thank you for teaching me how to do research (while listening to terrible music) and for the tripod memories! The lab just isn't the same without you two. Thank you so much also to Vladimir Kardelis; you've been an invaluable friend to me since you started. Thank you especially for the quirky comments and videos that always kept me (and everyone else) laughing, and for the stunning photos of my hydrogels – you are so talented!

I want to thank my friends outside McMaster, particularly Lisa and Janis, thank you so much for your love and support, and for being there for me through everything these past few years; I couldn't have done this without you.

To my Mom and Dad, who have been there for me since day one, I give my biggest thank you. You two are the most remarkable, talented, compassionate, smart, and all-around wonderful people I have ever met and I am so lucky and privileged to have you as my parents. Thank you for all you have done for me, and for constantly reminding me that "there's nothing I can't do".

Last but not least, I must thank my daughter Hailey. Thank you for your beautiful spirit, contagious smile, and endless hugs. Because of you, the sun shines a little brighter, and I know that anything is possible.

List of Abbreviations

AAm	Acrylamide
AcOH	Acetic Acid
AFCT	Addition-Fragmentation Chain Transfer
APA	Alginate/Poly-L-Lysine/Alginate
BARAC	Biarylazacyclooctynone
Bis-MPA	2,2-Bis(hydroxymethyl)Propanoic Acid
BMSC	Bone Marrow Derived Stromal Cell
BSA	Bovine Serum Albumin
CBS	Calf Bovine Serum
CMC	Carboxymethyl Cellulose
CuAAC	Copper(I)-Catalyzed Alkyne-Azide Cycloaddition
DA	Diels-Alder
DBA	Dimethyl-γ-Butyrolactone Acrylate
DBU	1,8-Diazabicyclo(5.4.0)undec-7-ene
DCM	Dichloromethane
DEPTq	Distortionless Enhancement by Polarisation Transfer with Retention of Quaternaries
DIBAC	Aza-Dibenzycyclooctyne
DLD	Dendritic-Linear-Dendritic
DMAP	4-Dimethylaminopyridine
DMF	Dimethylformamide
DMSO	Dimethylsulfoxide
DTT	Dithiothreitol
ECM	Extracellular Matrix
EDC	1-Ethyl-3-(3-dimethylaminopropyl)Carbodiimide
EHS	Engelbreth-Holm-Swarm
EO	Ethylene Oxide

ESD	Equilibrium Swelling Degree
ESI	Electrospray Mass Spectrometry
ESMN	Embryonic Stem Cell-Derived Motor Neurons
EtOAc	Ethyl Acetate
EtOH	Ethanol
FDA	Food and Drug Administration
FITC	Fluorescein Isothiocyanate
G	Generation
GelMA	Gelatin Methacrylamide
GPC	Gel Permeation Chromatography
HA	Hyaluronic Acid
HEMA	Hydroxyethylmethacrylate
HMDS	Hexamethyldisilane
hMSC	Human Mesenchymal Stem Cell
HPLC	High Performance Liquid Chromatography
HRMS	High-Resolution Mass Spectrometry
HSA	Human Serum Albumin
KHMDS	Potassium Bis(trimethylsilyl)Amide
KO^{t}Bu	Potassium *tert*-Butoxide
LCST	Lower Critical Solution Temperature
MALDI	Matrix Assisted Laser Desorption/Ionization
MeOH	Methanol
MMP	Matrix Metalloproteinase
MS	Mass Spectrometry
MTT	Thiazolyl Blue Tetrazolium Bromide
NBOC	Nitrobenzyloxycarbonyl
NMR	Nuclear Magnetic Resonance
OEGMA	Oligo(ethylene glycol) Methacrylate
PAAm	Polyacrylamide

PAMAM	Polyamidoamine
PBS	Phosphate Buffer Saline
PDI	Polydispersity Index
PEG	Poly(ethylene glycol)
PEGDA	Poly(ethylene glycol)-Diacrylate
PHEMA	Poly(hydroxyethylmethacrylate)
PLL	Poly-L-Lysine
PMAA	Poly(methacrylic acid)
PNIPAAm	Poly(*N*-isopropylacrylamide)
POEGMA	Poly(oligoethylene glycol methacrylate)
PVA	Poly(vinyl alcohol)
PVP	Poly(vinylpyrrolidone)
R_f	Retention Factor
RGD	Argenine – Glycine – Aspartic Acid
s.e.m	Standard Error of the Mean
SPAAC	Strain-Promoted Alkyne-Azide Cycloaddition
TBAB	Tetrabutylammonium Bromide
THF	Tetrahydrofuran
THP	Tetrahydropyran
TIPS	Triisopropylsilane
TLC	Thin Layer Chromatography
uDEFT	Uniform Driven Equilibrium Fourier Transform
UV	Ultraviolet
UV-Vis	Ultraviolet Visible
VIC	Valvular Interstitial Cell
YM	Young's Modulus

Contents

Abstract iii

Acknowledgements v

List of Abbreviations vii

List of Tables xiv

List of Figures xv

List of Schemes xxi

Chapter 1: Overview of Click-Crosslinked Hydrogels 1

1.1. Introduction to Hydrogels 1

1.1.1. Natural Hydrogels 2

1.1.2. Synthetic Hydrogels 4

1.1.2.1. PEG Hydrogels 6

1.2. Hydrogel Crosslinking 8

1.2.1. Physically-Crosslinked Hydrogels 10

1.2.2. Covalentely-Crosslinked Hydrogels 12

1.2.2.1. SPAAC-Crosslinked Hydrogels 15

1.2.3. Injectable Hydrogels 18

1.3. Hydrogel Swelling 20

1.4. Hydrogel Degradation 20

1.5. Dendrimers 22

1.5.1. Dendrimer Hydrogels 23

1.6. PEG Hydrogel Applications 26

1.7. Summary 30

1.8. References 32

Chapter 2: Scalable Synthesis of Strained Cyclooctyne Derivatives 42
2.1. Introduction 44
2.2. Results and Discussion 47
2.3. Conclusions 54
2.4. Experimental 54
2.4.1. General 54
2.4.2. Kinetic Experiments 54
2.4.3. Synthesis 55
2.5. Supporting Information 66
2.6. References 81

Chapter 3: Properties of Poly(ethylene glycol) Hydrogels Cross-Linked via Strain Promoted Alkyne-Azide Cycloaddition (SPAAC) 83
3.1. Introduction 85
3.2. Materials and Methods 87
3.2.1. Synthetic Procedures 87
3.2.2. Hydrogel Preparation 90
3.2.3. Characterization 91
3.2.3.1. UV-Vis Data 91
3.2.3.2. Swelling and Degradation Kinetics 92
3.2.3.3. Hydrogel Mechanics 93
3.2.4. Biological Evaluation 94
3.2.4.1. Protein Adsorption 94
3.2.4.2. Cell Cytotoxicity 95
3.3. Results and Discussion 95
3.3.1. Preparation of Polymers and Hydrogels 95
3.3.2. Hydrogel Formation and Gelation Time 98
3.3.3. UV-Vis Analysis of Cross-Linking 101

3.3.4. Swelling and Degradation 102
3.3.5. Young's Modulus Measurements 104
3.3.6. Protein Adsorption Study (BSA) 105
3.3.7. MTT Assay 106
3.4. Conclusions 108
3.5. References 108

Chapter 4: Reproducible Dendronized PEG Hydrogels via SPAAC Cross-Linking 114

4.1. Introduction 116
4.2. Materials and Methods 118
4.2.1. Hydrogel Formation 118
4.2.2. Hydrogel Characterization 119
4.2.2.1. Gelation Time 119
4.2.2.2. Swelling Kinetics (at 37°C) 119
4.2.2.3. Hydrogel Mechanics 119
4.2.2.4. Cell Culture 120
4.2.2.5. Cell Encapsulation and Live/Dead Assay 120
4.3. Results and Discussion 121
4.3.1. Preparation of Polymers 121
4.3.2. Hydrogel Formation and Gelation Time 122
4.3.3. Hydrogel Swelling 125
4.3.4. Hydrogel Rheology to Deduce Reproducibility 127
4.3.5. Cell Viability with hMSCs 128
4.4. Conclusions 130
4.5. Supporting Information 130
4.5.1. Materials and Methods 130
4.5.1.1. General 130
4.5.1.2. Synthesis 131

4.6. References 144

Chapter 5: Thesis Overall Conclusions and Recommendations for Future Work 147

5.1. General Conclusions 147

5.2. Recommendations for Future Work 150

List of Tables

3.1. Precursor Polymer and Functional Group Concentrations Used to Maintain 1:2 Strained Alkyne:Azide Functional Group Ratio Across All Tested Hydrogels 91
3.2 Functional Group and Polymer Concentrations Post-Gelation. . . . 99
3.3 Summary of Hydrogel Swelling, Degradation, and Young's Moduli. 104
4.1 Gelation times for linear, G1 and G2 Systems 123
4.2 Young's Modulus Values for Two Batches (A and B) of the Linear, G1 and G2 Hydrogels 128
4.3 hMSC viability in G2 hydrogels after 4, 8, and 15 days. Three different concentrations of G2 hydrogel were assessed: 9.6 wt%, 7.2 wt% and 4.8 wt% 130

List of Figures

1.1. Phase contrast optical microscopy image 7 days after encapsulation of C2C12 mouse cells in alginate/poly-L-lysine/alginate (APA) microcapsules. Scale bar: 500μm. Reproduced with permission.[22] Copyright Biomacromolecules, 2009. 2

1.2 Schematic formation and degradation of enzymatically-degradable PEG hydrogels synthesized via the Cu(I)-catalyzed azide-alkyne cycloaddition reaction. Reproduced with permission.[56] Copyright Biomacromolecules, 2010. 7

1.3 Scale of soft tissue elasticity expressed in Young's Modulus values (E, kPa). Reproduced with permission.[81] Copyright Science, 2009 . . . 9

1.4 ABA tri-block copolymer composed of catechol-functionalized PNIPAAm and PEG (A) form a self-healing hydrogel based on hydrogen bonding and aromatic interactions (B). Structures of ABA tri-block copolymer without catechol (C) and instead containing phenylethylacrylamide (D) to show lack of hydrogen bonding interactions (D) as well as lack of both hydrogen bonding and aromatic interactions (C). Reproduced with permission.[85] Copyright Advanced Materials, 2015. 11

1.5 Examples of click reactions 12

1.6 PEG-hydrogel based on thiol-ene chemistry with 4-arm PEG tetranorbornene (A) and a dicysteine(thiol)-terminated cleavable peptide (B). Schematic of the hydrogel undergoing spatial photopatterning (C) of RGD and a graph showing that the extent of photopatterning can be controlled by changing the light dosage (time/intensity) and the photoinitiator concentration. Reproduced with permission.[112] Copyright ACS Macro Letters, 2013 14

1.7 The strain-promoted alkyne-azide cycloaddition (SPAAC) 15

1.8 Figure 1.8. Various cyclooctynes for Cu-free click chemistry. Second-order rate constants are for reaction with benzyl azide. Reproduced with permission.[116] Copyright Accounts of Chemical Research, 2011. 16
1.9 Hydrogel formation (B, E), photopatterning (C, F) and photo-degradation (D, G) of SPAAC-crosslinked hydrogels made from a diazido degradeable peptide and a 4-arm PEG tetracyclooctyne (A). Reproduced with permission.[117] Copyright Nature Chemistry, 2011. 17
1.10 Formation of thiol-Michael addition crosslinked cell-containing micro-gels via microfluidic emulsification. Reproduced with permission.[127] Copyright Journal of the American Chemical Society, 2012 19
1.11 Schematic overview comparing the structures of linear polymers versus other macromolecules that fall under the dendritic category. Reproduced with permission.[139] Copyright Chemical Society Reviews, 2012 22
1.12 Anatomy of a third-generation dendrimer and dendron. Reproduced with permission.[140] Copyright Nature Biotechnology, 2005 23
1.13 Dendritic hydrogel formation via CuAAC crosslinking. Reproduced with permission.[145] Copyright Macomolecules, 2010. 24
1.14 Formation of a dual-purpose DLD PEG hydrogel. Linear PEG is the starting point, which is functionalized with thiols, or alkene or azide terminated dendrons (left). The hydrogel is formed using photoinitiated thiol-ene crosslinking, and biomolecules like Biotin, DOPA and Man can be incorporated using CuAAC. Reproduced with permission.[154] Copy-right Chemical Communications, 2013 25
1.15 Illustration of the stem cell niche involving cell-matrix interactions and adhesion, cell-cell contacts, and growth factors, which all direct cell fate. Reproduced with permission.[81] Copyright Science, 2009 . 27
1.16 Fluorescently labeled human mesenchymal stem cells (hMSCs) in a degradable PEG hydrogel. At the start of the experiment (left), the cells

appear rounded with few interactions, whereas after 2 weeks (right), the cells have formed interactions with the gel that promote attachment, migration and differentiation. Reproduced with permission.[31] Copyright Science, 2007. 28

1.17 Directed mobility of motor axons from ESMNs within photodegradable PEG hydrogels. Two-photon light was used to create an eroded fork-shaped pattern within the hydrogel. Left image shows axons hours before reaching the fork, and then right image shows the direction that was selected. Reproduced with permission.[165] Copyright Bio-macromolecules, 2014. 29

1.18 Cell encapsulation and hydrogel particle formation via a microfluidic device (A). NIH 3T3 cells at least 94% viable based on live-dead assay (B). pH-controlled release of cells after 3 days with maintained viability (C). Reproduced with permission.[168] Copyright Angewandte Chemie International Edition, 2013. 30

2.1 BARAC precursors for elimination attempts 50

2.2 Second order rate constants of **21**. Measured from the reaction with benzyl azide in acetonitrile at 25°C.[13] 53

2.3 ^{1}H (top) and ^{13}C DEPT-q (bottom, CH_2 down) NMR spectra for compound **1** 66

2.4 ^{1}H (top) and ^{13}C DEPT-q (bottom, CH_2 down) NMR spectra for compound **2** 67

2.5 ^{1}H (top) and ^{13}C DEPT-q (bottom, CH_2 down) NMR spectra for compound **3** 68

2.6 ^{1}H (top) and ^{13}C DEPT-q (bottom, CH_2 down) NMR spectra for compound **4** 69

2.7 ^{1}H (top) and ^{13}C DEPT-q (bottom, CH_2 down) NMR spectra for compound **5** 70

2.8 ^{1}H (top) and ^{13}C DEPT-q (bottom, CH_2 down) NMR spectra for compound **7** 71
2.9 ^{1}H (top) and ^{13}C DEPT-q (bottom, CH_2 up) NMR spectra for compound **8**. 72
2.10 ^{1}H (top) and ^{13}C DEPT-q (bottom, CH_2 up) NMR spectra for compound **10** 73
2.11 ^{1}H (top) and ^{13}C DEPT-q (bottom, CH_2 up) NMR spectra for compound **15** 74
2.12 ^{1}H (top) and ^{13}C DEPT-q (bottom, CH_2 down) NMR spectra for compound **16** 75
2.13 ^{1}H (top) and ^{13}C DEPT-q (bottom, CH_2 down) NMR spectra for compound **17** 76
2.14 ^{1}H (top) and ^{13}C DEPT-q (bottom, CH_2 down) NMR spectra for compound **18** 77
2.15 ^{1}H (top) and ^{13}C DEPT-q (bottom, CH_2 down) NMR spectra for compound **19** 78
2.16 ^{1}H (top) and ^{13}C DEPT-q (bottom, CH_2 down) NMR spectra for compound **20** 79
2.17 ^{1}H (top) and ^{13}C DEPT-q (bottom, CH_2 down) NMR spectra for compound **21** 80
3.1 ^{1}H NMR spectra in DMSO-d_6 of PEG_{10k}-diol (top) and $PEG_{10k}(DIBAC)_2$ (bottom). 96
3.2 ^{1}H NMR spectrum in $CDCl_3$ of $PEG_{10k}(N_3)_{12}$ 98
3.3 Graphical representation of hydrogel formation between $PEG_n(DIBAC)_2$ (blue polymer) and $PEG_{10k}(N_3)_m$ (red polymer) using a double barrel syringe (left). The photograph (top right) shows actual hydrogel disks produced, with a visual representation of an idealized hydrogel network formed between the strained alkyne (blue) and azide (red) polymers shown below 99

3.4 UV-Vis spectra of hydrogels made between $PEG_{4.6k}(DIBAC)_2$ and $PEG_{10k}(N_3)_9$ with varying functional group ratios of strained alkyne to azide 102
3.5 Mass-based swelling ratio of each hydrogel composition over time. Each measurement is represented as the mean ± standard error of the mean (s.e.m.) from triplicate experiments 103
3.6 Bovine serum albumin (BSA) adsorption onto hydrogel compositions $4.6k(D)_2$-$10k(N)_{12}$, $10k(D)_2$-$10k(N)_9$, and $10k(D)_2$-$10k(N)_{12}$ at 37°C as a function of the protein concentration in the loading solution. Error bars represent one standard deviation of five replicates 106
3.7 Cytotoxicity of $PEG_{4.6k}(DIBAC)_2$ (blue) and $PEG_{10k}(N_3)_{12}$ (red) polymer precursors via an MTT assay on NIH 3T3 fibroblasts relative to a cell-only control. Dotted line indicates relative viability = 1. Error bars represent one standard deviation of four replicates 107
4.1 Photograph of G1 (left) and G2 (right) hydrogels at 2.5 wt%. Insets show top-down view of the same gels, demonstrating their transparency 123
4.2 Structural comparison of the linear and corresponding dendritic azide-functionalized polymers. 124
4.3 Graph of hydrogel swelling over time for 2.5 wt% and 5 wt% G1 and G2 dendrimer hydrogels at 37°C. 126
4.4 Representative projections of 3D confocal images of encapsulated hMSC cells, showing viability over time at different hydrogel concentrations: 9.6 wt% (left column), 7.2 wt% (middle column), 4.8 wt% (right column). Cells are stained with calcein AM (live – green) and ethidium homodimer (red – dead). Scale bar 100 μm 129
4.5 NMR spectra of poly(ethylene glycol) (top), PEG-$G1(N_3)_4$ (middle) and PEG-$G2(N_3)_8$ (bottom). Disappearance of the PEG-O<u>H</u> peak at 4.6 ppm in the spectra of PEG-$G1(N_3)_4$ and PEG-$G2(N_3)_8$ is evidence that the final

step in the synthesis of the polymer was successful and that complete conversion was achieved 140
4.6 ^{1}H NMR spectra of two separately prepared batches of linear azide polymer 141
4.7 ^{1}H NMR spectra of two separately prepared batches of G1 azide polymer 142
4.8 ^{1}H NMR spectra of two separately prepared batches of G2 azide polymer 143

List of Schemes

2.1 Literature syntheses of DIBAC. (a) $PdCl_2(PPh_3)_2$, CuI, Et_3N, THF, N_2/H_2, r.t.; (b) Boc_2O, THF, 70 °C, 2d; (c) 10% $Pd/BaSO_4$, quinolone, H_2, MeOH, r.t. 1.5h; (d) Dess-Martin periodinane, $NaHCO_3$, CH_2Cl_2, r.t. 40 min; (e) (1) 2 M HCl in EtOAc, r.t. 1 h; (2) $NaBH_4$, H_2O, r.t., o.n.; (f) $NH_2OH{\cdot}HCl$, pyridine, EtOH, reflux, 12h; (g) Polyphosphoric acid, 125 °C, 1h; (h) $LiAlH_4$, Et_2O, reflux, 15h; (i) Various Conditions; (j) Br_2, DCM, 0 °C, 2h; (k) KO^tBu, THF, -40 °C, 2h. 46

2.2 Optimization of DIBAC Synthesis. (a) $NH_2OH{\cdot}HCl$, pyridine, EtOH, Reflux, o.n. (98%); (b) Eaton's Reagent, 100°C, 30 min (97%); (c) $LiAlH_4$, Et_2O, 35 °C, o.n. (91%); (d) Methyl 4-chloro-4-oxobutyrate, DCM, Et_3N, 0 °C, 2h (87%); (e) LiOH, $MeOH/H_2O$, reflux, 16h, 95%; (f) Br_2, DCM, 0 °C, 2h, 99%; (g) KO^tBu, THF, -40 °C, 2h, 95% 49

2.3 Attempted Synthesis of BARAC. (a) 1-Bromohexane, NaOH (sat.), toluene, TBABr (5 mol %), 60°C (85%); (b) Br_2, DCM, 0°C (88%); (c) KO^tBu, THF, -40°C (<10%) 50

2.4 *Reagents and conditions*: (a) HNO_3, H_2SO_4, 85 °C, 2h (49%); (b) $SnCl_2$, HCl/AcOH, reflux, 2h (73%) (c) (1) $NaNO_2$, HBF_4, H_2O, 0 °C -> r.t., 2h (89%); (d) Xylene, 125°C, 3h ; (48%) (e) $POCl_3/PCl_5$, 90 °C, 3h (55%) (f) $NH_2OH{\cdot}HCl$, pyridine, 110°C, o.n. (87%); (g) Eaton's Reagent, 100°C, 30 min (99%); (h) $LiAlH_4$, Et_2O, 35°C, o.n. (94%); (i) Palmitoyl chloride, pyridine, CH_2Cl_2, r.t., 4h (80%); (j) Br_2, CH_2Cl_2, 0°C, 1.5h (99%); (k) KO^tBu, THF, -40°C, 2h (83%) 52

2.5 Reaction of *para*-difluoro-DIBAC **21** with benzyl azide 53

3.1 Synthetic scheme for the synthesis of $PEG_n(DIBAC)_2$ from DIBAC. . 96

3.2 Synthetic scheme for $PEG_{10k}(N_3)_m$ from 5,5-bis(azidomethyl)-1,3-dioxan-2-one (azide monomer) 97

4.1 Synthesis of PEG-G1-$(N_3)_4$ (top) and PEG-G2-$(N_3)_8$ (bottom) starting with the corresponding bis-MPA dendrons **1** and **3** 121
4.2 Synthesis of PEG-$(DIBAC)_2$ from DIBAC 122

Chapter 1

Overview of Click-Cross-linked Hydrogels

1.1. Introduction to Hydrogels

Hydrogels are comprised of a three-dimensional network of hydrophilic polymer that has a high degree of swelling in water.[1] The ability hydrogels have of retaining an extensive amount of water without dissolving makes them ideal for a wide range of applications.[2–9] Among the unique properties of hydrogels is their similarity to natural tissue, which is due to their flexibility from being mostly water. The small amount of polymer that's present must have a hydrophilic backbone, and must be cross-linked to prevent complete dissolution. The cross-linked network makes hydrogels semi-permeable, allowing small molecules to transport into and out of the matrix.[10] This poses many advantages for a wide range of biomedical applications, such as tissue engineering,[11,12] cell encapsulation,[5,13] controlled release,[9,14] and wound healing.[15,16]

One of the first reported synthetic hydrogels was in 1960 by Wichterle and Lim and was made from poly(hydroxyethylmethacrylate) (PHEMA).[17] Since then, research on hydrogels has expanded across the globe. The material that is chosen to make a hydrogel impacts the resulting properties, quality and reproducibility.[18] Choosing the right precursor polymer, and adapting it to a specific application, can be challenging. Hydrogels can be made up of natural polymers, synthetic polymers, or a combination of both natural and synthetic elements. The polymer chosen must be stable, non-cytotoxic, and not elicit an immune response.

1.1.1. Natural Hydrogels

Some of the first successful examples of hydrogels involved natural polymers. In 1980, Lim and Sun created hydrogel microcapsules out of calcium alginate for the encapsulation of islet cells.[19] After that report, alginate became a common material for cell encapsulation, since it made microcapsule fabrication extremely easy.[20] To create hydrogel beads, sodium alginate is dropped into a calcium chloride solution, and the resulting anionic beads can be coated with cationic poly-L-lysine (PLL) to increase mechanical stability. Unfortunately, PLL elicits an immune response, so efforts have been made to mask it, for example, having a third coating of alginate.[21] In a study by Stöver and co-workers, C2C12 mouse cells exibited high viability 7 days post-encapsulation within alginate/poly-L-lysine/alginate (APA) microcapsules (Figure 1.1), proving the effectiveness of alginate hydrogels for cell encapsulation.[22]

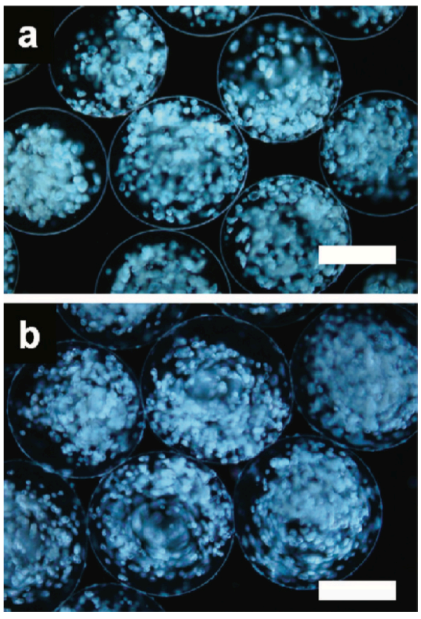

Figure 1.1. Phase contrast optical microscopy image 7 days after encapsulation of C2C12 mouse cells in alginate/poly-L-lysine/alginate (APA) microcapsules. Scale bar: 500μm. Reproduced with permission.[22] Copyright Biomacromolecules, 2009.

Since then, there have been many approaches toward perfecting hydrogel design. Many other materials of natural origin have been studied, including protein-based hydrogels like Matrigel™, collagen and fibrin. Matrigel™ is the trade name for a mixture of basement membrane proteins derived from Engelbreth-Holm-Swarm (EHS) mouse sarcoma cells.[23] It promotes cell differentiation, improves graft survival, and repairs damaged tissues. Other examples of natural polymers used for hydrogel synthesis include collagen, hyaluronic acid (HA) or hyaluronate, agarose, chitosan and dextran.[24] These materials have many advantages and have been utilized in the reconstruction of organs (collagen),[25,26] wound healing and implants (HA),[27,28] sealants and adhesives in surgery (fibrin).[29] However, the low mechanical stability, batch-to-batch variability, and sometimes difficult purification procedures, limits the range of applications of these natural polymers.[24]

There are still many researchers building hydrogels with natural polymers, but most have incorporated a synthetic aspect to the hydrogel in order to impart greater control over the structure and properties. Leossner and co-workers recently developed a three-dimensional cell culture platform for cancer research based on a synthetically modified gelatin hydrogel.[30] Gelatin, which is a derivative of collagen, has been used in many tissue-engineering applications due to its ease of gelation and compatibility in the body. The semi-synthetic gelatin methacrylamide (GelMA) hydrogel takes advantage of the natural cues provided by the gelatin, with the added bonus of having tunable properties.

The biggest advantage of natural hydrogels is their likeness to native extracellular matrix (ECM), which allows for facile incorporation into a host, and also means there are built-in cell-binding and cleavage sites. Unfortunately, complete elucidation of the matrix composition is often not possible due to the complex and ill-defined nature of the scaffold.[30,31] As natural polymers are derived from nature, purification is often difficult as

there are proteins, biomaterials, and other impurities present.[21] As an alternative, important biomaterials that are present in natural polymers can be synthetically engineered and incorporated into hydrogels to allow for greater control over structure, properties and consistency between batches.

1.1.2. Synthetic Hydrogels

Natural polymers helped pave the way for what was possible with hydrogel materials, however, over the years synthetic hydrogels have been investigated more and more. Synthetic polymers have structural control, versatility in molecular weight, as well as ease of purification and ability to incorporate stable cross-linking chemistry. The building block style of synthetic hydrogels allows for great control over desired properties such as strength, durability and degradability. The main drawbacks to synthetic hydrogels are the typically complex synthetic route to their formation, as well as the absence of natural bioactive ECM ligands. Synthetic procedures can be optimized to be less complex, and the absence of natural biomaterials can be easily corrected by manually adding synthetic versions, such as integrating adhesion peptides or growth factors.

Examples of synthetic polymers used to make hydrogels include poly(hydroxyethylmethacrylate) (PHEMA), poly(*N*-isopropylacrylamide) (PNIPAAm), polyacrylamide (PAAm), poly(vinylpyrrolidone) (PVP), poly(vinyl alcohol) (PVA), poly(ethylene glycol) (PEG) and several other water-soluble polymers.[24] PHEMA was the first reported polymer for hydrogel synthesis, and remains one of the most studied synthetic hydrogel polymers. It is very hydrolytically stable, and is most well known for its use in contact lenses,[32] although it has also been used in drug delivery applications,[33] wound dressings, and implants.[34] Since PHEMA is essentially non-degradable under physiological conditions, it must be modified to create

a degradable hydrogel, for example, by incorporating degradable crosslinks to dextran,[35] or PEG.[36]

PNIPAAm is another synthetic polymer that has been used in hydrogel synthesis. It has a lower critical solution temperature (LCST) in water of approximately 32°C. This is extremely advantageous for cell encapsulation and tissue engineering applications as a solution of cells and the polymer can be prepared below the LCST, and then once injected into the body, the solution forms a gel. Depending on the desired hydrogel properties, NIPAAm can be copolymerized with other polymers, such as acrylic acid, N-hydroxysuccinimide, acrylamide (AAm), and dimethyl-γ-butyrolactone acrylate (DBA).[37,38] Addition of DBA into the polymer increases the LCST above physiological temperature, allowing the polymer to be cleared from the body.[39] Typically, hydrogels made from PNIPAAm are opaque, which could pose a problem for specific applications in the eye. In that case, the hydrogel can be injected at the bottom of the vitreous, which does not affect sight.[40] In addition, using a temperature-responsive polymer for hydrogel synthesis enables cells to be easily recovered by simply lowering the temperature.

PVP, PAAm, and PVA are other examples of synthetic polymers used in making hydrogels. PVP hydrogels are typically made through physical crosslinking, and have been used in a number of applications including ophthalmic drug delivery, wound dressing, and even heavy metal removal from water.[41–43] PAAm hydrogels are non-degradable, stable and non-toxic and can be injected into soft tissue in the body for tissue implants.[44,45] Finally, PVA can be modified through the plethora of pendant hydroxyl groups, and can be physically or chemically crosslinked to form hydrogels.[2,46]

1.1.2.1. PEG Hydrogels

Of all the examples of synthetic polymers, PEG and PEG derivatives seem to be one of the best options for hydrogel applications, as they fit all the necessary criteria. PEG is hydrophilic, non-toxic, stable, and is easily modifiable to tune hydrogel crosslinking and properties. They can be adapted to be degradable or non-degradable, are completely transparent, can crosslink through either physical or chemical means, and are a good candidate for an injectable material. PEG has already obtained approval from the Food and Drug Administration (FDA), is inexpensive, and available in a wide range of molecular weights with narrow polydispersities. PEG is most well-known for its use in laxatives, excipients, skin creams, and toothpaste. It is also used in biopharmaceutical drugs to increase circulation times. Lower molecular weight PEG can be used as a solvent in oral liquids or soft capsules, whereas the larger molecular weight polymers are more solid and are useful as an ointment base, tablet binder, film coating, or lubricant.

It is important for the hydrogel material chosen to have low non-specific protein adsorption. Typically, the first step of an inflammatory response is protein adsorption, though hydrogels are less prone to this due to their highly hydrated nature. PEG is particularly well known for its low protein adsorption and antibiofouling properties, which further confirms its suitability as a hydrogel material.[47,48] In some cases, PEG is added to a hydrogel system specifically to reduce non-specific protein adsorption.[49–52]

PEG on its own is unable to form a crosslinked network, therefore, the end hydroxyl groups of PEG must be functionalized in order to create a hydrogel. An array of functional groups can be used, including acrylates,[53,54] azides,[55] alkynes,[56] thiols,[57] vinyl sulfones,[58] maleimides,[59,60] and many more.[57,61]

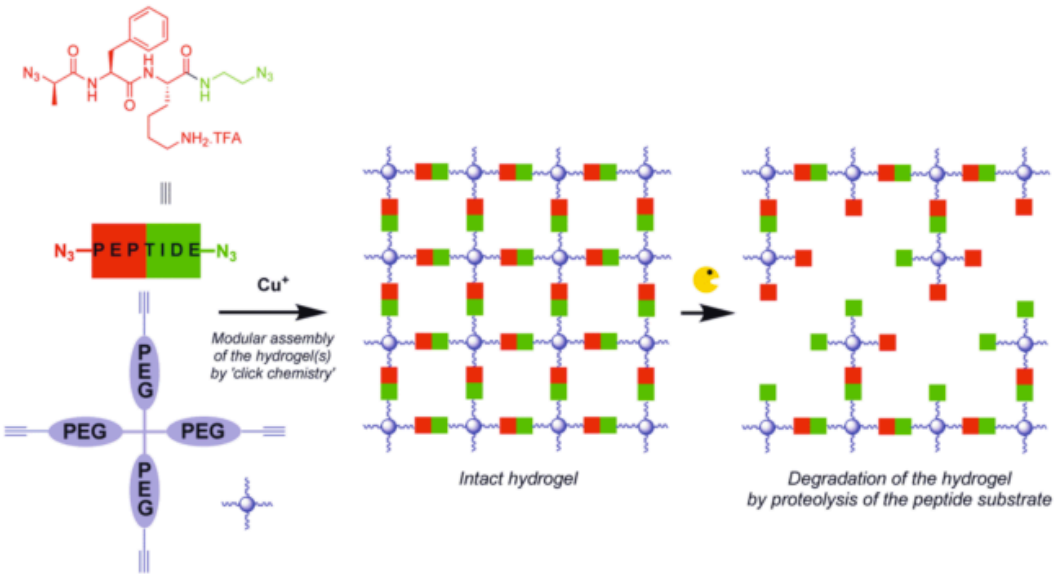

Figure 1.2. Schematic formation and degradation of enzymatically-degradable PEG hydrogels synthesized via the Cu(I)-catalyzed azide-alkyne cycloaddition reaction. Reproduced with permission.[56] Copyright Biomacromolecules, 2010.

Poly(ethylene glycol)-diacrylate (PEGDA), is PEG functionalized with unsaturated carbon-carbon double bonds, making the resulting polymer able to form a hydrogel through photopolymerization with UV light.[62] The PEGDA hydrogel system has been widely used for over 20 years for its ease in hydrogel formation.[63] Studies have demonstrated its use in photoencapsulating chondrocytes,[64,65] corneal keratocytes,[66] human mesenchymal stem cells (hMSCs),[67] as well as for cartilage, nerve cell, and cardiovascular repair.[12,68,69]

There are also reports of hydrogels made from non-linear, multifunctional PEG; most common are four-arm[59,61,70,71] and 8-arm PEG hydrogels.[72–74] Figure 1.2 depicts the formation of a PEG hydrogel using a four-arm PEG-alkyne and the Cu(I)-catalyzed azide-alkyne cycloaddition reaction. In this case, the diazide crosslinker is a short peptide sequence that can be cleaved

by trypsin and plasmin, two endogenous serine proteases produced by the pancreas (trypsin) and liver (plasmin).

An alternative to the typical PEG-based hydrogel systems is the fairly new poly(oligoethylene glycol methacrylate) (POEGMA).[75] This polymer is synthesized from controlled living free-radical polymerization, and offers the advantage of being made thermoresponsive by copolymerizing oligo(ethylene glycol) methacrylate (OEGMA) monomers with varying lengths of ethylene oxide (EO) side chains.[76,77] Hydrogels can be formed by complementary hydrazide and aldehyde functionalized POEGMA precursors, as proven successful by the Hoare group.[78–80]

1.2. Hydrogel Cross-linking

Finding the right cross-linking chemistry is imperative for successful hydrogel synthesis. Whether through click chemistry, or traditional polymerization, the ability to control the crosslink density of a hydrogel means control over the properties of that hydrogel, like flexibility and stiffness, as well as gelation time. Gelation must occur at physiologically relevant conditions, at a pH of 7.4 and a temperature of 37°C. It also must occur quickly, within seconds to minutes following injection, to minimize diffusion of the precursor polymers from the target site, which may cause adverse effects in neighboring tissues and/or prevent hydrogel formation entirely if the dilution is too significant.

The crosslink density affects the mechanical properties of the hydrogel. Different tissues in the body have varying mechanical properties, or elasticity, as depicted in Figure 1.3, therefore hydrogels meant for specific applications in the body can be tailored to mimic specific soft tissues.[81]

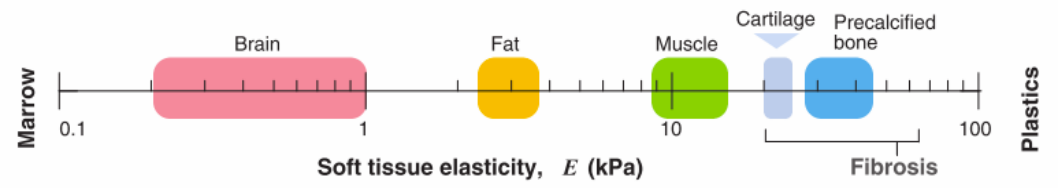

Figure 1.3. Scale of soft tissue elasticity expressed in Young's Modulus values (E, kPa). Reproduced with permission.[81] Copyright AAAS, 2009.

A statistical gelation model (Equation 1.1) developed by Flory and Stockmayer allows calculation of the theoretical gel point (ρ_c) in step growth networks.[82,83] This equation works for systems that have two reactive polymer species, for example, a PEG azide and a PEG alkyne. The conversion required for gelation to occur can be predicted based on equation 1.1 where *r* is the ratio of reactants and f_A and f_B are the degree of functionality of each reactive polymer. For gelation to occur, ρ_c must be less than or equal to 1. Using this equation, it is possible to determine the ratio of the two reactive polymers that is required for gelation, as well as the ratios at which a gel would not be formed.

$$\rho_c = \frac{1}{\sqrt{r(f_A-1)(f_B-1)}} \tag{1.1}$$

Formation of hydrogels typically involves either polymerizing hydrophilic monomers, or modifying or functionalizing existing polymers, and then combining them to form a gel. A wide range of crosslinking strategies has been used, though, they are only practical for biomedical applications if there are no toxic reagents or byproducts, and no harmful stimuli required for gelation.[9] Physically crosslinked polymers are an alternative option for hydrogel formation, which do not have any harsh requirements for hydrogel crosslinking, but these systems also fall apart faster since they are not held together by stable crosslinks. Ultimately, chemically-crosslinked systems

seem to be the ideal solution, and considerable effort has been made to create a hydrogel material that meets all the crosslinking requirements; bio-orthogonal, stable, fast (even at low concentrations), achievable under physiological conditions (pH and temperature), no toxic reagents or byproducts, and no harmful stimuli or catalysts.

1.2.1. Physically Cross-linked Hydrogels

Hydrogels can be formed through non-covalent, or physical crosslinks. The advantage of these hydrogels is they generally require little or no chemical modification, and therefore, the presence of any potentially harmful crosslinking agents or reaction byproducts is avoided. There are application-based advantages of physically crosslinked hydrogels; for example, they are often used in self-healing applications.[6] Self-healing hydrogels can be formed based on physicochemical interactions such as hydrogen bonding,[84] aromatic interactions,[85] ionic bonding,[86] supramolecular (guest-host) interactions,[87] and hydrophobic interactions.[88] Often, two types of physical crosslinks are used, as shown in Figure 1.4. In this example, an injectable self-healing hydrogel is formed through combined interactions of thermoresponsive PNIPAAm, and the hydrogen bonding and aromatic π-stacking of the mussel-inspired catechol moiety.[85] As an added bonus, the hydrogel has anti-biofouling properties due to the presence of PEG.

Examples of other physically crosslinked hydrogels use environmental triggers, like pH or temperature.[9,89] PNIPAAm is one of the most commonly used temperature-responsive polymers for hydrogels. In this case, when the temperature is raised above the LCST of 32°C, water molecules that were bound to the isopropyl side groups are released, increasing hydrophobic interactions and causing the polymer chains to collapse, which ultimately results in the phase separation of the hydrogel system.[90] The hydrogel is also

visually opaque above its LCST due to the phase transition. Agarose is another representative example of a temperature-responsive hydrogel, although the gelling properties are reversed from PNIPAAm, with gelation occurring upon cooling.[91] This is valuable for applications in drug delivery as physiological temperatures cause hydrogel dissolution and therefore, controlled release of the encapsulated drug.[92]

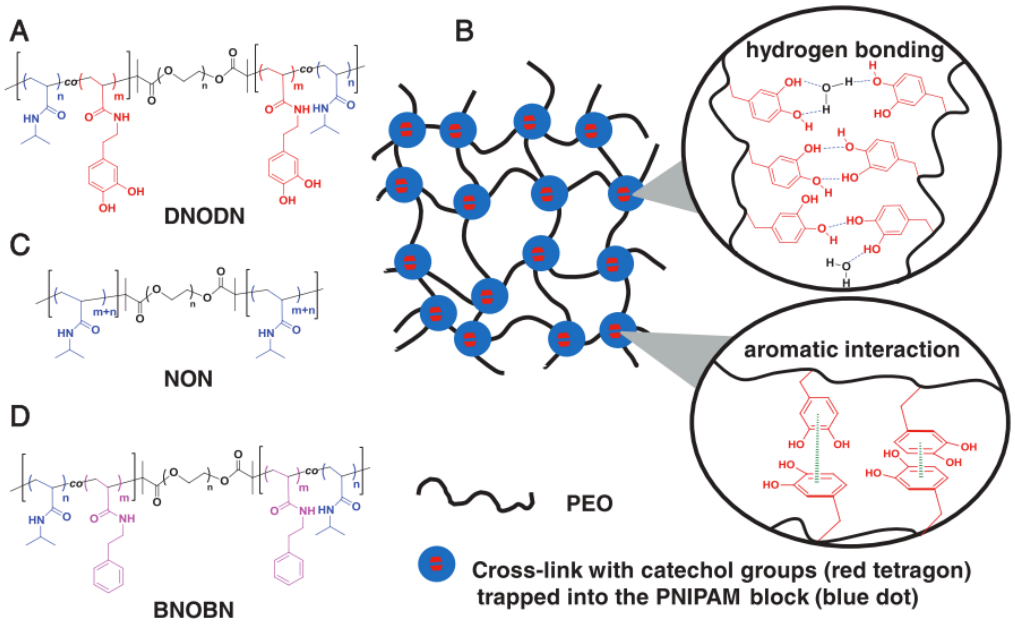

Figure 1.4. ABA tri-block copolymer composed of catechol-functionalized PNIPAAm and PEG (A) form a self-healing hydrogel based on hydrogen bonding and aromatic interactions (B). Structures of ABA tri-block copolymer without catechol (C) and instead containing phenylethylacrylamide (D) to show lack of hydrogen bonding interactions (D) as well as lack of both hydrogen bonding and aromatic interactions (C). Reproduced with permission.[85] Copyright Advanced Materials, 2015.

Physically crosslinked hydrogels can also be formed through freeze-thaw cycles and are termed cryogels; PVA, carboxymethyl cellulose (CMC), agarose, and startch are a few examples.[93] The major disadvantage of physically crosslinked hydrogels is overall lower mechanical strength compared to covalently crosslinked hydrogels.

1.2.2. Covalently Cross-linked Hydrogels

Covalently cross-linked hydrogels are preferred due to the higher mechanical properties, ability to control crosslink density, and preservation of the hydrogel over a longer period of time. A wider range of hydrogel properties is available, and increased tunability is achievable.

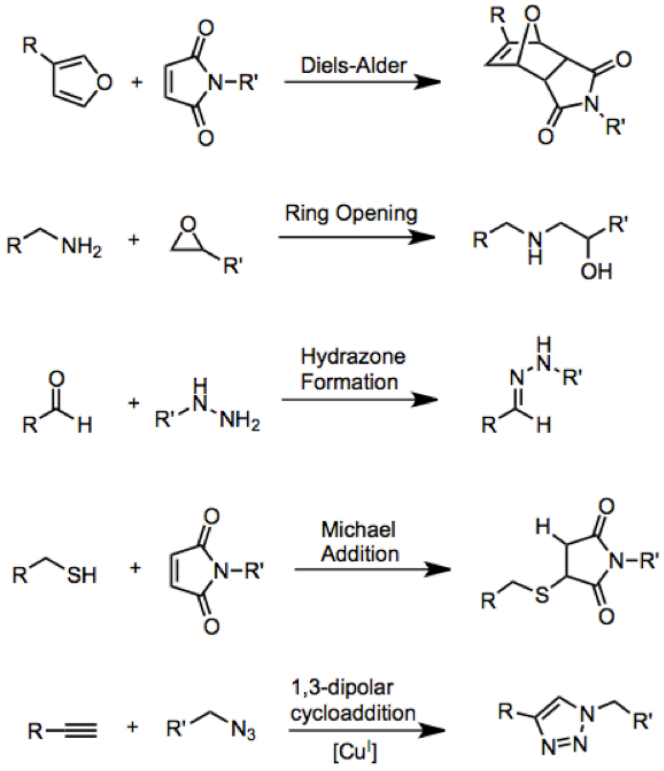

Figure 1.5. Examples of click reactions.

The most common covalent crosslinking in hydrogels involves click reactions (Figure 1.5). The term "click", coined by Sharpless and coworkers in 2001, refers to reactions that are modular, wide in scope, high yielding, and do not generate byproducts.[94] Examples of click reactions include 1,3-dipolar cycloadditions such as the copper(I)-catalyzed alkyne-azide cycloaddition (CuAAC) and the strain-promoted alkyne-azide cycloaddition

(SPAAC), as well as other cycloadditions like Diels-Alder (DA); nucleophilic substitutions such as ring-opening; carbonyl chemistry such as formation of oximes and hydrazones; and carbon-carbon double bond additions like Michael additions. Unfortunately, not all of these reactions are appropriate for biomedical applications. For example, CuAAC has been reported many times for hydrogel formation,[95–98] and would be ideal as it proceeds quickly under physiological conditions, except it requires a copper(I) catalyst that is cytotoxic if not removed.[99]

Another excellent click reaction that is often used in hydrogel formation is the DA cycloaddition between a diene and a dienophile. The most frequently reported version involves maleimide and furan functionalized precursors.[100–102] The downsides to the DA reaction are that it can require high temperatures, which is not conducive to biomedical applications, or if kept at physiological temperatures, the reaction may proceed slowly (hours to days). Also, the dienophile may be reactive toward thiols, which are present in proteins, making this reaction not bio-orthogonal in the presence of thiols. Recently, tetrazine-norbornene chemistry has been used to create hydrogels, which is a form of inverse electron demand DA.[103] This reaction is fast, irreversible, and has proven to be cytocompatible towards hMSCs postencapsulation.[104]

Michael additions are another click reaction used for developing step-growth hydrogels. The components required for this reaction are a Michael donor such as a thiol or amine and a Michael acceptor, which is an electrophilic carbon-carbon double bond that is conjugated to a carbonyl group. The first example of this reaction for hydrogel formation was reported by Hubbel and co-workers and used acrylates as the Michael acceptor.[105] From there, more hydrolytically stable hydrogels were formed with vinyl sulfones, which were used to study cell migration.[106] However, like the DA reaction, the Michael addition is not bio-orthogonal in the presence of thiols.

One type of covalent crosslinking that has shown a lot of promise for making hydrogel materials is the photoinitiated thiol-ene reaction.[107–109] Aside from the potentially harmful radicals that are formed, this reaction seems to be ideal for hydrogels. This chemistry has the added bonus of spatiotemporal control, which allows for site-specific incorporation of biochemical materials, proteins, or peptide sequences such as the adhesion peptide arginylglycylaspartic acid (RGD) (Figure 1.6).[110–112] The Anseth group has revolutionized this chemistry for PEG hydrogels, with the ability to form gels in seconds to minutes.[72]

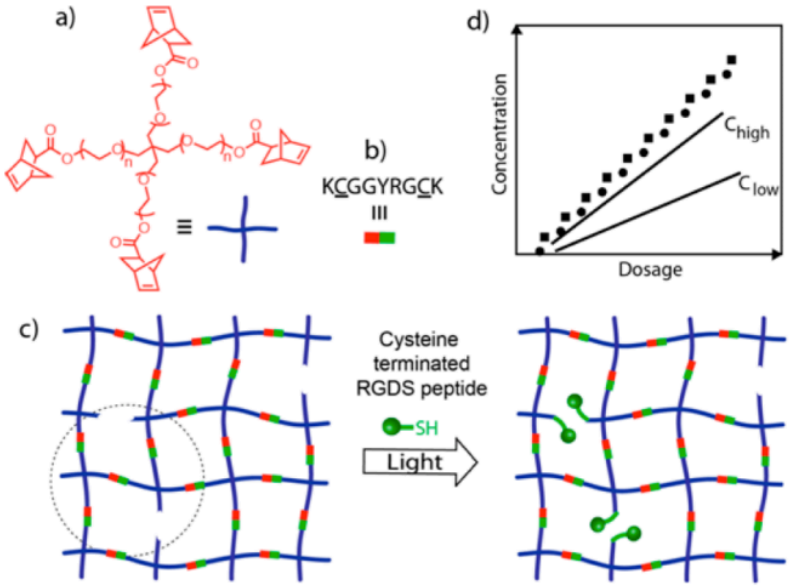

Figure 1.6. PEG-hydrogel based on thiol-ene chemistry with 4-arm PEG tetranorbornene (A) and a dicysteine(thiol)-terminated cleavable peptide (B). Schematic of the hydrogel undergoing spatial photopatterning (C) of RGD and a graph showing that the extent of photopatterning can be controlled by changing the light dosage (time/intensity) and the photoinitiator concentration. Reproduced with permission.[112] Copyright ACS Macro Letters, 2013.

1.2.2.1. SPAAC-Crosslinked Hydrogels

Of all the click reactions available for hydrogel synthesis, one of the most promising is the strain-promoted alkyne-azide cycloaddition (SPAAC, Figure 1.7). This reaction offers all the advantages of CuAAC without requiring a copper catalyst. SPAAC is a [3+2] cycloaddition reaction between a strained cyclooctyne and an azide. The reaction forms an irreversible triazole linkage without the need for any other reagents, catalysts, or external stimuli. It is a fast, efficient reaction that is bio-orthogonal and does not produce any by-products. The reaction occurs quickly, and is driven by the ring strain of the cyclooctyne, which is relieved upon reaction with the azide.

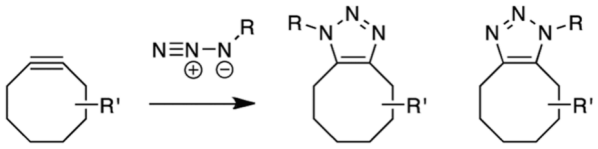

Figure 1.7. The strain-promoted alkyne-azide cycloaddition (SPAAC).

Blomquist and Liu were the first to discover the reactivity of cyclooctynes in 1953,[113] while the first report of the reaction between cyclooctynes and azides was in 1961 by Wittig and Krebs.[114] Many years went by before this reaction was properly noticed again. In 2004, Bertozzi uncovered the potential for SPAAC in living systems as a tool for bioconjugation.[115] Over the next few years, many variations of cyclooctynes were synthesized and their reactivity tested (Figure 1.8).[116] The first cyclooctyne that was used ("OCT" in Figure 1.8) had reactivity that was slower than CuAAC, but eventually other versions were made with an increase in electron-withdrawing groups. Adding one fluorine group ("MOFO" in Figure 1.8) increased reactivity four-fold. Once benzene rings are incorporated, along with other electron

withdrawing groups like carbonyls, the reactivity increases by several orders of magnitude.

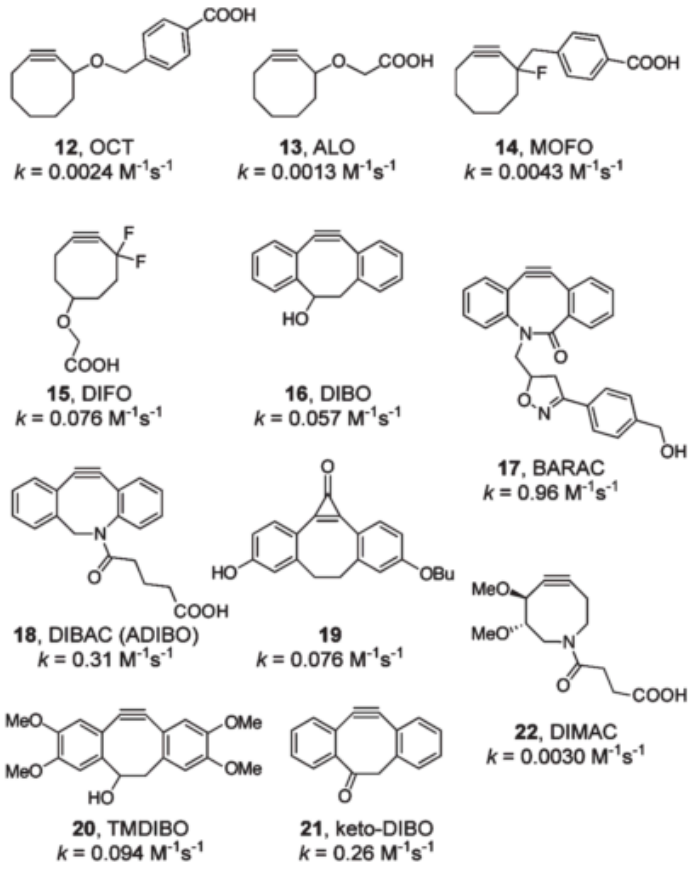

Figure 1.8. Various cyclooctynes for Cu-free click chemistry. Second-order rate constants are for reaction with benzyl azide. Reproduced with permission.[116] Copyright Accounts of Chemical Research, 2011.

Since Bertozzi's reintroduction of cyclooctynes with SPAAC, researchers have been finding ways to incorporate them into hydrogel chemistry, which has proven extremely successful. The Anseth group, who predominantly works with PEG hydrogels, has published many reports of PEG hydrogels crosslinked with SPAAC. At first, they used cyclooctynes containing a geminal difluoro moiety ("DIFO", Figure 1.8). For example, they used a synthetic polypeptide difunctionalized with DIFO and a 4-arm PEG tetrafunctionalized

with azides to create hydrogels with tunable mechanical properties.[110] They also incorporated an alkene group within the dipeptide to integrate postgelation photopatterning of biomolecules. By controlling the area in which the light is delivered, as well as the light intensity, a material can be created that has the potential to direct cell function within specific regions. They later took this one step further by adding a photodegradable unit into the backbone of the polypeptide crosslinker (Figure 1.9).[117] This enhanced hydrogel offers dynamic tunability of properties by spatiotemporally controlling photoconjugation as well as photocleavage.

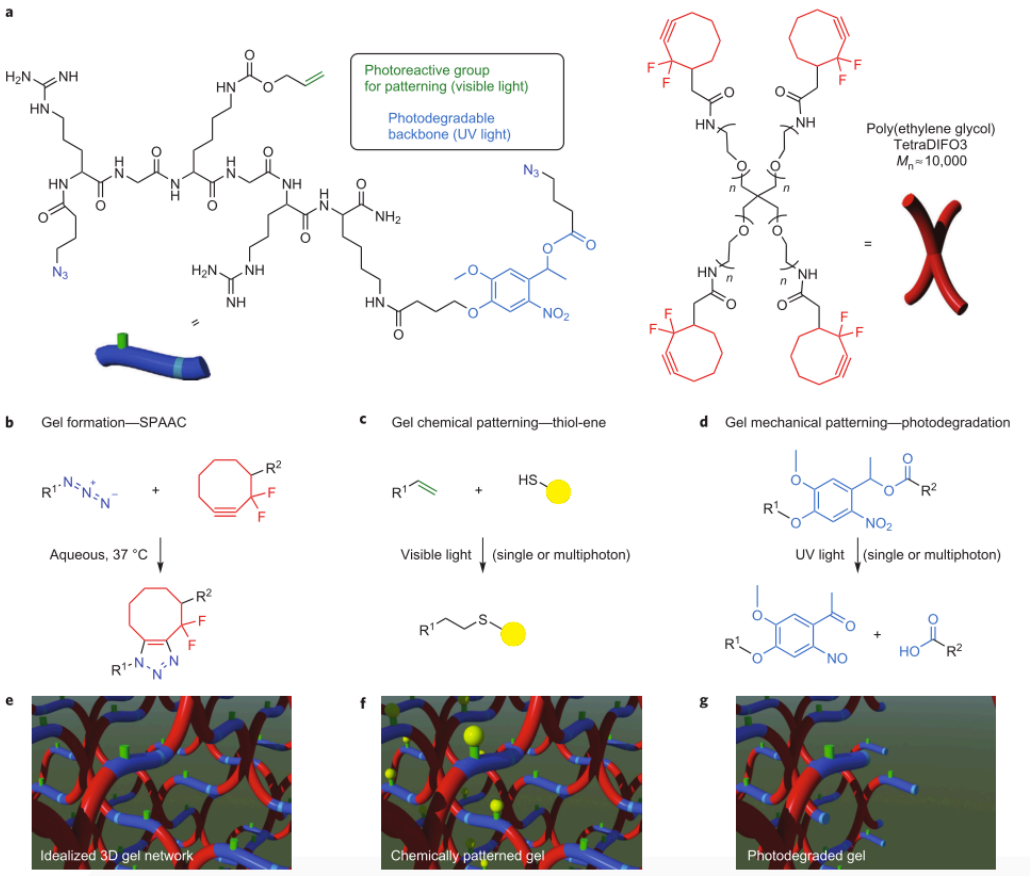

Figure 1.9. Hydrogel formation (B, E), photopatterning (C, F) and photodegradation (D, G) of SPAAC-crosslinked hydrogels made from a diazido degradeable peptide and a 4-arm PEG tetracyclooctyne (A). Reproduced with permission.[117] Copyright Nature Chemistry, 2011.

Other groups have also reported SPAAC-crosslinked hydrogels. Zheng and co-workers created an injectable hydrogel based on 4-dibenzocyclooctynol ("DIBO", Figure 1.8) functionalized PEG that formed within minutes and kept hMSCs viable for 24 hours *in vitro*.[118] Song and co-workers used aza-dibenzocyclooctyne ("DIBAC", Figure 1.8) to make PEG hydrogels that formed quickly and showed high viability of bone marrow derived stromal cells (BMSCs) 48 hours after encapsulation.[119] Zhong and co-workers synthesized an injectable PEG hydrogel containing fluorocyclooctyne ("MOFO", Figure 1.8).[120] They performed *in vivo* mouse studies, which involved a subcutaneous injection of the hydrogel precursors. The hydrogel caused a mild initial inflammatory response, though the surrounding tissue fully recovered within a week.

1.2.3. Injectable Hydrogels

The innate three-dimensional structure of hydrogels poses a challenge for delivery into the body. For biomedical applications, delivery into the body is a requirement, and therefore the focus of hydrogel preparation has turned to "injectable" or "*in situ* gelling" systems, which enable the use of minimally invasive surgical techniques. This has many advantages including greatly reducing patient discomfort, risk of infection, and recovery time.[48] This method relies on the ability of the hydrogel system to gel post-injection, and therefore gelation must be prevented prior to administration *in vivo*.[121] To accomplish this, the hydrogel precursor solution undergoes a solution-to-gel transition (sol-gel) *in situ* due to physical or chemical stimuli. This poses the advantage that these hydrogels can be injected into a cavity or area of any shape or size. For successful administration of the hydrogel through a needle, the precursor polymer solutions must have low viscosity, and they also must gel fairly quickly to limit the amount of diffusion from the injection site, though not so quickly as to clog the needle. Typically the gelation kinetics can

be controlled by the degree of crosslinking. There are many reviews on injectable hydrogels,[3,8,122–126] as these types of hydrogels are preferred for certain biomedical applications.

If not *in situ* or injectable, hydrogels can also be preformed into microparticles or hydrogel beads prior to injection. These microgels can be made using microfluidics (Figure 1.10).[91,127,128] Microfluidics is a high-throughput emulsification technique used to generate droplets with precise dimensions. To make hydrogels, precursor polymer solutions can be incorporated into individual channels that are then combined and formed into droplets via emulsion. Microfluidics works well for the synthesis of hydrogel beads as the number of cells per microparticle can be controlled, and the hydrogel composition can be controlled, by adjusting the flow rate of the individual channels.[129]

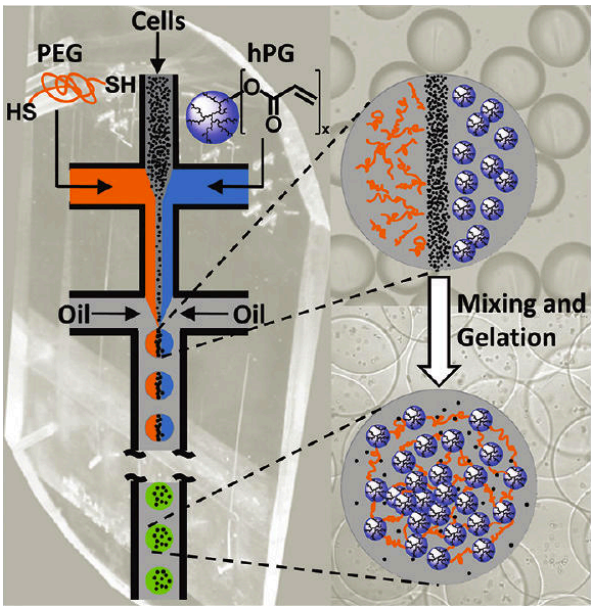

Figure 1.10. Formation of thiol-Michael addition crosslinked cell-containing microgels via microfluidic emulsification. Reproduced with permission.[127] Copyright Journal of the American Chemical Society, 2012.

1.3. Hydrogel Swelling

Three-dimensional hydrogel networks swell in aqueous solutions due to the hydrophilic nature of the polymer chains. They do not dissolve, and instead remain insoluble, because of the crosslinks that create the network. The degree of crosslinking between polymer chains, as well as the dispersion forces acting on them affects the amount of swelling that occurs.[130] Swelling in a hydrogel is not continuous, and eventually reaches an equilibrium state based on balancing the forces of osmosis and elasticity.[131] These forces prevent the network from deforming while still allowing the appropriate amount of solvent to enter. The equilibrium swelling ratio can be calculated using the Flory-Rehner equation.[132] A simpler equation, which describes the weight equilibrium swelling ratio (Q) is described in Equation 1.2, where W_s is the swollen hydrogel weight and W_d is the dry hydrogel weight.[133]

$$Q = \frac{W_s}{W_d} \tag{1.2}$$

1.4. Hydrogel Degradation

Injectable hydrogels must be able to degrade over time, otherwise surgical intervention would be required once the hydrogel is no longer needed. The degradation products must also be non-toxic, and able to clear the body. Therefore, the degradation time of the hydrogel must be controlled. For natural polymer hydrogels, the components typically degrade and are metabolized into small molecules in the body. Synthetic polymer hydrogels do not always have the same ease of degradation. To control the degradation mechanism and rate, reversible crosslink chemistry or degradable linkages in the polymer backbone can be introduced. Depending on the application, degradation and clearance from the body might not be desired, for example

in dermal fillers or contact lenses. If degradation via the polymer backbone is desired, there are a few mechanisms to achieve this; oxidation, hydrolysis, photodegradation or by enzymatic cleavage. An example of oxidation-driven degradation involves HA hydrogels connected with disulfide bonds.[134] In this example, the hydrogel can be reduced with dithiothreitol (DTT) to break the disulfide bond into two corresponding thiols. Varying the amount of DTT controls the extent of hydrogel degradation.

The Anseth group has reported successful matrix metalloproteinase (MMP) degradeable PEG hydrogels. These enzyme-degradable hydrogels give encapsulated stem cells the control to remodel their own environment,[70] which results in an increase in the levels of specific differentiation markers (osteogenic, chondrogenic, or adipogenic) compared to hydrogels that are not cell-degradable. Hydrogels containing this degradable linker have also been successful for housing valvular interstitial cells (VICs).[135]

Hydrogels can also degrade via hydrolysis of the polymer backbone. One of the more common examples of this uses ester groups, as they degrade naturally over time in physiological environments.[120] Song and co-workers developed a series of four SPAAC crosslinked PEG hydrogels that predictably degrade via hydrolysis in 1.5, 2, 52 or greater than 250 days in cell culture medium.[55] These times were slightly longer in phosphate buffer saline (PBS). All four hydrogels have comparable macroscopic properties including stiffness and swelling, yet the degradation time can be controlled by changing the number of specific functional linkages near the crosslinks; either amide, ester or ether.

Another way to controllably degrade hydrogels is through photodegradation. Using this method, photodegradable moieties can be incorporated within the polymer backbone of the hydrogel network, such as nitrobenzyloxycarbonyl (NBOC) or nitrobenzyl ether.[136–138] Recently, Anseth and co-workers reported the synthesis of hydrogels with amplified

photodegradable properties.[83] By incorporating an allyl sulfide group in one of the polymer precursors, the resulting hydrogel can be degraded via a radical addition-fragmentation chain transfer (AFCT) process. Unlike typical photodegradation chemistry where one photon breaks one bond, in this process, one photon initiates multiple events, ultimately breaking many bonds and amplifying the degradation process. For example, they were able to degrade a 1 cm thick hydrogel in 1 minute.

1.5. Dendrimers

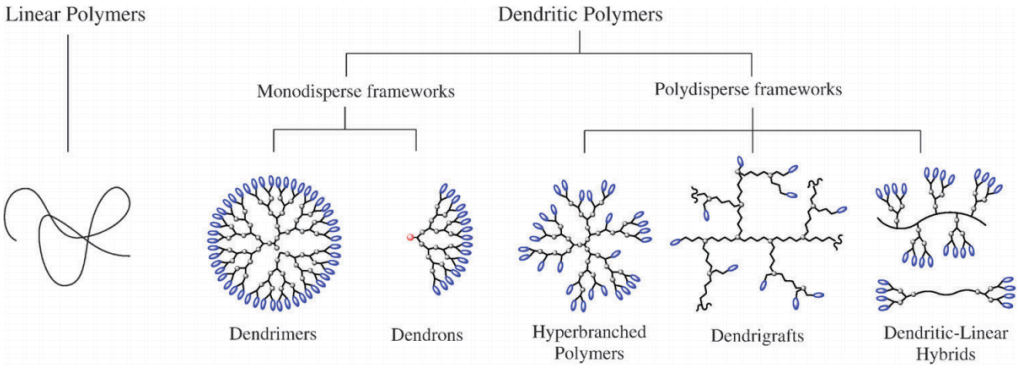

Figure 1.11. Schematic overview comparing the structures of linear polymers versus other macromolecules that fall under the dendritic category. Reproduced with permission.[139] Copyright Chemical Society Reviews, 2012.

Within the field of macromolecular chemistry is a class of polymers called dendrimers (Figure 1.11). Unlike traditional polymers, dendrimers are structurally perfect and monodisperse.[139] Three-dimensionally, dendrimers are globular structures that are prepared using a stepwise synthesis that results in well-defined repeat branching units (generations, G) from the core to the periphery, where there are a set number of peripheral end groups based on the generation number (Figure 1.12). Each component of the dendrimer; the core, monomer units and periphery, can be controlled.

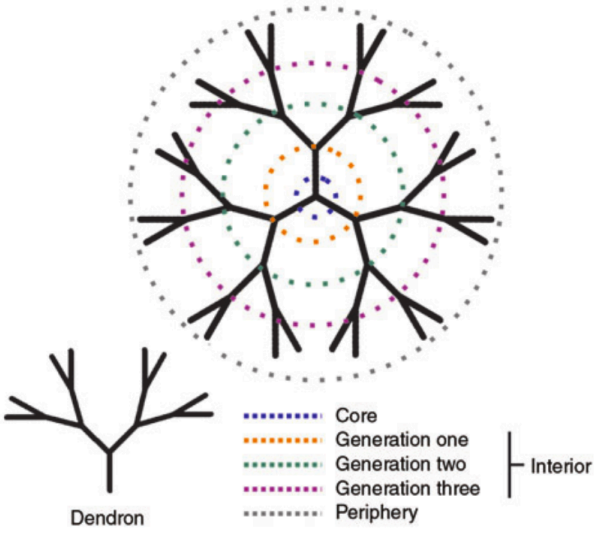

Figure 1.12. Anatomy of a third-generation dendrimer and dendron. Reproduced with permission.[140] Copyright Nature Biotechnology, 2005.

1.5.1. Dendrimer Hydrogels

The use of dendrimers in hydrogel materials is still fairly novel, with one of the first reports of covalently crosslinked dendritic hydrogels in 2002 by Grinstaff and co-workers.[141] This work outlined the synthesis of a photocrosslinkable hydrogel for sealing corneal lacerations.[142] The hydrogel was made using a dendritic-linear-dendritic (DLD) structure made of PEG that was end functionalized with poly(glycerol-succinic acid) dendrons. The periphery of the dendrons was functionalized with methacrylate groups to allow photocrosslinking.

The advantage to incorporating dendrimers in hydrogel materials is that, due to the complete preciseness and structural control of the dendrimer precursor, hydrogels are created that have reliable, reproducible properties. Often, when polymers are functionalized with reactive groups for crosslinking, the exact number of crosslinking moieties is unknown, and

therefore different batches of the polymer will result in variations in the resulting hydrogels.[119] The integration of dendrimers allows for complete batch-to-batch reproducibility, which facilitates ongoing research and ultimately helps create hydrogels with specific, optimized properties. Additionally, dendrimers of different generations can be used to change the crosslink density without having to adjust the dendrimer concentration. Due to the high degree of functionality at the periphery of dendrimers, incorporation of biomolecules or other reactive groups is possible. Finally, the spherical dendrimers help limit the swelling and improve mechanical properties.[143,144]

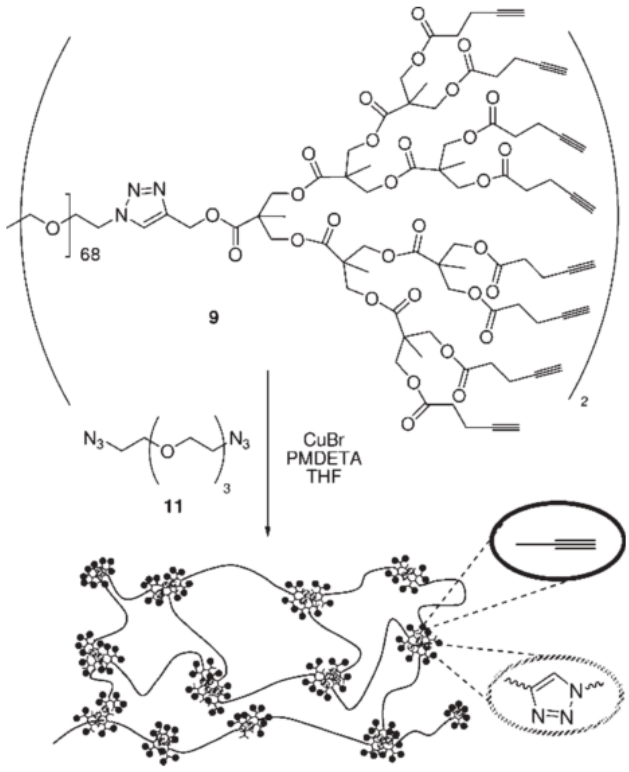

Figure 1.13. Dendritic hydrogel formation via CuAAC crosslinking. Reproduced with permission.[145] Copyright Macomolecules, 2010.

Most reports of dendrimer hydrogels use PEG, and typically they are functionalized with acrylates that require UV light for crosslinking.[144,146] There are other reports that use materials such as PAMAM,[147,148] or PAMAM and PEG,[149–151] or that incorporate linear PEG as a crosslinker between dendritic benzyl ether groups.[152,153] Aside from photocrosslinking, few other reactions have been used to make dendritic hydrogels. One example by Sanyal and co-workers uses CuAAC to crosslink linear PEG diazide with a DLD structure made from a PEG chain that is functionalized at its ends with polyester dendrons (Figure 1.13).[145] The dendrons were made from second and third generation 2,2-bis(hydroxymethyl)propanoic acid (bis-MPA) dendrons that were functionalized at the periphery with terminal alkynes.[145] Another example involves dual-purpose PEG DLD hydrogels that are crosslinked using photoinitiated thiol-ene chemistry, but also contain pendant azide groups for controlled incorporation of biomolecules via CuAAC (Figure 1.14).[154]

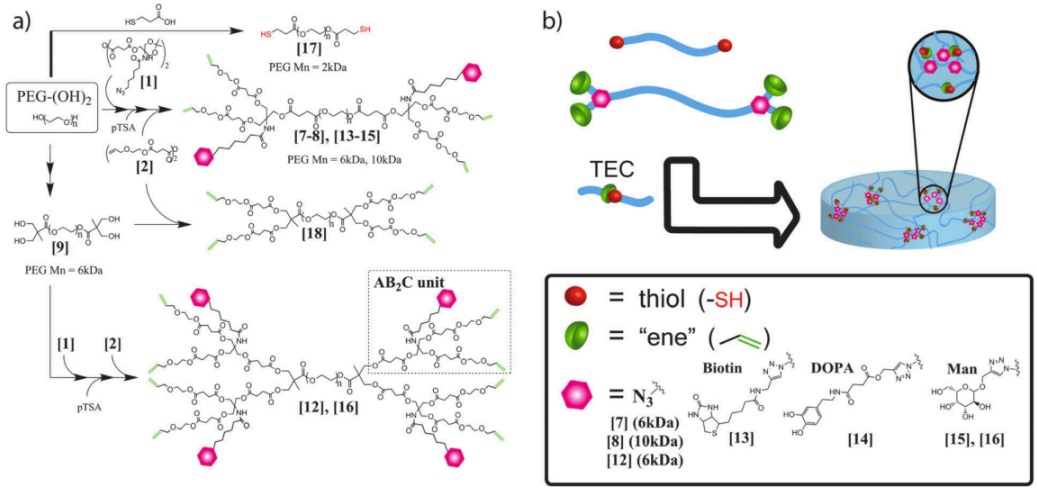

Figure 1.14. Formation of a dual-purpose DLD PEG hydrogel. Linear PEG is the starting point, which is functionalized with thiols, or alkene or azide terminated dendrons (left). The hydrogel is formed using photoinitiated thiol-ene crosslinking, and biomolecules like Biotin, DOPA and Man can be incorporated using CuAAC. Reproduced with permission.[154] Copyright The Royal Society of Chemistry, 2013.

1.6. PEG Hydrogel Applications

PEG hydrogels are widely used for biomedical applications, including controlled release and tissue engineering. In controlled release applications, the goal is to enable a molecular, macromolecular, or biomolecular payload to exit the delivery vehicle in a manner that allows a therapeutic dose to be sustained over a desired period of time. The payload delivery can occur through diffusion, swelling, or chemical means. Since PEG hydrogels typically have high permeability, there is little control over the exit of small molecules, even if the crosslink density is adjusted.[155] To control the release from these materials, the use of stimuli-responsive hydrogels, such as hydrogels that collapse or swell in response to a change in pH or temperature, has been reported.[156–158] As the hydrogel swells, the encapsulated molecules are released.

The highly porous nature of hydrogels is ideal for cell encapsulation, as it allows for facile transport of oxygen, nutrients, waste, and any potential therapeutic agents that are released from the cells. For cell encapsulation applications, other components must be added to the hydrogel, such as targeted cells, growth factors, and adhesion peptides. Hydrogels that are made of PEG have the advantage of being able to integrate into the body with minimal protein adsorption.[159] PEG hydrogels have proven successful in cell encapsulation, particularly when coupled with RGD, a tripeptide that supports cell adhesion.[70,104,160] PEG is a biochemically inert polymer that has inadequate cell adhesion properties, so incorporation of peptides like RGD is not only advantageous, it is necessary.

As an example for therapeutic cell encapsulation, PEG hydrogels have shown promise in islet encapsulation for the treatment of type 1 diabetes.[161,162] As an alternative to manual insulin injections, islet cells (that produce insulin) can be encapsulated within a hydrogel matrix and injected into the body to auto-regulate blood glucose levels.[163,164]

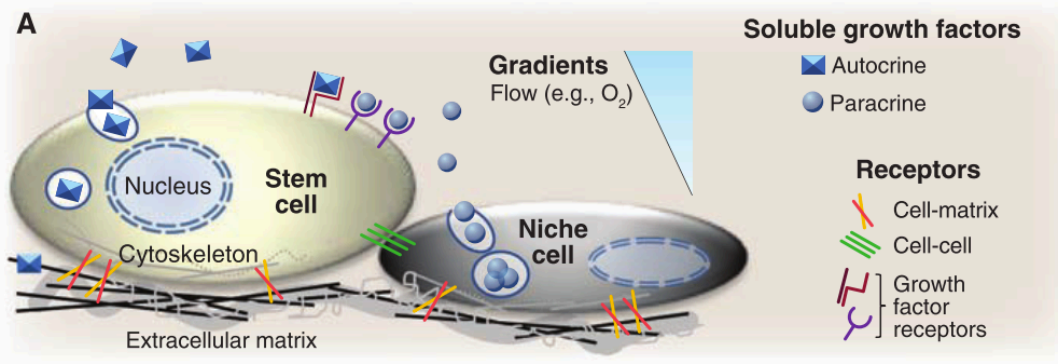

Figure 1.15. Illustration of the stem cell niche involving cell-matrix interactions and adhesion, cell-cell contacts, and growth factors, which all direct cell fate. Reproduced with permission.[81] Copyright AAAS, 2009.

One aspect of tissue engineering involves stem cells, with the goal of directing differentiation of the stem cells toward a specific cell line in order to regenerate damaged or diseased tissue. Cell-matrix and cell-cell interactions take place, and the presence of growth factors and adhesion peptides is important (Figure 1.15). Stem cells that are encapsulated within a hydrogel that contains specific signals can proliferate and grow. They also have the potential to differentiate into a particular cell line, secrete new ECM and restore damaged tissue. Figure 1.16 shows fluorescently-labeled hMSCs within a degradable PEG hydrogel that contains signals promoting hMSC proliferation. At the start of the experiment (left image), the cells are round and have few interactions with the matrix or each other. After two weeks (right image), it is clear that they have formed cell-matrix interactions, which is key for differentiation to occur.

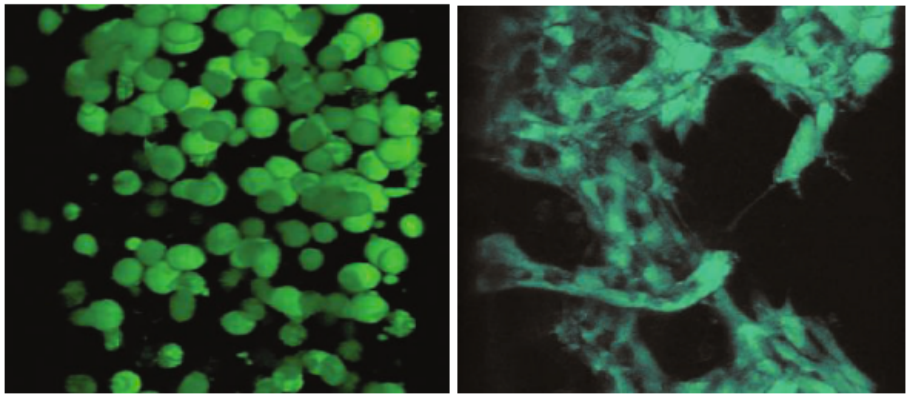

Figure 1.16. Fluorescently labeled human mesenchymal stem cells (hMSCs) in a degradable PEG hydrogel. At the start of the experiment (left), the cells appear rounded with few interactions, whereas after 2 weeks (right), the cells have formed interactions with the gel that promote attachment, migration and differentiation. Reproduced with permission.[31] Copyright AAAS, 2007.

The Anseth group has done extensive *in vitro* testing using various cell lines within PEG hydrogels. One particularly impressive example involves the encapsulation of embryonic stem cell-derived motor neurons (ESMNs) in a photodegradeable SPAAC-crosslinked PEG hydrogel.[165] Using two-photon infrared light, they were able to spatiotemporally control hydrogel degradation, which ultimately allowed them to direct the formation of neural networks (Figure 1.17). Additionally, they cocultured ESMNs and C2C12 myotubes in the hydrogel and connected the two cell types via eroded channels. Results showed that motor axons from the ESMNs extended through the channel toward the myotube aggregates and formed functional neuromuscular junctions. Another example by the same group describes induced differentiation of hMSCs down osteogenic and adipogenic pathways within three-dimensional PEG hydrogels.[166] Differentiation was controlled using tethered small-molecules; charged phosphate groups led to osteogenesis, and hydrophobic *t*-butyl groups induced adipogenesis. The

Anseth group has also reported a PEG hydrogel system that influences chondrogenic differentiation of hMSCs.[167]

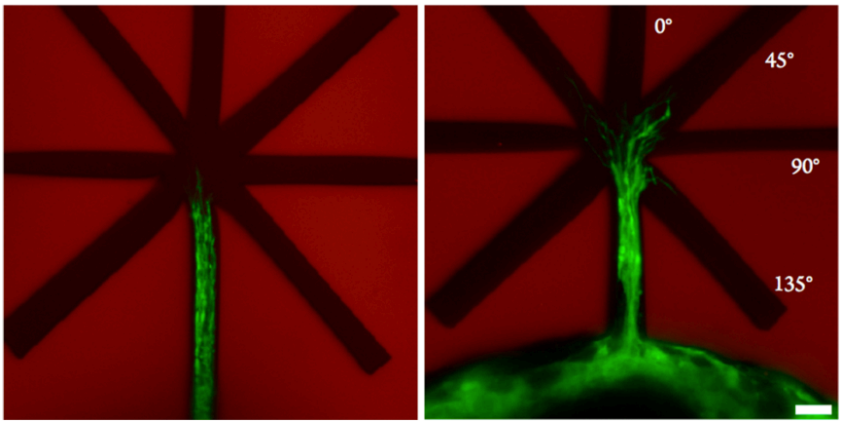

Figure 1.17. Directed mobility of motor axons from ESMNs within photodegradable PEG hydrogels. Two-photon light was used to create an eroded fork-shaped pattern within the hydrogel. Left image shows axons hours before reaching the fork, and then right image shows the direction that was selected. Reproduced with permission.[165] Copyright Biomacromolecules, 2014.

Combining several different hydrogel tools, Haag and co-workers created a "microgel construction kit" to controllably encapsulate cells within a hydrogel matrix and then controllably release them (Figure 1.18). They did this using SPAAC crosslinked PEG hydrogels with either an acid-cleavable linker, a physiological pH-cleavable linker, or a non-cleavable linker (Figure 1.18A). Using microfluidics, the microgels were formed with NIH 3T3 cells inside, and postencapsulation the cells maintained 94% viability (Figure 1.18B). On day 3, degradation of the hydrogel and release of the cells could be controlled with pH, while maintaining cell viability (Figure 1.18C).

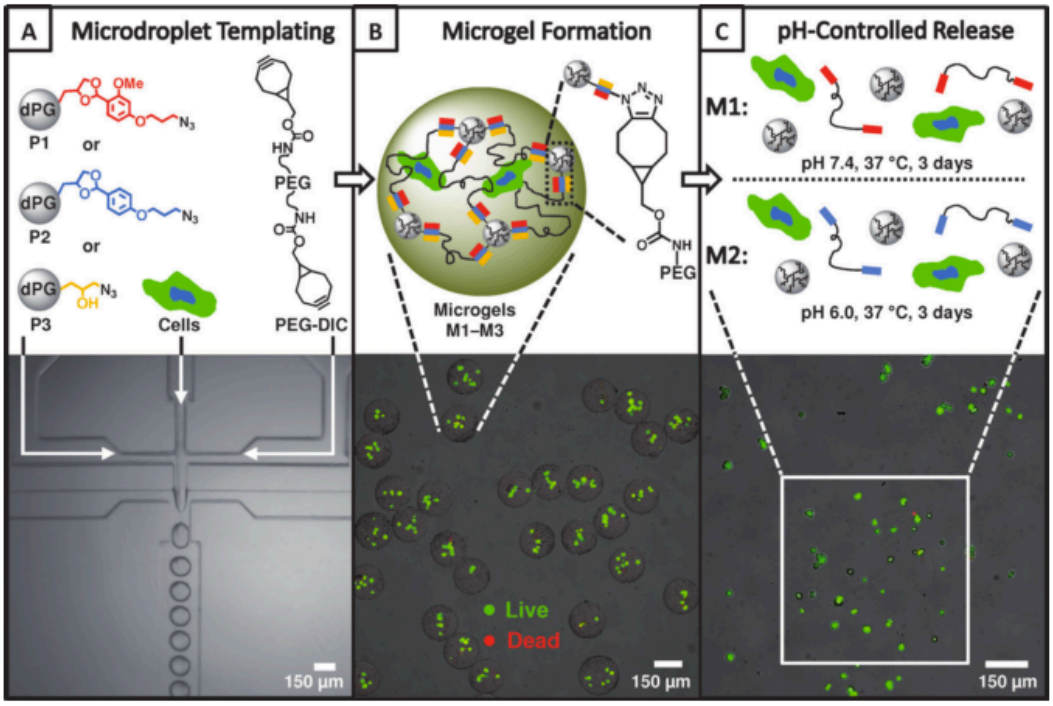

Figure 1.18. Cell encapsulation and hydrogel particle formation via a microfluidic device (A). NIH 3T3 cells at least 94% viable based on live-dead assay (B). pH-controlled release of cells after 3 days with maintained viability (C). Reproduced with permission.[168] Copyright Angewandte Chemie International Edition, 2013.

1.7. Summary

Over the past several decades, researchers have been forming hydrogel networks for biomedical applications. Whether the goal is cell encapsulation, tissue engineering, wound dressing, controlled drug delivery, or corneal adhesives, hydrogels have proven to be the appropriate material of choice. Extensive work has been done in an effort to create hydrogels that are appropriate for a wide range of biomedical applications. Research is also ongoing to find hydrogels that work well for specific applications and that have specific goals in mind. Whatever the ultimate goal, hydrogel research requires expertise in many different fields, including chemistry, physics and biology. Choosing the appropriate material and crosslinking chemistry is

challenging, yet there are many additional aspects of hydrogel formation that must be considered. Hydrogel research is made all the more complicated by adding components such as post-gelation functionalization with biomolecules, controlled swelling, controlled degradation, tunable mechanical properties, injectability, reproducibility, as well as *in vitro* and *in vivo* studies.

One of the major goals of this thesis was to design a hydrogel that was relatively simple to make, yet met all of the requirements for biomedical applications including using a material that has low non-specific protein adsorption and that can be functionalized easily with bio-orthogonal cross-linking chemistry. Significant effort was put toward optimizing the synthesis of the crosslinking chemistry, which allowed for a facile route to creating hydrogels quickly without the need for cytotoxic catalysts or external stimuli. Taking into account the complexities that can arise once cells are encapsulated and the hydrogel is put into the body, extensive measurements were done to understand the properties of the hydrogel at varying concentrations.

The second major goal of this thesis was to improve the hydrogel design one step further by creating a reproducible system. By incorporating dendrimers, while keeping the material and the crosslinking chemistry the same, a new hydrogel system with superior qualities was developed that did not vary from batch-to-batch. Additionally, an adhesion peptide was incorporated into the hydrogel, and *in vitro* studies were performed with hMSCs to test stem cell viability and proliferation over time.

1.8. References

(1) Ahmed, E. M. *J. Adv. Res.* **2015**, *6*, 105–121.

(2) Tan, H.; Marra, K. G. *Materials* **2010**, *3*, 1746–1767.

(3) Yang, J. A.; Yeom, J.; Hwang, B. W.; Hoffman, A. S.; Hahn, S. K. *Prog. Polym. Sci.* **2014**, *39*, 1973–1986.

(4) Kopecek, J. *J. Polym. Sci. Part A Polym. Chem.* **2009**, *47*, 5929–5946.

(5) Caliari, S. R.; Burdick, J. A. *Nat. Methods* **2016**, *13*, 405–414.

(6) Taylor, D. L.; in het Panhuis, M. *Adv. Mater.* **2016**, *28*, 9060–9093.

(7) Oelker, A. M.; Grinstaff, M. W. *J. Mater. Chem.* **2008**, *18*, 2521–2536.

(8) Pakulska, M. M.; Ballios, B. G.; Shoichet, M. S. *Biomed. Mater.* **2012**, *7*, 24101.

(9) Hoare, T. R.; Kohane, D. S. *Polymer* **2008**, *49*, 1993–2007.

(10) Nafea, E. H.; Marson, A.; Martens, P. J. *J. Control. Release* **2011**, *154*, 110–122.

(11) Shin, H.; Jo, S.; Mikos, A. G. *Biomaterials* **2003**, *24*, 4353–4364.

(12) Bryant, S. J.; Anseth, K. S. *J. Biomed. Mater. Res. A* **2003**, *64*, 70–79.

(13) Schmidt, J. J.; Rowley, J.; Kong, H. J. *J. Biomed. Mater. Res. Part A* **2008**, *87*, 1113–1122.

(14) Lin, C. C.; Anseth, K. S. *Pharm. Res.* **2009**, *26*, 631–643.

(15) Boateng, J. S.; Matthews, K. H.; Stevens, H. N. E.; Eccleston, G. M. *J. Pharm. Sci.* **2008**, *97*, 2892–2923.

(16) Hubbell, J. A. *J. Control. Release* **1996**, *39*, 305–313.

(17) Wichterle, O.; Lim, D. *Nature* **1960**, *185*, 117–118.

(18) Mathur, A. M.; Moorjani, S. K.; Scranton, A. B. *J. Macromol. Sci. Part C* **1996**, *36*, 405–430.

(19) Lim, F.; Sun, A. M. *Science* **1980**, *210*, 908–910.

(20) Orive, G.; Maria Hernández, R.; Rodríguez Gascón, A.; Calafiore, R.; Swi Chang, T. M.; Vos, P. De; Hortelano, G.; Hunkeler, D.; Lacík, I.; Luis Pedraz, J. *Trends Biotechnol.* **2004**, *22*, 87–92.

(21) Orive, G.; Tam, S. K.; Pedraz, J. L.; Hallé, J.-P. *Biomaterials* **2006**, *27*, 3691–3700.

(22) Mazumder, M. A. J.; Burke, N. A. D.; Shen, F.; Potter, M. A.; Stöver, H. D. H. *Biomacromolecules* **2009**, *10*, 1365–1373.

(23) Kleinman, H. K.; Martin, G. R. *Semin. Cancer Biol.* **2005**, *15*, 378–386.

(24) Lee, K. Y.; Mooney, D. J. *Chem. Rev.* **2001**, *101*, 1869–1879.

(25) Kaufmann, P. M.; Heimrath, S.; Kim, B. S.; Mooney, D. J. *Cell Transplant.* **1997**, *6*, 463–468.

(26) Voytik-Harbin, S. L.; Brightman, A. O.; Waisner, B. Z.; Robinson, J. P.; Lamar, C. H. *Tissue Eng.* **1998**, *4*, 157–174.

(27) Duranti, F.; Salti, G.; Bovani, B.; Calandra, M.; Rosati, M. L. *Dermatologic Surg.* **1998**, *24*, 1317–1325.

(28) Radomsky, M. L.; Aufdemorte, T. B.; Swain, L. D.; Fox, W. C.; Spiro, R. C.; Poser, J. W. *J. Orthop. Res.* **1999**, *17*, 607–614.

(29) Sierra, D. H. *J. Biomater. Appl.* **1993**, *7*, 309–352.

(30) Kaemmerer, E.; Melchels, F. P. W.; Holzapfel, B. M.; Meckel, T.; Hutmacher, D. W.; Loessner, D. *Acta Biomater.* **2014**, *10*, 2551–2562.

(31) Cushing, M. C.; Anseth, K. S. *Science* **2007**, *316*, 1133–1134.

(32) Kidane, A.; Szabocsik, J. M.; Park, K. *Biomaterials* **1998**, *19*, 2051–2055.

(33) Lu, S.; Anseth, K. S. *J. Control. Release* **1999**, *57*, 291–300.

(34) Chirila, T. V; Constable, I. J.; Crawford, G. J.; Vijayasekaran, S.; Thompson, D. E.; Chen, Y.; Fletcher, W. A.; Griffin, B. J. *Biomaterials* **1993**, *14*, 26–38.

(35) Meyvis, T. K. L.; De Smedt, S. C.; Demeester, J.; Hennink, W. E. *Macromolecules* **2000**, *33*, 4717–4725.

(36) Son, Y.-K.; Jung, Y. P.; Kim, J.-H.; Chung, D. J. *Macromol. Res.* **2006**, *14*, 394–399.

(37) Stile, R. A.; Burghardt, W. R.; Healy, K. E. *Macromolecules* **1999**, *32*, 7370–7379.

(38) Prosperi-Porta, G.; Muirhead, B.; Sheardown, H. *J. Biomed. Mater. Res. Part B* **2017**, *105*, 53–62.

(39) Cui, Z.; Lee, B. H.; Vernon, B. L. *Biomacromolecules* **2007**, *8*, 1280–1286.

(40) Fitzpatrick, S. D.; Jafar Mazumder, M. A.; Muirhead, B.; Sheardown, H. *Acta Biomater.* **2012**, *8*, 2517–2528.

(41) Sheikholeslami, P.; Muirhead, B.; Baek, D. S. H.; Wang, H.; Zhao, X.; Sivakumaran, D.; Boyd, S.; Sheardown, H.; Hoare, T. *Exp. Eye Res.* **2015**, *137*, 18–31.

(42) Hilmy, N.; Darwis, D.; Hardiningsih, L. *Radiat. Phys. Chem.* **1993**, *42*, 911–914.

(43) El-Hag Ali, A.; Shawky, H. A.; Abd El Rehim, H. A.; Hegazy, E. A. *Eur. Polym. J.* **2003**, *39*, 2337–2344.

(44) Breiting, V.; Aasted, A.; Jørgensen, A.; Opitz, P.; Rosetzsky, A. *Aesthetic Plast. Surg.* **2004**, *28*, 45–53.

(45) Caliari, S. R.; Burdick, J. A. *Nat. Methods* **2016**, *13*, 405–414.

(46) Martens, P.; Anseth, K. S. *Polymer* **2000**, *41*, 7715–7722.

(47) Benoit, D. S. W.; Anseth, K. S. *Acta Biomater.* **2005**, *1*, 461–470.

(48) Bakaic, E.; Smeets, N. M. B.; Hoare, T. *RSC Adv.* **2015**, *5*, 35469–35486.

(49) Charles, P. T.; Stubbs, V. R.; Soto, C. M.; Martin, B. D.; White, B. J.; Taitt, C. R. *Sensors* **2009**, *9*, 645–655.

(50) Unsworth, L. D.; Sheardown, H.; Brash, J. L. *Langmuir* **2005**, *21*, 1036–1041.

(51) Du, H.; Chandaroy, P.; Hui, S. W. *Biochim. Biophys. Acta* **1997**, *1326*, 236–248.

(52) Lowe, S.; O'Brien-Simpson, N. M.; Connal, L. A. *Polym. Chem.* **2015**, *6*, 198–212.

(53) Fairbanks, B. D.; Schwartz, M. P.; Bowman, C. N.; Anseth, K. S. *Biomaterials* **2009**, *30*, 6702–6707.

(54) Hou, Y.; Schoener, C. A.; Regan, K. R.; Munoz-Pinto, D.; Hahn, M. S.;

Grunlan, M. A. *Biomacromolecules* **2010**, *11*, 648–656.

(55) Xu, J.; Feng, E.; Song, J. *J. Am. Chem. Soc.* **2014**, *136*, 4105–4108.

(56) Van Dijk, M.; Van Nostrum, C. F.; Hennink, W. E.; Rijkers, D. T. S.; Liskamp, R. M. J. *Biomacromolecules* **2010**, *11*, 1608–1614.

(57) Truong, V. X.; Ablett, M. P.; Richardson, S. M.; Hoyland, J. A.; Dove, A. P. *J. Am. Chem. Soc.* **2015**, *137*, 1618–1622.

(58) Seliktar, D.; Zisch, A. H.; Lutolf, M. P.; Wrana, J. L.; Hubbell, J. A. *J. Biomed. Mater. Res.* **2004**, *68A*, 704–716.

(59) Phelps, E. A.; Enemchukwu, N. O.; Fiore, V. F.; Sy, J. C.; Murthy, N.; Sulchek, T. A.; Barker, T. H.; García, A. J. *Adv. Mater.* **2012**, *24*, 64–70.

(60) García, A. J. *Ann. Biomed. Eng.* **2014**, *42*, 312–322.

(61) Freudenberg, U.; Hermann, A.; Welzel, P. B.; Stirl, K.; Schwarz, S. C.; Grimmer, M.; Zieris, A.; Panyanuwat, W.; Zschoche, S.; Meinhold, D.; Storch, A.; Werner, C. *Biomaterials* **2009**, *30*, 5049–5060.

(62) DeLong, S. A.; Gobin, A. S.; West, J. L. *J. Control. Release* **2005**, *109*, 139–148.

(63) West, J. L.; Hubbell, J. A. *React. Polym.* **1995**, *25*, 139–147.

(64) Rice, M. A.; Anseth, K. S. *J. Biomed. Mater. Res. A* **2004**, *70*, 560–568.

(65) Bryant, S. J.; Bender, R. J.; Durand, K. L.; Anseth, K. S. *Biotechnol. Bioeng.* **2004**, *86*, 747–755.

(66) Garagorri, N.; Fermanian, S.; Thibault, R.; Ambrose, W. M.; Schein, O. D.; Chakravarti, S.; Elisseeff, J. *Acta Biomater.* **2008**, *4*, 1139–1147.

(67) Jongpaiboonkit, L.; King, W. J.; Murphy, W. L. *Tissue Eng. Part A* **2009**, *15*, 343–353.

(68) Nakayama, Y.; Matsuda, T. *J. Biomed. Mater. Res.* **1999**, *48*, 511–521.

(69) Cai, L.; Lu, J.; Sheen, V.; Wang, S. *Biomacromolecules* **2012**, *13*, 342–349.

(70) Anderson, S. B.; Lin, C. C.; Kuntzler, D. V.; Anseth, K. S. *Biomaterials* **2011**, *32*, 3564–3574.

(71) Jin, R.; Moreira Teixeira, L. S.; Krouwels, A.; Dijkstra, P. J.; van

Blitterswijk, C. A.; Karperien, M.; Feijen, J. *Acta Biomater.* **2010**, *6*, 1968–1977.

(72) Mabry, K. M.; Lawrence, R. L.; Anseth, K. S. *Biomaterials* **2015**, *49*, 47–56.

(73) Metters, A.; Hubbell, J. *Biomacromolecules* **2005**, *6*, 290–301.

(74) Mahou, R.; Wandrey, C. *Macromolecules* **2010**, *43*, 1371–1378.

(75) Lutz, J.-F. *J. Polym. Sci. Part A Polym. Chem.* **2008**, *46*, 3459–3470.

(76) Smeets, N. M. B.; Bakaic, E.; Patenaude, M.; Hoare, T. *Acta Biomater.* **2014**, *10*, 4143–4155.

(77) Smeets, N. M. B.; Bakaic, E.; Patenaude, M.; Hoare, T. *Chem. Commun.* **2014**, *50*, 3306–3309.

(78) Smeets, N. M. B.; Patenaude, M.; Kinio, D.; Yavitt, F. M.; Bakaic, E.; Yang, F.-C.; Rheinstädter, M.; Hoare, T. *Polym. Chem.* **2014**, *5*, 6811–6823.

(79) Bakaic, E.; Smeets, N. M. B.; Dorrington, H.; Hoare, T. *RSC Adv.* **2015**, *5*, 33364–33376.

(80) Smeets, N. M. B.; Bakaic, E.; Yavitt, F. M.; Yang, F. C.; Rheinstädter, M. C.; Hoare, T. *Macromolecules* **2014**, *47*, 6017–6027.

(81) Discher, D. E.; Mooney, D. J.; Zandstra, P. W. *Science* **2009**, *324*, 1673–1677.

(82) DeForest, C. A.; Polizzotti, B. D.; Anseth, K. S. *Nat. Mater.* **2009**, *8*, 659–664.

(83) Brown, T. E.; Marozas, I. A.; Anseth, K. S. *Adv. Mater.* **2017**, *29*, 1605001.

(84) Phadke, A.; Zhang, C.; Arman, B.; Hsu, C.-C.; Mashelkar, R. A.; Lele, A. K.; Tauber, M. J.; Arya, G.; Varghese, S. *Proc. Natl. Acad. Sci.* **2012**, *109*, 4383–4388.

(85) Li, L.; Yan, B.; Yang, J.; Chen, L.; Zeng, H. *Adv. Mater.* **2015**, *27*, 1294–1299.

(86) Bai, T.; Liu, S.; Sun, F.; Sinclair, A.; Zhang, L.; Shao, Q.; Jiang, S.

Biomaterials **2014**, *35*, 3926–3933.

(87) Kakuta, T.; Takashima, Y.; Nakahata, M.; Otsubo, M.; Yamaguchi, H.; Harada, A. *Adv. Mater.* **2013**, *25*, 2849–2853.

(88) Jiang, G.; Liu, C.; Liu, X.; Zhang, G.; Yang, M.; Liu, F. *Macromol. Mater. Eng.* **2009**, *294*, 815–820.

(89) Cheng, E.; Xing, Y.; Chen, P.; Yang, Y.; Sun, Y.; Zhou, D.; Xu, L.; Fan, Q.; Liu, D. *Angew. Chemie* **2009**, *121*, 7796–7799.

(90) Wu, C.; Wang, X. *Phys. Rev. Lett.* **1998**, *80*, 4092–4094.

(91) Kumachev, A.; Greener, J.; Tumarkin, E.; Eiser, E.; Zandstra, P. W.; Kumacheva, E. *Biomaterials* **2011**, *32*, 1477–1483.

(92) Wang, N.; Wu, X. S. *Pharm. Dev. Technol.* **1997**, *2*, 135–142.

(93) Zhang, H.; Zhang, F.; Wu, J. *React. Funct. Polym.* **2013**, *73*, 923–928.

(94) Kolb, H. C.; Finn, M. G.; Sharpless, K. B. *Angew. Chemie Int. Ed.* **2001**, *40*, 2004–2021.

(95) Malkoch, M.; Vestberg, R.; Gupta, N.; Mespouille, L.; Dubois, P.; Mason, A. F.; Hedrick, J. L.; Liao, Q.; Frank, C. W.; Kingsbury, K.; Hawker, C. J. *Chem. Commun.* **2006**, 2774–2776.

(96) Crescenzi, V.; Cornelio, L.; Di Meo, C.; Nardecchia, S.; Lamanna, R. *Biomacromolecules* **2007**, *8*, 1844–1850.

(97) Liu, S. Q.; Rachel Ee, P. L.; Ke, C. Y.; Hedrick, J. L.; Yang, Y. Y. *Biomaterials* **2009**, *30*, 1453–1461.

(98) Zhang, J.; Xu, X. D.; Wu, D. Q.; Zhang, X. Z.; Zhuo, R. X. *Carbohydr. Polym.* **2009**, *77*, 583–589.

(99) Gaetke, L. M.; Chow, C. K. *Toxicology* **2003**, *189*, 147–163.

(100) Owen, S. C.; Fisher, S. A.; Tam, R. Y.; Nimmo, C. M.; Shoichet, M. S. *Langmuir* **2013**, *29*, 7393–7400.

(101) Nimmo, C. M.; Owen, S. C.; Shoichet, M. S. *Biomacromolecules* **2011**, *12*, 824–830.

(102) Stewart, S. A.; Backholm, M.; Burke, N. A. D.; Stöver, H. D. H. *Langmuir*

2016, *32*, 1863–1870.

(103) Desai, R. M.; Koshy, S. T.; Hilderbrand, S. A.; Mooney, D. J.; Joshi, N. S. *Biomaterials* **2015**, *50*, 30–37.

(104) Alge, D. L.; Azagarsamy, M. a.; Donohue, D. F.; Anseth, K. S. *Biomacromolecules* **2013**, *14*, 949–953.

(105) Elbert, D. L.; Pratt, A. B.; Lutolf, M. P.; Halstenberg, S.; Hubbell, J. A. *J. Control. Release* **2001**, *76*, 11–25.

(106) Raeber, G. P.; Lutolf, M. P.; Hubbell, J. A. *Biophys. J.* **2005**, *89*, 1374–1388.

(107) Fairbanks, B. D.; Schwartz, M. P.; Halevi, A. E.; Nuttelman, C. R.; Bowman, C. N.; Anseth, K. S. *Adv. Mater.* **2009**, *21*, 5005–5010.

(108) Mongkhontreerat, S.; Öberg, K.; Erixon, L.; Löwenhielm, P.; Hult, A.; Malkoch, M. *J. Mater. Chem. A* **2013**, *1*, 13732–13737.

(109) Lin, C.-C.; Raza, A.; Shih, H. *Biomaterials* **2011**, *32*, 9685–9695.

(110) DeForest, C. A.; Sims, E. A.; Anseth, K. S. *Chem. Mater.* **2010**, *22*, 4783–4790.

(111) Kyburz, K. A.; Anseth, K. S. *Acta Biomater.* **2013**, *9*, 6381–6392.

(112) Azagarsamy, M. a.; Anseth, K. S. *ACS Macro Lett.* **2013**, *2*, 5–9.

(113) Blomquist, A. T.; Liu, L. H. *J. Am. Chem. Soc.* **1953**, *75*, 2153–2154.

(114) Wittig, G.; Krebs, A. *Chem. Ber.* **1961**, *94*, 3260–3275.

(115) Agard, N. J.; Prescher, J. a; Bertozzi, C. R. *J. Am. Chem. Soc.* **2004**, *126*, 15046–15047.

(116) Sletten, E. M.; Bertozzi, C. R. *Acc. Chem. Res.* **2011**, *44*, 666–676.

(117) DeForest, C. A.; Anseth, K. S. *Nat. Chem.* **2011**, *3*, 925–931.

(118) Zheng, J.; Smith Callahan, L. A.; Hao, J.; Guo, K.; Wesdemiotis, C.; Weiss, R. A.; Becker, M. L. *ACS Macro Lett.* **2012**, *1*, 1071–1073.

(119) Xu, J.; Filion, T. M.; Prifti, F.; Song, J. *Chem. Asian J.* **2011**, *6*, 2730–2737.

(120) Jiang, H.; Qin, S.; Dong, H.; Lei, Q.; Su, X.; Zhuo, R.; Zhong, Z. *Soft Matter* **2015**, *11*, 6029–6036.

(121) Patenaude, M.; Smeets, N. M. B.; Hoare, T. *Macromol. Rapid Commun.* **2014**, *35*, 598–617.

(122) Kretlow, J. D.; Klouda, L.; Mikos, A. G. *Adv. Drug Deliv. Rev.* **2007**, *59*, 263–273.

(123) Macaya, D.; Spector, M. *Biomed. Mater.* **2012**, *7*, 12001.

(124) Amini, A. A.; Nair, L. S. *Biomed. Mater.* **2012**, *7*, 24105.

(125) Van Tomme, S. R.; Storm, G.; Hennink, W. E. *Int. J. Pharm.* **2008**, *355*, 1–18.

(126) Yu, L.; Ding, J. *Chem. Soc. Rev.* **2008**, *37*, 1473–1481.

(127) Rossow, T.; Heyman, J. A.; Ehrlicher, A. J.; Langhoff, A.; Weitz, D. A.; Haag, R.; Seiffert, S. *J. Am. Chem. Soc.* **2012**, *134*, 4983–4989.

(128) Chau, M.; Abolhasani, M.; Thérien-Aubin, H.; Li, Y.; Wang, Y.; Velasco, D.; Tumarkin, E.; Ramachandran, A.; Kumacheva, E. *Biomacromolecules* **2014**, *15*, 2419–2425.

(129) Velasco, D.; Tumarkin, E.; Kumacheva, E. *Small* **2012**, *8*, 1633–1642.

(130) Peppas, N. A. *J. Bioact. Compat. Polym.* **1991**, *6*, 241–246.

(131) Ganji, F.; Vasheghani-Farahani, S.; Vasheghani-Farahani, E. *Iran. Polym. J.* **2010**, *19*, 375–398.

(132) Emileh, A.; Vasheghani-Farahani, E.; Imani, M. *Eur. Polym. J.* **2007**, *43*, 1986–1995.

(133) Dinerman, A. A.; Cappello, J.; Ghandehari, H.; Hoag, S. W. *J Contr Rel* **2002**, *82*, 277–287.

(134) Shu, X. Z.; Liu, Y.; Luo, Y.; Roberts, M. C.; Prestwich, G. D. *Biomacromolecules* **2002**, *3*, 1304–1311.

(135) Benton, J. A.; Fairbanks, B. D.; Anseth, K. S. *Biomaterials* **2009**, *30*, 6593–6603.

(136) Lewis, K. J. R.; Tibbitt, M. W.; Zhao, Y.; Branchfield, K.; Sun, X.; Balasubramaniam, V.; Anseth, K. S. *Biomater. Sci.* **2015**, *3*, 821–832.

(137) Kloxin, A. M.; Tibbitt, M. W.; Kasko, A. M.; Fairbairn, J. A.; Anseth, K. S.

Adv. Mater. **2010**, *22*, 61–66.

(138) Johnson, J. A.; Baskin, J. M.; Bertozzi, C. R.; Koberstein, J. T.; Turro, N. J. *Chem. Commun.* **2008**, 3064–3066.

(139) Walter, M. V.; Malkoch, M. *Chem. Soc. Rev.* **2012**, *41*, 4593–4609.

(140) Lee, C. C.; MacKay, J. A.; Fréchet, J. M. J.; Szoka, F. C. *Nat. Biotechnol.* **2005**, *23*, 1517–1526.

(141) Carnahan, M. A.; Middleton, C.; Kim, J.; Kim, T.; Grinstaff, M. W. *J. Am. Chem. Soc.* **2002**, *124*, 5291–5293.

(142) Velazquez, A. J.; Carnahan, M. A.; Kristinsson, J.; Stinnett, S.; Grinstaff, M. W.; Kim, T. *Arch. Ophthalmol.* **2004**, *122*, 867–870.

(143) Wang, Y.; Zhao, Q.; Zhang, H.; Yang, S.; Jia, X. *Adv. Mater.* **2014**, *26*, 4163–4167.

(144) Degoricija, L.; Bansal, P. N.; Sontjens, S. H. M.; Joshi, N. S.; Takahashi, M.; Snyder, B.; Grinstaff, M. W. *Biomacromolecules* **2008**, *9*, 2863–2872.

(145) Altin, H.; Kosif, I.; Sanyal, R. *Macromolecules* **2010**, *43*, 3801–3808.

(146) Yang, H.; Tyagi, P.; Kadam, R. S.; Holden, C. A.; Kompella, U. B. *ACS Nano* **2012**, *6*, 7595–7606.

(147) Abou Taleb, M. F.; Elsigeny, S. M.; Ibrahim, M. M. *Radiat. Phys. Chem.* **2007**, *76*, 1612–1618.

(148) Zhang, J. T.; Huang, S. W.; Zhuo, R. X. *Macromol. Biosci.* **2004**, *4*, 575–578.

(149) Desai, P. N.; Yuan, Q.; Yang, H. *Biomacromolecules* **2010**, *11*, 666–673.

(150) Holden, C. A.; Tyagi, P.; Thakur, A.; Kadam, R.; Jadhav, G.; Kompella, U. B.; Yang, H. *Nanomedicine Nanotechnology, Biol. Med.* **2012**, *8*, 776–783.

(151) Unal, B.; Hedden, R. C. *Polymer* **2006**, *47*, 8173–8182.

(152) Zhu, C.; Hard, C.; Lin, C.; Gitsov, I. *J. Polym. Sci. Part A Polym. Chem.* **2005**, *43*, 4017–4029.

(153) Gitsov, I.; Zhu, C. *Macromolecules* **2002**, *35*, 8418–8427.

(154) Öberg, K.; Hed, Y.; Rahmn, I. J.; Kelly, J.; Löwenhielm, P.; Malkoch, M. *Chem. Commun.* **2013**, *49*, 6938–6940.

(155) Lin, C.-C.; Anseth, K. S. *Pharm. Res.* **2009**, *26*, 631–643.

(156) Patel, V.; Amiji, M. *Pharm. Res.* **1996**, *13*, 588–593.

(157) Amiji, M.; Tailor, R.; Ly, M.-K.; Goreham, J. *Drug Dev. Ind. Pharm.* **1997**, *23*, 575–582.

(158) Bhattarai, N.; Ramay, H. R.; Gunn, J.; Matsen, F. A.; Zhang, M. *J. Control. Release* **2005**, *103*, 609–624.

(159) Uludag, H.; De Vos, P.; Tresco, P. *Adv. Drug Deliv. Rev.* **2000**, *42*, 29–64.

(160) Kraehenbuehl, T. P.; Ferreira, L. S.; Zammaretti, P.; Hubbell, J. A.; Langer, R. *Biomaterials* **2009**, *30*, 4318–4324.

(161) Weber, L. M.; Lopez, C. G.; Anseth, K. S. *J. Biomed. Mater. Res. Part A* **2009**, *90A*, 720–729.

(162) Brubaker, C. E.; Kissler, H.; Wang, L. J.; Kaufman, D. B.; Messersmith, P. B. *Biomaterials* **2010**, *31*, 420–427.

(163) Souza, Y. E. D. M. de; Chaib, E.; Lacerda, P. G. de; Crescenzi, A.; Bernal-Filho, A.; D'Albuquerque, L. A. C. *Arq. Gastroenterol.* **2011**, *48*, 146–152.

(164) Beck, J.; Angus, R.; Madsen, B.; Britt, D.; Vernon, B.; Nguyen, K. T. *Tissue Eng.* **2007**, *13*, 589–599.

(165) McKinnon, D. D.; Brown, T. E.; Kyburz, K. A.; Kiyotake, E.; Anseth, K. S. *Biomacromolecules* **2014**, *15*, 2808–2816.

(166) Benoit, D. S. W.; Schwartz, M. P.; Durney, A. R.; Anseth, K. S. *Nat. Mater.* **2008**, *7*, 816–823.

(167) Kloxin, A. M.; Kasko, A. M.; Salinas, C. N.; Anseth, K. S. *Science* **2009**, *324*, 59–63.

(168) Steinhilber, D.; Rossow, T.; Wedepohl, S.; Paulus, F.; Seiffert, S.; Haag, R. *Angew. Chemie Int. Ed.* **2013**, *52*, 13538–13543.

Chapter 2

Scalable Synthesis of Strained Cyclooctyne Derivatives

This chapter has been reprinted with permission from Synthesis; Ryan C. Chadwick, Sabrina Van Gyzen, Sophie Liogier and Alex Adronov, **2014**, *46*, 0669-0677, DOI: 10.1055/s-0033-1340509.

Ryan Chadwick and Sabrina Hodgson (née Van Gyzen) are co-first authors on this publication and were both involved in the planning of this study. Ryan Chadwick and Sabrina Hodgson both synthesized the aza-dibenzocyclooctyne (DIBAC). Ryan Chadwick synthesized the biarylazacyclooctynone (BARAC). Sophie Liogier and Sabrina Hodgson synthesized the difluorinated DIBAC, and its reactivity was measured by Sabrina Hodgson and Ryan Chadwick. Ryan Chadwick and Sabrina Hodgson both contributed to the writing of the manuscript.

Abstract

Herein we describe modifications to the Popik synthesis of aza-dibenzocyclooctyne (DIBAC) derivatives, which avoids tedious purifications and dramatically improves the yield. We also attempt a new and analogous route to biarylazacyclooctynone (BARAC) through an amide disconnection. The BARAC derivatives prepared were found to be unstable under the conditions we employed, undergoing a known rearrangement. Finally, we describe the synthesis of a difluoro-DIBAC derivative with a second-order rate constant intermediate between DIBAC and BARAC derivatives (0.50 M^{-1}). While more difficult to synthesize, we found this molecule to be considerably more stable than any BARAC derivatives that we prepared.

2.1. Introduction

The reactivity of cyclooctynes toward azides in 1,3-dipolar cycloadditions was first discovered by Blomquist and Liu in 1953,[1] and later confirmed by Wittig and Krebs in 1961.[2] Cyclooctynes are the smallest all-carbon cyclic alkynes that are isolable and stable under ambient conditions. Larger cyclooctynes have minimal ring strain and are much less reactive.[3] Smaller cyclic alkynes can be made *in situ*, and some are isolable, but, in most cases they quickly decompose.[4] Only a handful of stable, smaller, heteroatom-containing derivatives are known, such as the thiepin derivatives explored by Krebs and colleagues in the 1970's.[5,6] The increased stability of these molecules results from the addition of a sulfur atom within the 7–membered ring to relieve ring strain. These "angle-strained' cyclooctynes attracted a great deal of attention in the 1970's and 1980's, and the literature was exhaustively reviewed by Krebs and Wilke in 1983.[4]

The notion of using cyclooctynes for rapid bio-conjugation or as "Click" reagents[7] did not appear in the literature until 2004 when Bertozzi introduced the idea of using cyclooctynes instead of terminal alkynes in the 1,3-dipolar Huisgen cycloaddition reaction.[8] This reaction, now referred to as the Strain-Promoted Alkyne-Azide Cycloaddition (SPAAC) reaction, does not require a copper catalyst, eliminating the dependency of this reaction on a toxic metal, and thereby allowing its use *in vivo*.[8] Cyclooctynes are also subject to fewer side reactions with nucleophiles relative to other active alkynes, such as acetylene esters, which react with a variety of nucleophiles, hampering their chemical compatibility and rendering them generally unsuitable for biological work.[9]

The parent compound, cyclooctyne, is not sufficiently strained to be reactive at low concentrations and temperatures.[4,10] Thus, in most cases where SPAAC is used, a modified or substituted cyclooctyne is needed.[11] The second-order rate constants of several different cyclooctyne derivatives have

been measured, including those functionalized with fluorine atoms, amides, and aryl rings.[11] Typically, this rate constant is measured for the reaction between the cyclooctyne in question and benzyl azide in a polar solvent (typically acetonitrile or methanol), and is used to compare the relative reactivities of various cyclooctynes.[11] In general, it has been found that substituents with greater electron-withdrawing character, or ones that introduce additional ring strain via sp^2 centers on the cyclooctyne, increase the reactivity of the alkyne. These effects and their consequences have recently been explored using DFT calculations.[12]

SPAAC has required the development of a new series of cyclooctynes with reactivities, stabilities, and chemical handles suited to their use in larger bio- or macro-molecules.[3,11] The most reactive of the stable cyclooctynes are aza-dibenzocyclooctynes (DIBAC)[13,14] and biarylazacyclooctynones (BARACs).[11,15] In particular, reactions of di-fluorinated BARAC derivatives with azides exhibit the largest rate constants.[16] The orthogonality of SPAAC reactions to acid, base, and biological conditions[17] has enabled their use in biological applications, such as drug delivery,[18] live cell labeling[8], bioconjugation of proteins, nucleic acids and polysaccharides,[19] and the synthesis of hydrogels for 3D cell cultures.[20]

Outside of chemical biology, cyclooctynes have had limited application, presumably a result of the synthetic difficulty in their production. The two most commonly used synthetic methods toward DIBAC rely on the synthesis of a common intermediate **3**, followed by bromination and elimination to generate the product (Scheme 2.1C). The first method, developed by van Delft and co-workers (Scheme 2.1A),[13] utilizes a Sonogashira cross-coupling, followed by a Dess-Martin oxidation and reductive amination to generate intermediate **3**. The Popik method[14] (Scheme 2.1B) instead starts with a commercially available tri-cyclic compound (dibenzosuberenone); the

central 7-membered ring is expanded using a Beckmann rearrangement, followed by a lithium aluminum hydride reduction to generate **3**.

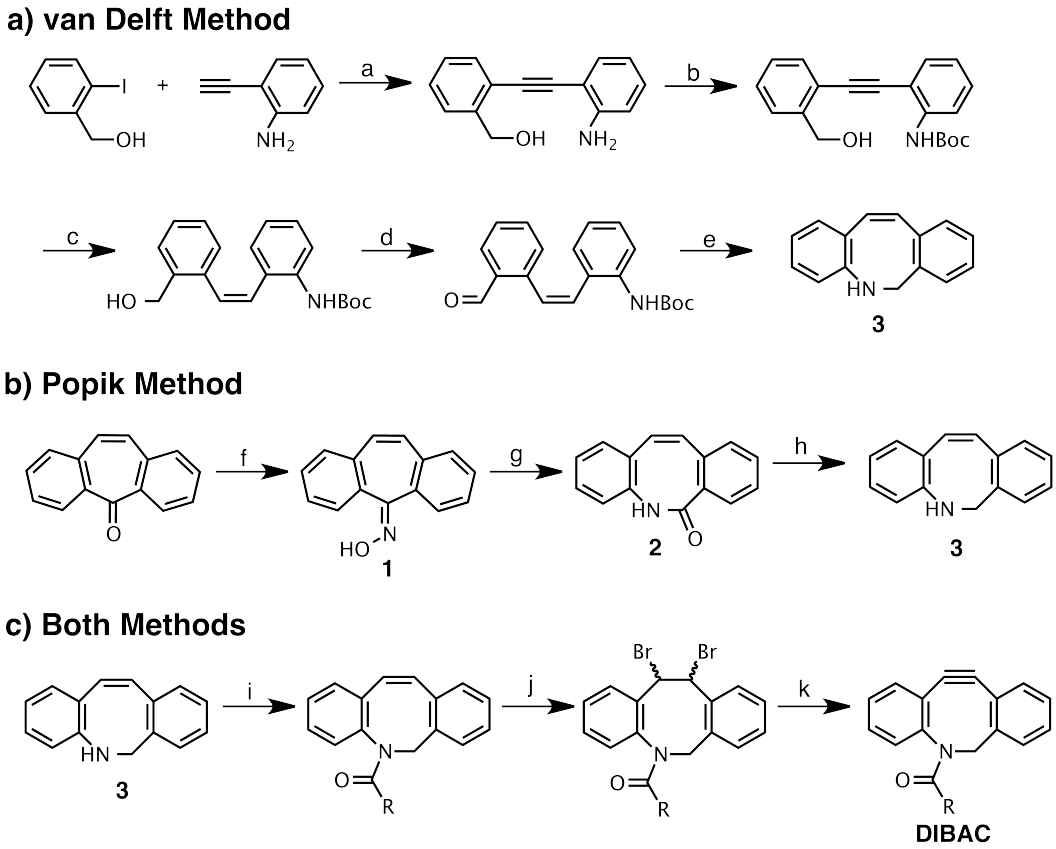

Scheme 2.1. Literature syntheses of DIBAC. (a) $PdCl_2(PPh_3)_2$, CuI, Et_3N, THF, N_2/H_2, r.t.; (b) Boc_2O, THF, 70 °C, 2d; (c) 10% $Pd/BaSO_4$, quinolone, H_2, MeOH, r.t. 1.5h; (d) Dess-Martin periodinane, $NaHCO_3$, CH_2Cl_2, r.t. 40 min; (e) (1) 2 M HCl in EtOAc, r.t. 1 h; (2) $NaBH_4$, H_2O, r.t., o.n.; (f) $NH_2OH{\cdot}HCl$, pyridine, EtOH, reflux, 12h; (g) Polyphosphoric acid, 125 °C, 1h; (h) $LiAlH_4$, Et_2O, reflux, 15h; (i) Various Conditions; (j) Br_2, DCM, 0 °C, 2h; (k) KO^tBu, THF, -40 °C, 2h.

The biggest advantage to the van Delft method is the high yield obtained at each step. An overall 70% yield was obtained over 5 steps to synthesize **3**. The Popik method, although having fewer steps, has a much lower overall yield of ca. 40 % for the three steps leading to **3**. Nonetheless, the Popik

method uses less expensive reagents, is simpler to perform and displays excellent atom economy. We chose to adapt and further develop the Popik method for synthesizing DIBAC with the aim of producing an easily scalable synthetic route.

Here, we describe our development of a streamlined synthesis of DIBAC derivatives with a focus on scale and simplicity of purification for materials chemists. It also discusses attempts to synthesize BARAC by an analogous route and outlines the synthesis of a di-fluorinated DIBAC derivative with reactivity intermediate to those of DIBAC and BARAC.

2.2. Results and Discussion

En route to synthesizing DIBAC using the Popik method, substantial improvements were made on the original synthesis. In particular, the ring-expanding Beckmann rearrangement, discovered in 1886,[21] which converts an oxime into an amide using an acid catalyst, was the focus of our attention. For the reaction shown in Scheme 2.2A, Popik and co-workers used polyphosphoric acid at 125°C, affording a 73% yield, Kim and co-workers recently obtained an 89% under the same conditions,[22] and Feringa and colleagues completed the same reaction, but with trichlorotriazine, which resulted in a yield of 67%.[23] The subsequent $LiAlH_4$ reduction has been shown to be equally problematic.[22] Our experience suggests that the root of these problems with inconsistent yield is the poor solubility of the compounds during reaction and work-up. Accordingly, we attempted the Beckmann reaction with Eaton's Reagent, developed in 1973, consisting of a 1:10 solution by weight of phosphorus pentoxide and methanesulfonic acid.[24] Eaton's reagent has been shown to be much more effective in dissolving poorly soluble, non-polar organic molecules, as well as being more active and amenable to easy work-up. The reaction was done in undiluted Eaton's

reagent at 100°C, and, after 30 minutes, showed complete conversion to the product with quantitative yield. When the reaction was scaled up to 50 g, the same quantitative yields were observed. Furthermore, with this improvement in yield, purification (aside from washing the precipitate with a small volume of ethyl acetate) was not required for either of the first two synthetic steps. The reduction of the amide with $LiAlH_4$, followed by acylation with an acyl chloride was facile. By improving the efficacy of the earlier reactions, we were able to avoid a chromatographic purification until after introduction of the solubilizing side-chain, greatly enhancing the overall yield. This allowed us to generate compound **3** in three steps from the commercially available dibenzosuberenone with greater than 90% yield, on a multi-gram scale.

Acylation, bromination, and elimination of the olefin was straightforward (Scheme 2.2B), and performed as in the literature.[13] It should be noted that elimination with *tert*-butoxide can be problematic if an ester functionality is used as a side-chain protecting group. Yields are highest when ~2.5 eq. are added slowly, portion-wise, as per van Delft and colleagues.[13] However, if the methyl protecting group is removed prior to elimination, this side-reaction is suppressed, and yields are in excess of 90%.

Using this improved synthetic scheme, we were able to substantially increase the yield of the desired DIBAC derivative **7** to 71% over 6 steps, and reduce purification to only 1 chromatographic step. It is quite reasonable to complete this procedure in 2 to 3 laboratory days – even on a multi-gram scale. (Scheme 2.2)

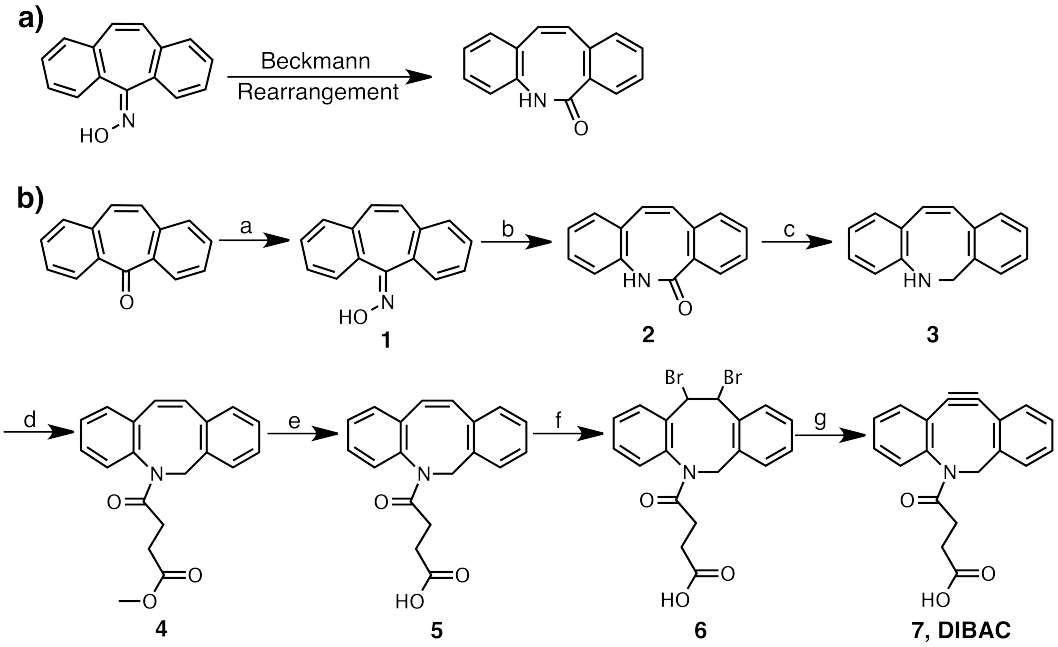

Scheme 2.2. Optimization of DIBAC Synthesis. (a) $NH_2OH{\cdot}HCl$, pyridine, EtOH, Reflux, o.n. (98%); (b) Eaton's Reagent, 100°C, 30 min (97%); (c) $LiAlH_4$, Et_2O, 35 °C, o.n. (91%); (d) Methyl 4-chloro-4-oxobutyrate, DCM, Et_3N, 0 °C, 2h (87%); (e) LiOH, $MeOH/H_2O$, reflux, 16h, 95%; (f) Br_2, DCM, 0 °C, 2h, 99%; (g) KO^tBu, THF, -40 °C, 2h, 95%.

Considering that our optimized production of the precursor amide **2** is straightforward and scalable, we decided to attempt the synthesis of the more reactive BARAC derivatives using an analogous approach (Scheme 2.3). Through the use of a toluene-water phase-transfer system (to minimize ring opening), we were able to rapidly alkylate **2** with a number of alkyl-bromides in near-quantitative yield. This alkylation chemistry was found to be compatible with silyl ether, methyl ester and tetrahydropyran (THP) protecting groups. This was followed by clean bromination of the double bond in excellent yield.

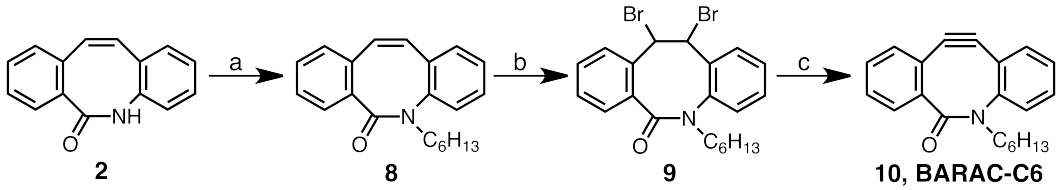

Scheme 2.3. Attempted Synthesis of BARAC. (a) 1-Bromohexane, NaOH (sat.), toluene, TBABr (5 mol %), 60°C (85%); (b) Br_2, DCM, 0°C (88%); (c) KO^tBu, THF, -40°C (<10%).

Unfortunately, elimination of the dibromide precursor using either potassium *tert*-butoxide or KHMDS was ineffective, unpredictable, and low-yielding. We attempted this route on several N-alkylated derivatives. Our side chains included methyl, hexyl, and hexadecyl alkyl chains; THP and TIPS protected propanols; and a 4-carbon methyl ester (Figure 2.1). We were able to produce two BARAC derivatives in very low yield (hexyl, and TIPS-propanol). The synthesis of these products was confirmed by *in situ* reaction with benzyl azide and TLC-M/S, as well as ^{1}H-NMR (hexyl derivative). Product yields were less than 10%, and both products partially decomposed during flash chromatography on silica. Eliminations on the other derivatives showed no evidence of product, but rather yielded highly fluorescent products that failed to react with benzyl azide, yet had the correct mass (determined by electrospray mass-spectrometry). We attribute these results to rearrangement products as observed by Chigrinova *et al*.[17]

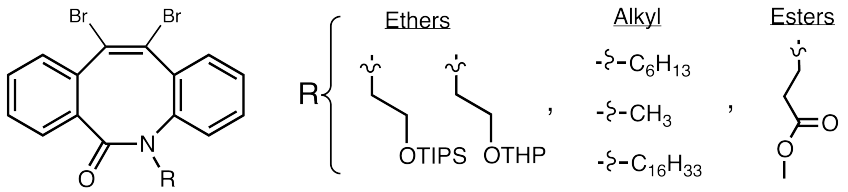

Figure 2.1. BARAC precursors for elimination attempts.

As mentioned, in the rare cases where cyclooctyne compounds were accessible, the yields were low, and the compounds showed only modest stability under ambient conditions. While we have only attempted the synthesis of a relatively small number of the possible derivatives, we do not believe that this is a viable route to BARAC compounds on the scale required for materials chemistry, nor do we believe that BARAC derivatives are sufficiently stable for these uses.

van Delft and co-workers have calculated the second-order rate constant (*k*) of DIBAC to be 0.31 $M^{-1}s^{-1}$. To date, this is the most reactive DIBAC reported in the literature. In order to produce a DIBAC compound with reactivity similar to BARAC, we synthesized a DIBAC derivative that was di-substituted in the 2 and 7 positions with fluorine atoms. The synthetic route to difluoro-DIBAC (F_2-DIBAC, **21**) is outlined in Scheme 2.4A.

Using literature procedures,[25,26] we generated 3,7-difluorosuberone in modest yield (Scheme 2.4A). The bridging double-bond was introduced using $POCl_3/PCl_5$ according to literature procedures for other suberone derivatives.[27,28] Once the fluorine atoms were in place, the synthesis was carried out in the same manner as the parent DIBAC, with similar yield (Scheme 2.4B). A 16-carbon side chain was used to provide solubility to the final alkyne. Following bromination and elimination, *para*-difluoro-DIBAC (**21**) was successfully isolated and its synthesis was confirmed by ^{1}H and ^{13}C NMR spectroscopy, as well as mass spectrometry.

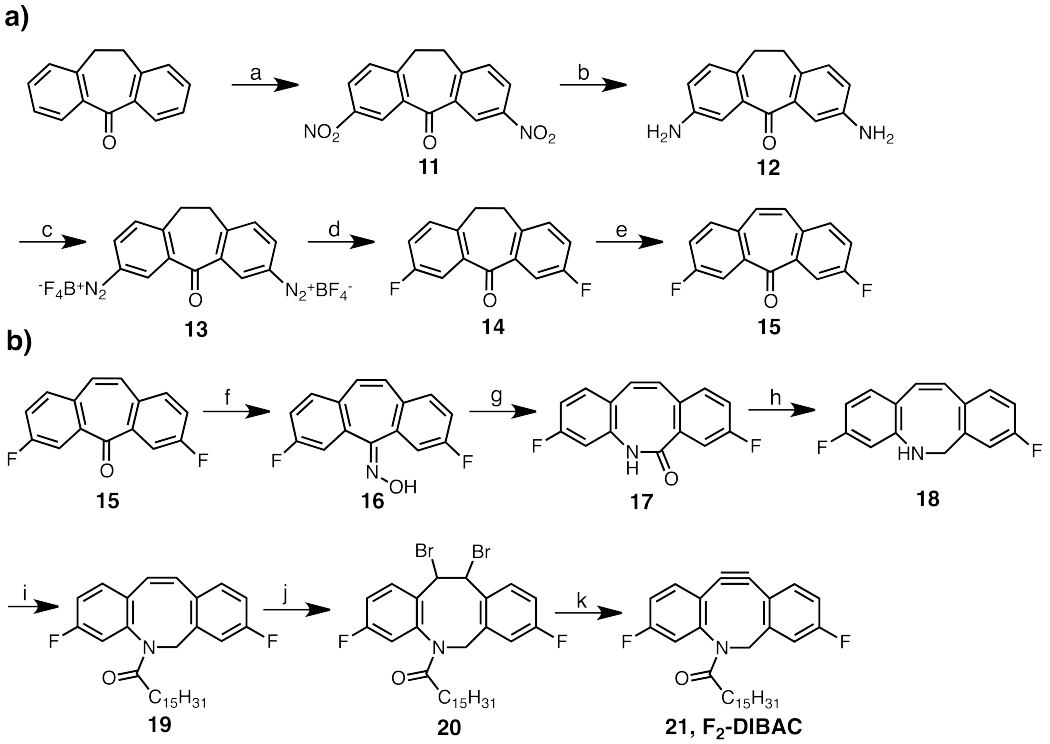

Scheme 2.4. *Reagents and conditions*: (a) HNO_3, H_2SO_4, 85 °C, 2h (49%); (b) $SnCl_2$, HCl/AcOH, reflux, 2h (73%) (c) (1) $NaNO_2$, HBF_4, H_2O, 0 °C -> r.t., 2h (89%); (d) Xylene, 125°C, 3h ; (48%) (e) $POCl_3/PCl_5$, 90 °C, 3h (55%) (f) $NH_2OH{\cdot}HCl$, pyridine, 110°C, o.n. (87%); (g) Eaton's Reagent, 100°C, 30 min (99%); (h) $LiAlH_4$, Et_2O, 35°C, o.n. (94%); (i) Palmitoyl chloride, pyridine, CH_2Cl_2, r.t., 4h (80%); (j) Br_2, CH_2Cl_2, 0°C, 1.5h (99%); (k) KO^tBu, THF, -40°C, 2h (83%).

The reactivity of **21** was compared to the parent DIBAC compound. We measured the second-order rate constant (*k*) by reacting **21** with benzyl azide (Scheme 2.5) in acetonitrile-d_6 and monitoring the disappearance of the starting material by ^1H NMR, using hexamethyl disilane (HMDS) as an internal standard. The reciprocal of the concentration of *para*-difluoro-DIBAC was plotted against time to give k = 0.50 $M^{-1}s^{-1}$. The same procedure was performed on the parent DIBAC, and the observed rate constant was consistent with that reported in the literature (k = 0.31 $M^{-1}s^{-1}$).[13] The kinetic plot for **21** is shown in Figure 2.2. Thus, a 60% increase in reactivity was

achieved with *para*-difluoro-DIBAC, as compared to the parent molecule. This increase in reactivity was almost identical to what has been observed for the 2,7-difluorinated BARAC relative to the non-fluorinated parent compound. As expected, *para*-difluoro-DIBAC is substantially more stable than BARAC; it is stable when stored at room temperature over the course of months, and has no proclivity to react with acetonitrile, even when heated to reflux, unlike BARAC.[17] To our knowledge, difluoro-DIBAC is the most reactive cyclooctyne that remains fully stable under ambient conditions.

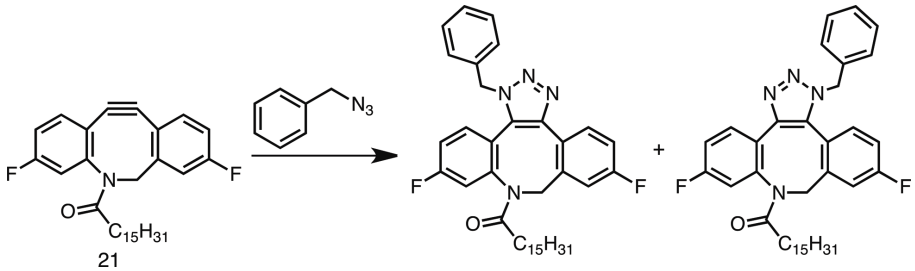

Scheme 2.5. Reaction of *para*-difluoro-DIBAC **21** with benzyl azide.

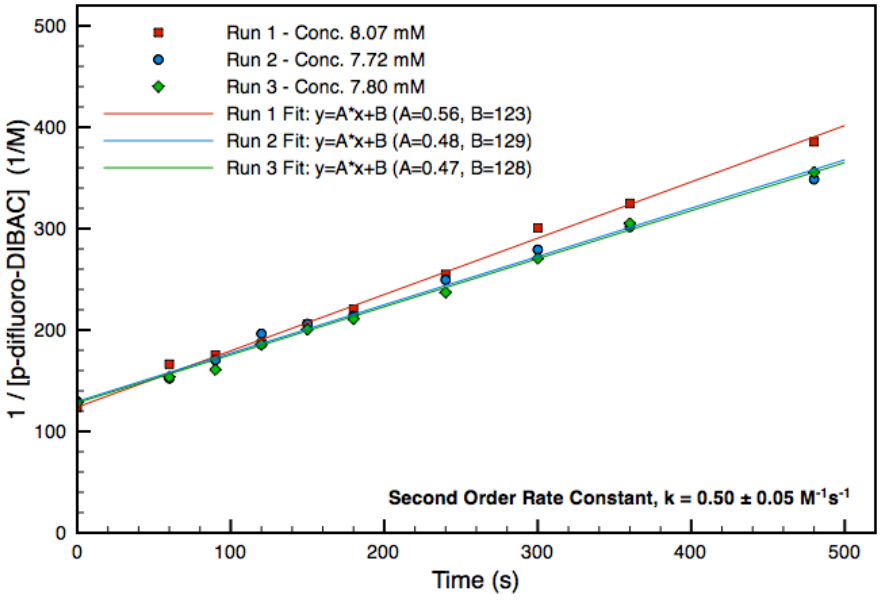

Figure 2.2. Second order rate constants of **21**. Measured from the reaction with benzyl azide in acetonitrile at 25°C.[13]

2.3. Conclusions

Dibenzocyclooctynes have many potential uses as orthogonal, reactive functional groups in polymer and materials chemistry. Until now, their use has been limited by the tedious and low-yielding synthetic procedures reported for their preparation. In order to facilitate their adoption in materials chemistry, we have optimized the synthetic route to DIBAC. A key to this improved synthesis was the use of Eaton's Reagent to carry out the ring-expanding Beckman rearrangement, which allowed for a substantial increase in reaction scale and a dramatic improvement in yield. While we were unable to develop a similar route to BARAC, we were able to produce the more stable, yet highly reactive cyclooctyne, *para*-difluro-DIBAC. We have found this derivative to exhibit the highest reactivity toward azides of any DIBAC derivative that has been reported thus far.

2.4. Experimental

2.4.1. General

LRMS was performed using Electrospray Ionization with quadrupole mass analysis (Micromass Quattro Ultima), HRMS was performed using Electrospray Ionization with quadrupole/TOF mass analysis. All mass-spectra were recorded in positive ion mode (ESI+). ^{1}H, ^{13}C NMR were performed in DMSO-d6 or $CDCl_3$ and all spectra referenced to the residual solvent peaks. ^{13}C-NMR spectra were recorded using the DEPTq or uDEFT pulse sequences.

2.4.2. Kinetic Experiments

Kinetic experiments were performed according to a literature procedure[15] The C16 derivatives of DIBAC and F_2-DIBAC were reacted with benzyl azide

in $CDCl_3$ at a 1:1 ratio and at concentrations of 7.7-8.1 mM. Hexamethyldisilane was used as an internal standard. The conversion was calculated by ^{1}H-NMR integration ratios relative to the internal standard. All experiments were performed in triplicate. The second order rate constant was calculated by plotting the reciprocal of substrate concentration vs. time and fitting the plot to a linear regression.

2.4.3. Synthesis

5*H*-dibenzo[a,d]cyclohepten-5-one oxime (1)[14]

A mixture of absolute ethanol (600 mL) and pyridine (130 mL) was added to a 1 L round bottom flask containing hydroxylamine hydrochloride (84.2 g, 1.2 mol), and dibenzosuberenone (50.0 g, 240 mmol). The mixture was stirred and heated to reflux via heating mantle for 15 hours. At this point, TLC showed the complete consumption of starting material (TLC: 5% MeOH in CH_2Cl_2). Once cooled to ca. 35°C, the reaction mixture was diluted in 500 mL CH_2Cl_2 and washed 3 times with 200 mL of 1M HCl, followed by 200 mL brine. The organic layer was dried over sodium sulfate, filtered and evaporated to yield 52.9 grams of light brown solid **1** (98%). ^{1}H-NMR: (600 MHz, $CDCl_3$): δ = 7.68-7.67 (m, 1H), 7.60-7.59 (m, 1H), 7.45-7.35 (m, 6H), 6.92 (q, *J* = 12, 18.6 Hz, 2H). ^{13}C-NMR: (151 MHz, $CDCl_3$): δ = 156.6, 135.5, 134.7, 133.9, 130.9, 130.8, 129.6, 129.3, 129.2, 129.1, 128.9, 127.9, 127.8.

Dibenzo[*b,f*]azocin-6(5H)-one (2)[14]

A flask was charged with 5H-dibenzo[a,d]cyclohepten-5-one oxime **1** (50.0 g, 225 mmol) and flushed with dry argon. Eaton's reagent[24] (P_2O_5-$MeSO_3H$, 300 mL) was added in a single portion. The reaction mixture immediately turned dark red. The reaction was placed into an oil bath and stirred at 100°C. After 30 min, TLC (5% MeOH in CH_2Cl_2) showed complete conversion.

The reaction was quenched by the addition of 1 L of water and the product was collected by extraction with multiple volumes of hot ethyl acetate. The ethyl acetate fractions were combined and concentrated to ca. 100 mL volume, allowed to cool to ambient temperature and the product was collected by filtration, then washed with an additional 100 mL ethyl acetate to yield **2** (48.4 g, 97%) as a light brown powder. ^{1}H-NMR (600 MHz; DMSO-d6): δ 9.87 (s, 1H), 7.33-7.31 (m, 2H), 7.27-7.21 (m, 2H), 7.17-7.09 (m, 4H), 7.01 (d, *J* = 11.6 Hz, 1H), 6.90 (d, *J* = 11.6 Hz, 1H).^{13}C-NMR (151 MHz, $CDCl_3$): δ = 171.7, 136.3, 136.1, 134.4, 133.4, 132.6, 130.1, 128.9, 128.8, 128.0, 127.8, 127.7, 127.4, 126.4, 126.2.

5,6-Dihydrodibenzo[*b,f*]azocine (3)[13,14]

Dibenzo[*b,f*]azocin-6(5H)-one (**2**) (3.00 g, 13.6 mmol) and $LiAlH_4$ (10.3 g, 271 mmol) were added to a 200 mL flame-dried, Ar-purged round bottom flask. Anhydrous ether (35 mL) was slowly added to the reaction via syringe. The reaction was stirred and heated to reflux for 15 h. TLC (2:1, Hexanes:EtOAc) showed complete disappearance of starting material. The reaction mixture was cooled via ice/water bath at 0^{o}C, and 150 mL of dichloromethane was added to the flask, followed by the dropwise addition of water until all the $LiAlH_4$ was quenched. Another 50 mL of water was added, and the inorganic precipitate was removed by filtration. The organic layer was separated, dried over sodium sulfate, filtered, and the solvent removed by rotary evaporation to yield **3** as a yellow solid (2.54 g, 91%). ^{1}H-NMR (600 MHz, $CDCl_3$): δ = 7.28-7.25 (m, 1H), 7.21-7.17 (m, 3H), 6.98 (dd, *J* = 7.8 Hz, 1H), 6.89 (td, *J* = 7.2 Hz, 1H), 6.61 (t, *J* = 7.8 Hz, 1H), 6.55 (d, *J* = 13.2 Hz, 1H), 6.48 (d, *J* = 7.8 Hz, 1H), 6.37, (d, *J* = 13.2 Hz, 1H), 4.59 (s, 2H). ^{13}C-NMR (151 MHz, $CDCl_3$): δ = 147.2, 139.4, 138.3, 134.9, 132.9, 130.3, 129.1, 128.2, 127.9, 127.6, 127.6, 122.0, 118.2, 117.9. MS (ESI-Quad.) *m/z* for $C_{15}H_{14}N$ $[M+H]^+$ Calculated: 208.10, Found: 208.2.

Methyl 4-dibenzo[b,f]azoncin-5(6H)-yl-4-oxobutanoate (4)[29]

Under an argon atmosphere, amine **3** (3.00 g, 14.5 mmol) was dissolved in 100 mL CH_2Cl_2, and 4 mL triethylamine (ca. 2 eq.) was added, and the mixture was cooled to 0°C in an ice bath. Methyl 4-chloro-4-oxobutyrate (3.27 g, 2.67 mL, 21.7 mmol) was added dropwise via syringe. The reaction was stirred for 2 h at room temperature, at which time TLC (2:1, Hexanes:EtOAc) showed complete conversion. The solution was washed with 3 x 50 mL 2M NaOH, 3 x 50 mL 2M HCl, 1 x 100 mL brine, dried over sodium sulfate, and filtered. The solvent was evaporated and the product purified by column chromatography (3:1 Hex:EtOAc). The product **4** was obtained as a white amorphous solid (4.05 g, 87%). ^{1}H NMR (600 MHz, $CDCl_3$): δ 7.26-7.24 (m, 5H), 7.17-7.11 (m, 3H), 6.79 (d, *J* = 13.2 Hz, 1H), 6.61 (d, *J* = 13.2 Hz, 1H), 5.51 (d, *J* = 15 Hz, 1H), 4.25 (d, *J* = 15 Hz, 1H), 3.61 (s, 3H), 2.62-2.57 (m, 1H), 2.49-2.39 (m, 2H), 2.04-1.91 (m, 1H).^{13}C NMR (151 MHz, $CDCl_3$): δ 173.6, 171.0, 140.7, 136.7, 136.0, 134.8, 132.8, 131.9, 131.0, 130.3, 128.7, 128.4, 128.1, 127.5, 127.1, 54.7, 51.8, 29.7, 29.2.

4-dibenzo[b,f]azoncin-5(6H)-yl-4-oxobutanoic acid (5)

A round-bottom flask equipped with a stir bar was charged with **4** (4.86 g, 15.1 mmol) and 100 mL of methanol. A solution of LiOH (2.17 g, 90.8 mmol) in water (50 mL) was added to the flask. A condenser was attached to the round-bottom flask and the reaction was stirred and heated to reflux for 16 h. The reaction was quenched with 1M $NaHSO_4$ (100 mL), and then extracted three times with CH_2Cl_2 (3 x 100 mL). The organic layers were combined and washed with water (100 mL) and brine (100 mL), and then dried over sodium sulfate and filtered. The solvent was removed under reduced pressure to yield compound **5** as a white solid (4.45 g, 95%), which was used without further purification. ^{1}H NMR (600 MHz, $CDCl_3$): δ = 7.30-7.26 (m, 3H), 7.25-7.22 (m, 2H), 7.19-7.11 (m, 3H), 6.81 (d, *J* = 12.6 Hz, 1H), 6.61 (d, *J* =

12.6 Hz, 1H), 5.53 (d, *J* = 15.6 Hz, 1H), 4.30 (d, *J* = 15 Hz, 1H), 2.63-2.58 (m, 1H), 2.53-2.49 (m, 1H), 2.44-2.39 (m, 1H), 2.08-2.03 (m, 1H). ^{13}C NMR (151 MHz, $CDCl_3$): δ = 176.3, 172.1, 140.2, 136.7, 136.0, 134.3, 133.1, 132.0, 131.0, 130.3, 128.9, 128.6, 128.2, 127.6, 127.4, 127.3, 54.8, 29.9, 29.7.

5-(11,12-didehydrodibenzo[b,f]azocin-5(6H)-yl)-4-oxobutanoic acid, DIBAC (7)

A round-bottom flask was charged with **5** (0.910 g, 2.96 mmol) and CH_2Cl_2 (40 mL). The flask was flushed with argon and the solution was stirred and cooled to 0°C in an ice/water bath. Br_2 (1.42 g, 0.46 mL, 8.89 mmol) was added dropwise to the flask via syringe. According to TLC (10% MeOH in CH_2Cl_2), the reaction was complete after 2 h, at which point the flask was removed from the ice/water bath and 50 mL CH_2Cl_2 was added to the reaction mixture. The mixture was washed with 3 x 50 mL aqueous saturated Na_2SO_3, 1 x 50 mL water and 1 x 50 mL NaCl brine. The organic layer was dried over sodium sulfate and filtered. Finally, the solvent was removed under reduced pressure to yield **6** as an off-white solid (1.38 g, 99%, two regioisomers, identity confirmed by TLC-MS and ^{1}H-NMR) that was used immediately in the next reaction. ^{1}H NMR (600 MHz, $CDCl_3$, both regioisomers): δ = 7.74 (d, *J* = 7.8 Hz, 1H), 7.66 (d, *J* = 7.2 Hz, 0.5H), 7.29-7.27 (m, 1H), 7.23-7.04 (m, 7.5H), 6.94-6.90 (m, 2H), 5.88 (d, *J* = 10.2 Hz, 1H), 5.83 (d, *J* = 15 Hz, 1H), 5.81 (d, *J* = 7.8 Hz, 0.5H), 5.25 (d, *J* = 9.6 Hz, 0.5H), 5.16 (d, *J* = 10.2 Hz, 1H), 5.15 (d, *J* = 14.4 Hz, 0.5H), 5.05 (d, *J* = 14.4 Hz, 0.5H), 4.22 (d, *J* = 15 Hz, 1H), 2.92-2.87 (m, 1H), 2.80-2.62 (m, 2.5H), 2.59-2.51 (m, 2H), 2.29-2.24 (m, 0.5H).

Compound **6** (1.34 g, 2.88 mmol), was dissolved in dry THF (50 mL), under argon atmosphere. The reaction mixture was stirred and cooled to -40°C in an acetonitrile/dry ice bath. A 1M solution of KO^{t}Bu in THF (10.0 mL, 10 mmol) was added dropwise to the reaction mixture via syringe. After 1.5

hours, another equivalent of KO^{t}Bu in THF (3 mL) was added to the reaction mixture. According to TLC (10% MeOH in CH_2Cl_2), the reaction was complete after another 30 min of stirring. The flask was removed from the acetonitrile/dry ice bath and warmed to room temperature. The reaction was quenched with 1M $NaHSO_4$ until the pH reached 1. The aqueous layer was extracted with 3 x 50 mL CH_2Cl_2, the organic layers were combined then washed with water and brine (50 mL each), followed by drying over sodium sulfate. The solvent was removed under reduced pressure to yield **7** (0.85 g, 95%) off white solid. ^{1}H NMR (600 MHz, DMSO-d_6): δ = 11.98 (s, 1H), 7.66 (d, *J* = 8.4 Hz, 1H), 7.62 (d, *J* = 7.2 Hz, 1H), 7.52-7.45 (m, 3H), 7.39-7.33 (m, 2H), 7.29 (d, *J* = 7.2 Hz, 1H), 5.03 (d, *J* = 14.4 Hz, 1H), 3.63 (d, *J* = 14.4 Hz, 1H), 2.61-2.56 (m, 1H), 2.32-2.27 (m, 1H), 2.21-2.16 (m, 1H), 1.80-1.76 (m, 1H). ^{13}C NMR (151 MHz, DMSO-d_6): δ = 173.5, 170.7, 151.4, 148.4, 132.4, 129.6, 128.9, 128.2, 127.9, 127.6, 126.8, 125.1, 122.5, 121.5, 144.3, 108.0, 54.9, 29.2, 28.9. Anal. calc'd for $C_{19}H_{15}NO_3$: C, 74.74; H, 4.95; N, 4.59. Found: C, 74.27; H, 4.97; N, 4.57. HRMS (ESI-TOF) *m/z* calcd for $C_{19}H_{15}NO_3$ $[M+H]^+$ 306.1130, found 306.1119.

3,7-Difluorodibenzosuberenone (15)[26]

Adapting a literature procedure,[28,27] 3,7-Difluorodibenzosuberone (4.6 g, 18.7 mmol) **14** was dissolved in 12 mL $POCl_3$ under nitrogen atmosphere and PCl_5 (8.5 g, 41 mmol) was added in one portion. The mixture was heated for 5 h at 90°C. CH_2Cl_2 (10 mL), MeOH (5 mL) and water (5 mL) were added to quench the reaction. This mixture spontaneously refluxed, and was stirred for 4 hours. The mixture was extracted with chloroform (100 mL), then the organic layer was washed with 100 mL water. After drying with Na_2SO_4, filtration, and evaporation, the mixture was re-crystallized from ethanol to yield the product **15** as colorless crystals (2.5 g, 55%). ^{1}H-NMR (600 MHz; $CDCl_3$): δ 7.96 (dd, *J* = 9.9, 2.8 Hz, 2H), 7.57 (dd, *J* = 8.6, 5.3 Hz, 2H), 7.37 (ddd,

J = 8.6, 7.4, 2.8 Hz, 2H), 7.02 (s, 2H). ^{13}C NMR (151 MHz; CDCl3): δ 133.75, 133.70, 130.1, 120.39, 120.24, 116.86, 116.70. HRMS (ESI-TOF) *m/z* calcd for $C_{15}H_9OF_2$ $[M+H]^+$ 243.0633, found 243.0632.

3,7-Difluoro-5*H*-dibenzo[7]annulen-5-one oxime (16)

Compound **15** (1.5 g, 6.2 mmol) and $NH_2OH{\cdot}HCl$ (1.7 g, 24.3 mmol) were added to a flask followed by pyridine (6 mL) and ethanol (12 mL). The reaction was heated to reflux for 15 h, until TLC (20% Et_2O in Hexanes) showed full conversion. The mixture was diluted with ethyl acetate (200 mL), and washed with 1M HCl (3 x 50 mL). The organic layers were washed with brine (40 mL), and then dried over magnesium sulfate followed by filtration. The solvent was removed under reduced pressure to obtain compound **16** as off white crystals (1.42 g, 87%). ^{1}H-NMR (600 MHz, DMSO-d_6) δ 11.72 (s, 1H), 7.56 (dd, *J* = 9, 6 Hz, 1H), 7.51 (dd, *J* = 8.4, 6 Hz, 1H), 7.35-7.28 (m, 4H), 6.94 (dd, *J* = 12, 1.2 Hz, 2H). ^{13}C-NMR (151 MHz, DMSO-d_6) δ 163.1, 162.2, 161.4, 160.5, 151.5, 137.2, 137.1, 132.2, 132.1, 131.6, 131.5, 131.3, 131.2, 130.9, 129.9, 129.0, 128.8, 116.1, 116.0, 115.9, 115.8, 115.7, 114.5, 114.4. HRMS (ESI-TOF) *m/z* calcd for $C_{15}H_{10}F_2NO$ $[M+H]^+$ 258.0730, found 258.0723.

3,8-Difluorodibenzo[*b*,*f*]azocin-6(5*H*)-one (17)

Compound **16** (1.4 g, 5.4 mmol) and Eaton's reagent (P_2O_5-$MeSO_3H$, 20 mL) were added to a flask under Ar atmosphere. The mixture was stirred and heated to 100°C. After 30 min, the mixture was cooled, quenched with 100 mL water, then extracted with 3 x 100 mL hot ethyl acetate. While still warm, the organic layer was washed with water (100 mL), and brine (100 mL). The organic layer was dried over magnesium sulfate, filtered, and concentrated *in vacuo* to obtain compound **17** (1.4 g, 99%) as a light brown powder. R_F = 0.6 (CH_2Cl_2:MeOH, 95:5). ^{1}H-NMR (600 MHz, DMSO-d_6) δ 10.05 (s, 1H), 7.22-7.13 (m, 4H), 7.06 (td, *J* = 8.4, 2.4 Hz, 1H), 6.98 (d, *J* = 10.8 Hz, 2H), 6.86 (d, *J* = 11.4

Hz, 1H). ^{13}C-NMR (151 MHz, DMSO-d_6) δ 170.0, 161.8, 160.2, 137.8, 137.7, 137.6, 137.5, 131.9, 130.7, 130.6, 130.3, 130.2, 129.7, 129.6, 129.5, 116.6, 116.4, 114.3, 114.1, 113.7, 113.6, 113.1, 112.9. HRMS (ESI-TOF) *m/z* calcd for $C_{15}H_{10}F_2NO$ $[M+H]^+$ 258.0730, found 258.0736.

3,8-Difluoro-5,6-dihydrodibenzo[*b,f*]azocine (18)

Compound **17** (0.20 g, 0.78 mmol) and $LiAlH_4$ (0.542 g, 14.28 mmol) were added to an Ar-purged flask along with dry diethyl ether (8 mL). The reaction was heated to 35°C for 16 h, whereupon the TLC (2:1 Hexanes:EtOAc) showed complete conversion. The reaction mixture was diluted with diethyl ether (50 mL) and then slowly poured into a beaker of ice water to quench the $LiAlH_4$. The mixture was filtered and extracted with diethyl ether (2 × 50 mL). The combined organic layers were washed with water (50 mL) and brine (50 mL). The organic layer was dried over sodium sulfate, filtered, and concentrated *in vacuo* to obtain compound **18** (0.18 g, 94%) as a yellow solid. R_F = 0.7 (Hexanes:EtOAc, 2:1). ^{1}H-NMR (600 MHz, $CDCl_3$) δ 7.14 (dd, *J* = 8.4, 5.4 Hz, 1H), 6.97 (td, *J* = 8.4, 2.4 Hz, 1H), 6.93-6.89 (m, 2H), 6.48 (d, *J* = 13.2 Hz, 1H), 6.32 (td, *J* = 7.8, 2.4 Hz, 1H), 6.27 (d, *J* = 12.6 Hz, 1H), 6.16 (dd, *J* = 10.8, 2.4 Hz, 1H), 4.54 (s, 2H). ^{13}C-NMR (151 MHz, DMSO-d_6) δ 163.2, 162.3, 140.1, 136.4, 136.3, 132.1, 131.9, 131.8, 126.3, 117.9, 115.8, 115.6, 115.0, 114.9, 105.3, 105.2, 104.0, 103.9, 48.9, 29.9. HRMS (ESI-TOF) *m/z* calcd for $C_{15}H_{12}F_2N$ $[M+H]^+$ 244.0938, found 244.0945.

1-(3,8-Difluorodibenzo[*b,f*]azocin-5(6*H*)-yl)hexadecan-1-one (19)

Compound **18** (0.15 g, 0.62 mmol) and pyridine (0.15 mL, 1.85 mmol) were added to an argon-purged flask along with CH_2Cl_2 (5 mL). Palmitoyl chloride (0.37 mL, 1.23 mmol) was added drop-wise via syringe and the reaction was left to stir at room temperature. Two hours later, the reaction mixture was diluted with CH_2Cl_2 (20 mL) and washed with 1M HCl (3 × 20

mL), water (20 mL) and brine (20 mL). After drying over sodium sulfate, filtering, and concentrating *in vacuo*, the crude product was purified by column chromatography (1:1, CH_2Cl_2:Hexanes) to obtain **19** as a slow-to-solidify, white, amorphous solid (0.24 g, 80%). R_f = 0.4 (CH_2Cl_2). ^{1}H-NMR (600 MHz, $CDCl_3$) δ 7.28-7.25 (m, 1H), 7.12-7.09 (m, 1H), 7.03-6.99 (m, 2H), 6.92-6.87 (m, 2H), 6.69 (d, *J* = 13.2 Hz, 1H), 6.49 (d, *J* = 13.2 Hz, 1H), 5.45 (d, *J* = 15 Hz, 1H), 4.14 (d, *J* = 15 Hz, 1H), 2.06-2.01 (m, 1H), 1.93-1.88 (m, 1H), 1.49-1.44 (m, 2H), 1.31-1.05 (m, 25H), 0.88 (t, *J* = 6.6 Hz, 3H). ^{13}C-NMR (151 MHz, $CDCl_3$) δ 195.3, 134.3, 134.2, 132.9, 132.8, 131.5, 126.1, 117.4, 117.3, 115.6, 115.5, 115.4, 114.5, 114.3, 54.5, 34.7, 29.9, 29.8, 29.7, 29.6, 29.5, 29.4, 29.2, 25.4, 22.9, 14.3. HRMS (ESI-TOF) *m/z* calcd for $C_{31}H_{42}F_2NO$ $[M+H]^+$ 482.3234, found 482.3233.

1-(11,12-Dibromo-3,8-difluoro-11,12-dihydrodibenzo[*b,f*]azocin-5(6*H*)-yl)hexadecan-1-one (20)

Compound **19** (0.15 g, 0.31 mmol) was placed in an Ar purged flask along with CH_2Cl_2 (10 mL) and the solution was cooled to 0°C. Br_2 (0.03 mL, 0.62 mmol) was added via syringe and the reaction was left to stir for 1.5 hours at 0°C until full conversion was observed by TLC (1:1, CH_2Cl_2:Hex). The reaction was diluted with CH_2Cl_2 (50 mL), washed with aqueous sat'd Na_2SO_3 (2 × 50 mL) and then washed with water (50 mL) and brine (50 mL). The organic layer was dried over sodium sulfate, filtered, and concentrated *in vacuo* to obtain compound **20** (0.20 g, 99%, 2 regioisomers). TLC/MS confirmed the presence of two regioisomers. R_f = 0.2 (1:1, CH_2Cl_2:Hex). ^{1}H-NMR (600 MHz, $CDCl_3$, both regioisomers) δ 7.72 (dd, *J* = 9, 5.4 Hz, 1H), 7.04 (dd, *J* = 9, 6 Hz, 1H), 6.91-6.88 (m, 2H), 6.73 (dd, *J* = 8.4, 2.4 Hz, 1H), 6.65 (dd, *J* = 9, 2.4 Hz), 5.85 (d, *J* = 10.2 Hz, 1H), 5.81 (d, *J* = 15 Hz, 1H), 5.11 (d, *J* = 10.2 Hz, 1H), 4.08 (d, *J* = 15 Hz, 1H), 2.33-2.28 (m, 1H), 2.13-2.07 (m, 1H), 1.72-1.63 (m, 2H), 1.30-1.22 (m, 33H), 0.87 (t, *J* = 7.2 Hz, 4H). ^{13}C-NMR (151 MHz, $CDCl_3$, both

regioisomers) δ 173.6, 163.9, 163.2, 162.3, 161.5, 139.1, 139.0, 135.3, 135.2, 134.7, 134.6, 133.2, 132.4, 132.3, 131.0, 130.9, 118.1, 117.9, 117.1, 116.9, 116.8, 116.7, 116.0, 115.9, 59.2, 54.8, 52.2, 36.2, 32.1, 29.9, 29.8, 29.7, 29.6, 29.5, 25.3, 22.9, 14.3. HRMS (ESI-TOF) *m/z* calcd for $C_{31}H_{42}Br_2F_2NO$ $[M+H]^+$ 640.1601, found 640.1589.

1-(3,8-Difluoro-11,12-didehydrodibenzo[*b,f*]azocin-5(6*H*)-yl)hexadecane-1-one (21, F_2-DIBAC)

Compound **20** (0.15 g, 0.23 mmol) was placed in an Ar-purged flask along with dry THF (5 mL) and the solution was stirred and cooled to -40°C. 1 M KO^{t}Bu in THF (0.47 mL, 0.47 mmol) was added dropwise and the reaction was stirred at -40°C. After 1 h, another portion of 1 M KO^{t}Bu in THF (0.23 mL, 0.23 mmol) was also added dropwise. After 1 additional hour the reaction was completed and the mixture was poured into water (50 mL). The product was then extracted with CH_2Cl_2 (3 × 30 mL). The organic layers were combined and washed with water (50 mL) and brine (50 mL). After drying over sodium sulfate, filtering, and concentrating *in vacuo*, the crude product was purified by column chromatography (1:10, Et_2O:Hex) to obtain **21** as a white solid (0.093 g, 83%). R_f = 0.3 (1:5, Et_2O:Hex). ^{1}H-NMR (600 MHz, $CDCl_3$) δ 7.43 (dd, *J* = 9.6, 3 Hz, 1H), 7.36 (dd, *J* = 8.4, 6 Hz, 1H), 7.19 (dd, *J* = 8.4, 5.4 Hz, 1H), 7.11 (td, *J* = 8.4, 2.4 Hz, 1H), 7.07 (dd, *J* = 9, 2.4 Hz, 1H), 7.00 (td, *J* = 8.4, 2.4 Hz, 1H), 5.09 (d, *J* = 13.8 Hz, 1H), 3.63 (d, *J* = 13.8 Hz, 1H), 2.22-2.17 (m, 1H), 1.98-1.93 (m, 1H), 1.44-1.36 (m, 2H), 1.30-0.98 (m, 25H), 0.88 (t, *J* = 7.2 Hz, 3H). ^{13}C-NMR (151 MHz, $CDCl_3$) δ 173.7, 163.3, 162.8, 161.7, 153.3, 153.2, 150.6, 150.5, 128.1, 128.0, 126.9, 126.8, 120.4, 120.2, 117.4, 117.2, 115.5, 115.4, 115.3, 115.1, 114.1, 106.9, 66.1, 55.1, 34.9, 32.1, 29.9, 29.8, 29.7, 29.6, 29.4, 29.0, 25.5, 22.9, 14.3. Anal. calc'd for $C_{31}H_{39}F_2NO$: C, 77.63; H, 8.20; N, 2.92. Found: C,77.75; H, 8.20; N, 2.82. HRMS (ESI-TOF) *m/z* calcd for $C_{31}H_{40}F_2NO$ $[M+H]^+$ 480.3078, found 480.3060.

N-Hexyldibenzo[*b,f*]azocin-6(5H)-one (8)

Compound **2** (1.105 g, 5.00 mmol) was suspended in 30 mL toluene. Hexyl bromide (1.8 g, 10 mmol), and tetra-n-butylammonium bromide (200 mg, 0.6 mmol) were added, followed by 30 mL of a saturated solution of NaOH (in water). The mixture was stirred at 90°C for 30 min until the reaction turned completely clear and TLC (20% EtOAc in hexanes) showed complete conversion. The reaction was diluted with 30 mL additional toluene, and the NaOH layer separated. The organic layer was washed with 3 x 50 mL water, and 1 x 50 mL brine, then dried over magnesium sulfate and filtered. The reaction mixture was then adsorbed onto silica gel and the hexyl bromide was eluted with 100% hexanes, followed by the product with 100% CH_2Cl_2 to yield 1.30 g of **8** (85%) as a white, amorphous solid. ^{1}H-NMR (600 MHz; $CDCl_3$): δ 7.36 (s, 1H), 7.19 (s, 4H), 7.13 (td, *J* = 7.1, 2.1 Hz, 1H), 7.08 (d, *J* = 7.7 Hz, 1H), 6.98-6.96 (m, 1H), 6.96 (d, *J* = 11.5 Hz, 1H), 6.85 (d, *J* = 11.4 Hz, 1H), 4.45 (ddd, *J* = 13.2, 9.2, 6.6 Hz, 1H), 3.23 (ddd, *J* = 13.3, 9.3, 4.9 Hz, 1H), 1.49 (m, 1H), 1.39 (m, 1H), 1.32 (m, 1H), 1.25 (m, 5H), 0.85 (t, *J* = 7.0 Hz, 3H). ^{13}C-NMR (151 MHz; CDCl3, uDEFT): δ 170.9, 141.5, 137.7, 136.3, 133.5, 133.3, 129.7, 128.6, 128.5, 127.6, 127.6, 127.3, 126.9, 126.9, 105.1, 50.7, 31.7, 28.0, 26.8, 22.7, 14.2.

N-Hexyl-11,12-didehydrodibenzo[*b,f*]azocin-6(5H)-one (C6-BARAC, 10)

Compound **8** (0.36 g, 1.2 mmol) was placed in an Ar purged flask along with CH_2Cl_2 (10 mL) and the solution was cooled to 0°C. Br_2 (220 mg, 1.4 mmol) was added via syringe and the reaction was left to stir for 2 h at 0°C until full conversion was observed by TLC (Product R_f = 0.6, CH_2Cl_2). The reaction was diluted with CH_2Cl_2 (50 mL), washed with Na_2SO_3 (2 × 50 mL) and then washed with water (50 mL) and brine (50 mL). The organic layer was dried over sodium sulfate and concentrated. The yellow residue was filtered through silica gel (Eluent: 100% CH_2Cl_2) to obtain compound **9**

(0.490 g, 88%, 2 regioisomers) as a white, amorphous solid. The presence of two regioisomers and the identity of **9** were confirmed by TLC/MS (ESI-Quad.). The product was used immediately in the next reaction.

Compound **9** (490 mg, 1.05 mmol) was dissolved in 50 mL dry THF under Ar atmosphere. 1M KO^{t}Bu in THF (2.1 mL, 2.1 mmol) was added dropwise and the reaction was stirred at -40°C. After 1 h, another portion of 1 M KO^{t}Bu in THF (1.05 mL, 1.05 mmol) was also added dropwise. The solution turned bright purple. After one additional hour the mixture was poured into water (50 mL). The product was then extracted with CH_2Cl_2 (3 × 30 mL). The red/orange organic layers were combined and washed with water (50 mL) and brine (50 mL), then dried over magnesium sulfate, filtered, and evaporated to dryness *in vacuo*. Purification of the product **10** by column chromatography was fruitless, as the product decomposed in solution and on the column. Nonetheless, after 2 columns (10% EtOAc in Hex), ca. 50 mg of partially pure (ca. 80%) product was obtained. ^{1}H-NMR, ESI+ MS, and derivatization with benzyl azide confirmed the product identity. ^{1}H-NMR (600 MHz; $CDCl_3$): δ 7.60-7.59 (m, 1H), 7.56 (dd, 1H), 7.47-7.43 (m, 4H), 7.40-7.35 (m, 2H), 3.08-3.03 (m, 1H), 2.66 (m, *J* = 4.5 Hz, 1H), 1.56-1.50 (m, 1H), 1.43-1.31 (m, 3H), 1.30-1.23 (m, 2H), 1.23-1.16 (m, 2H), 0.88-0.84 (m, 3H). ^{13}C-NMR (151 MHz; uDEFT, $CDCl_3$): δ 176.8, 155.2, 149.8, 130.5, 129.40, 129.38, 128.8, 128.1, 127.88, 127.88, 126.5, 126.0, 122.8, 122.4, 110.1, 109.3, 51.7, 31.5, 29.2, 26.4, 22.7, 14.1. MS (ESI-TOF) *m/z* calcd for $C_{21}H_{21}NO$ $[M+H]^+$ 304.17, found 304.2. NOTE: The product decomposed at room temperature on the timescale of days. Attempts with other side-chains, using the same procedure, were less successful.

2.5. Supporting Information

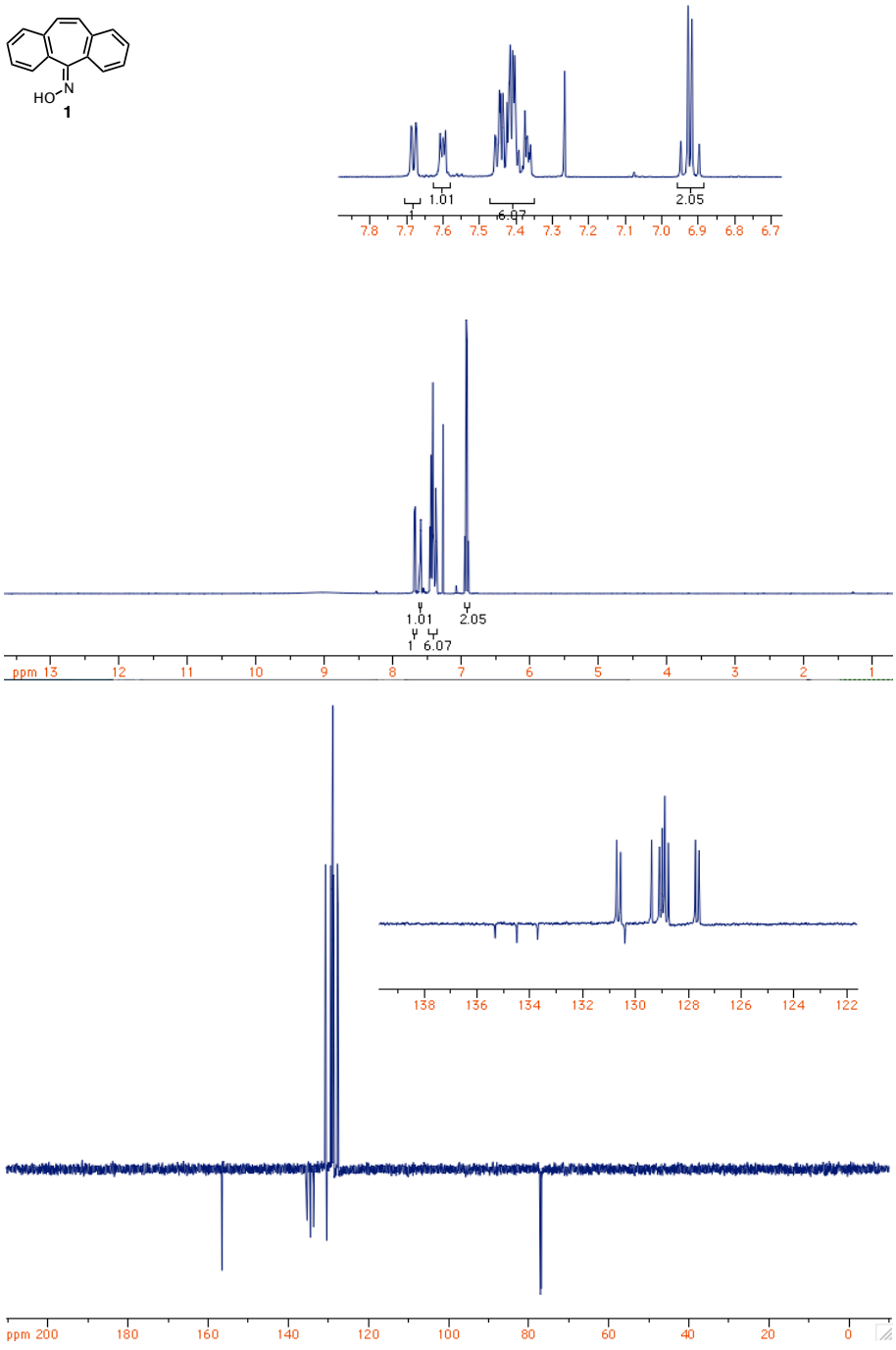

Figure 2.3. ^{1}H (top) and ^{13}C DEPT-q (bottom, CH_2 down) NMR spectra for compound **1**.

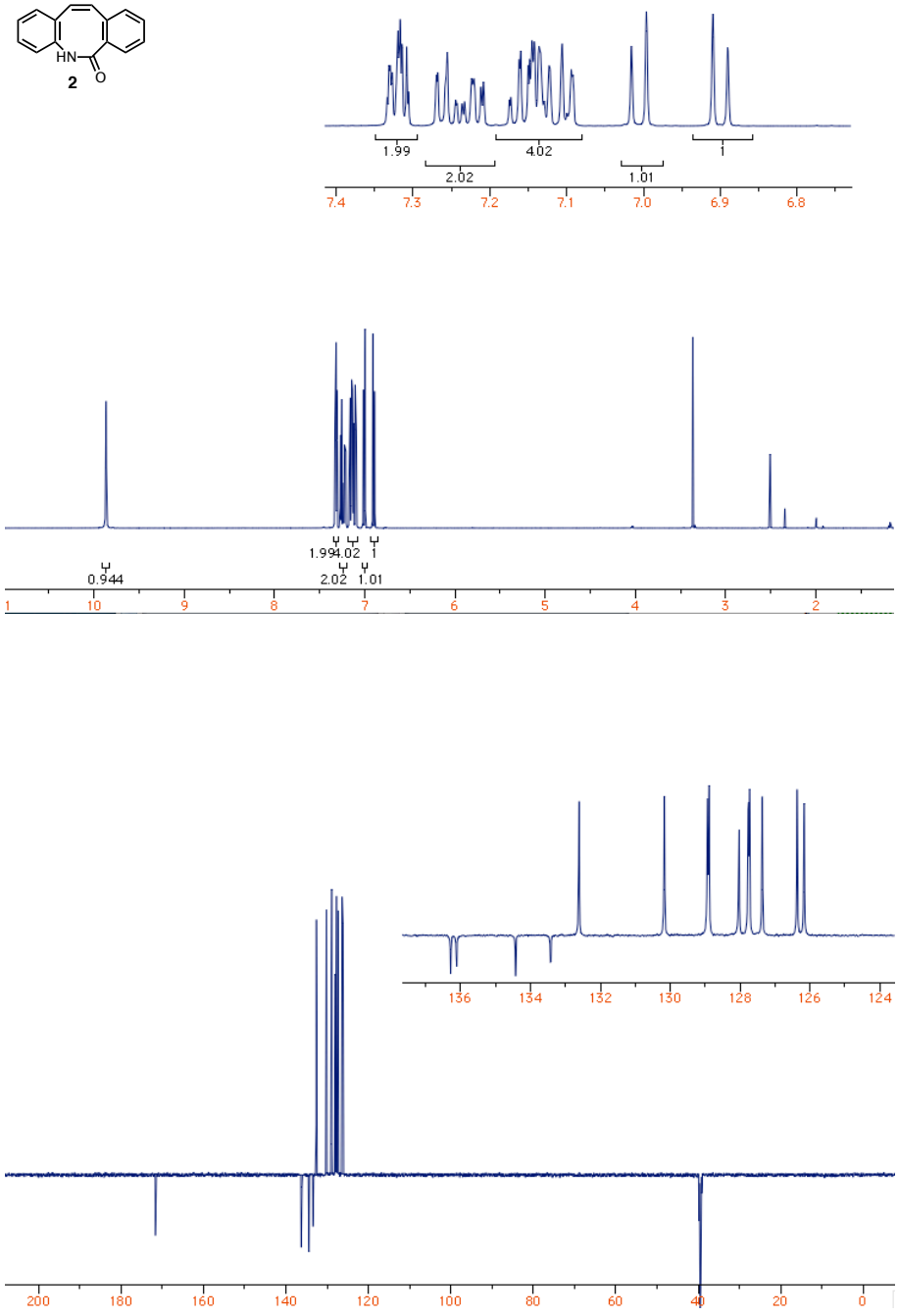

Figure 2.4. ^{1}H (top) and ^{13}C DEPT-q (bottom, CH_2 down) NMR spectra for compound **2**.

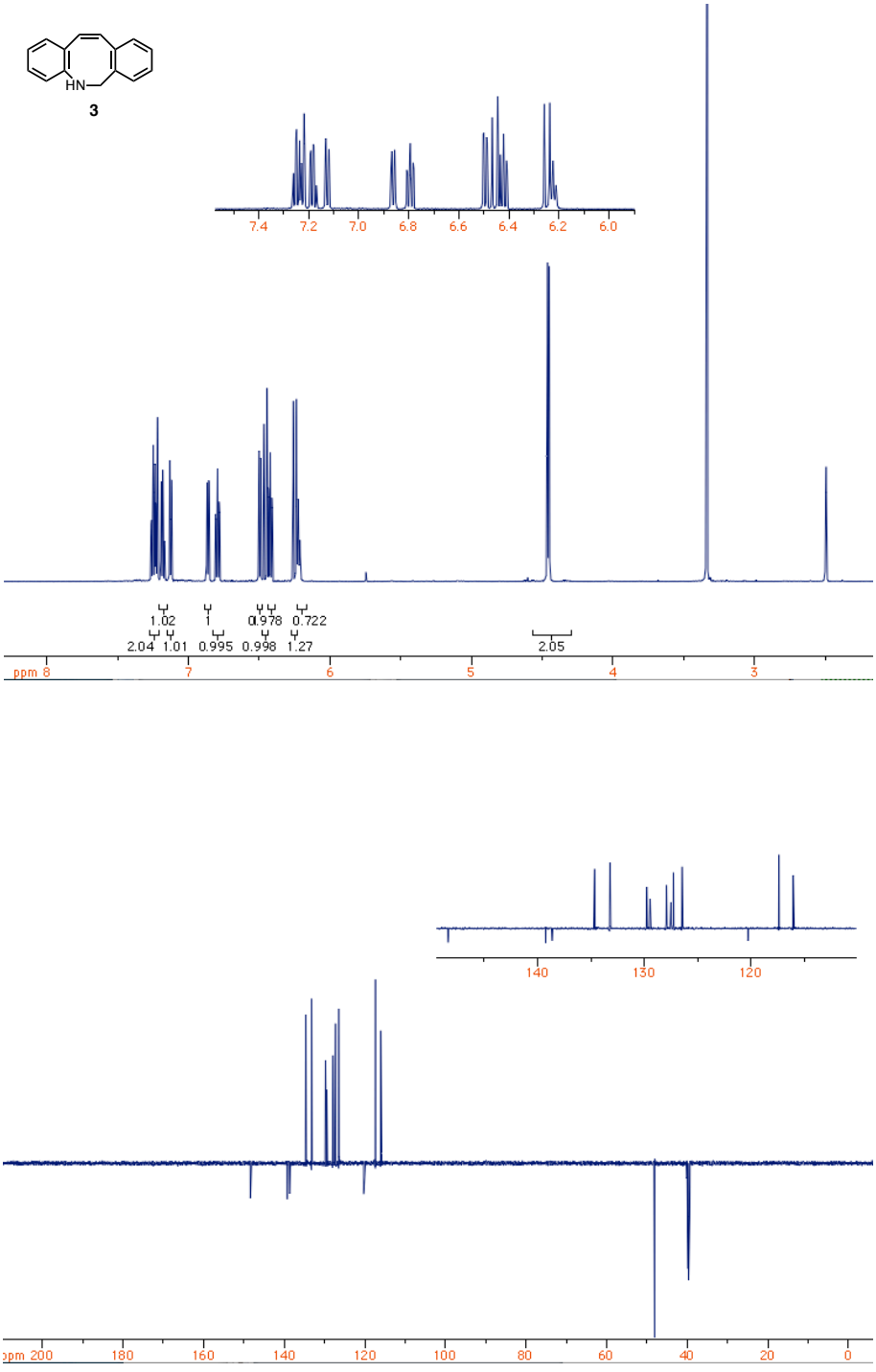

Figure 2.5. ^{1}H (top) and ^{13}C DEPT-q (bottom, CH_2 down) NMR spectra for compound **3**.

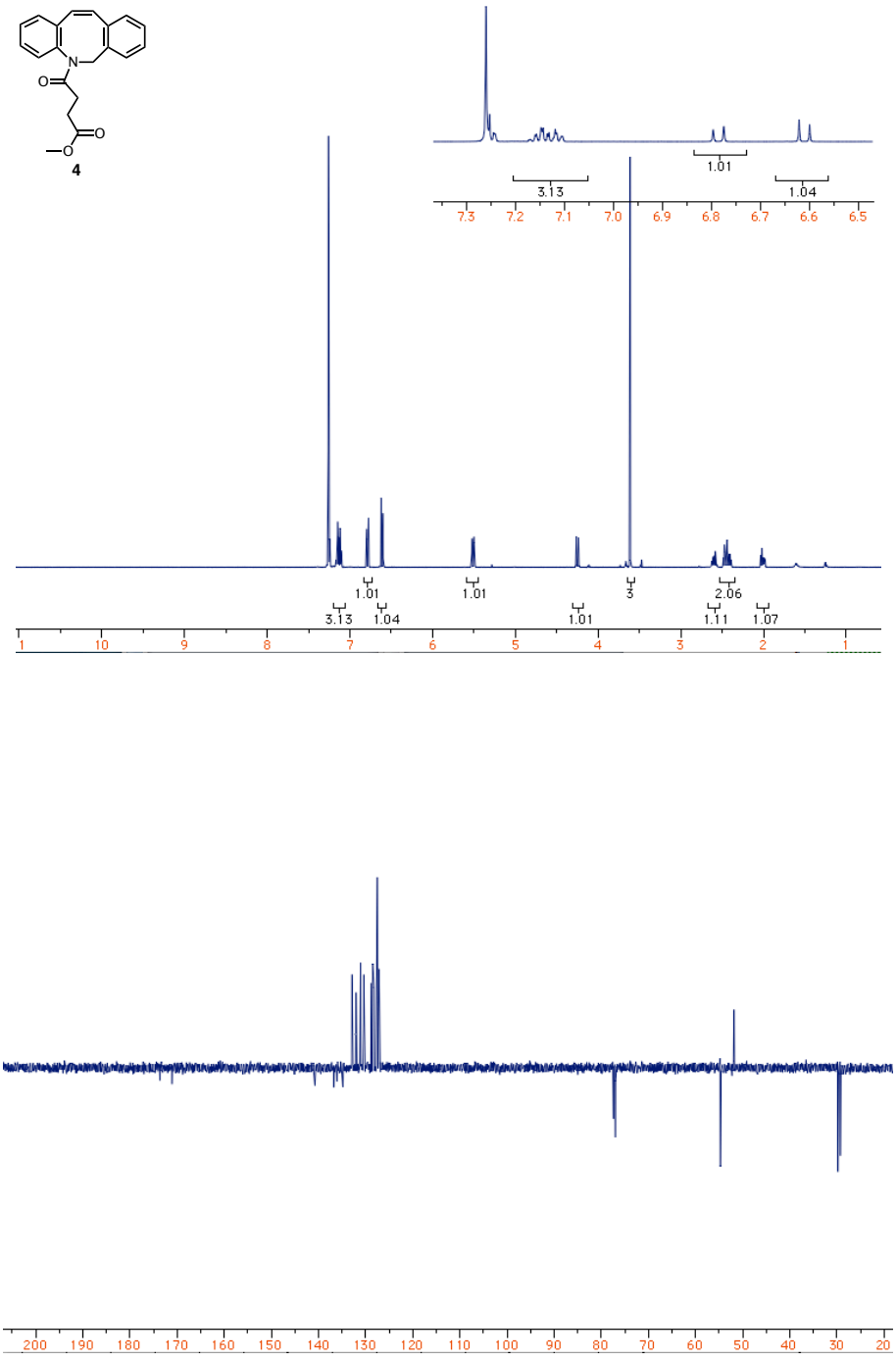

Figure 2.6. ^{1}H (top) and ^{13}C DEPT-q (bottom, CH_2 down) NMR spectra for compound **4**.

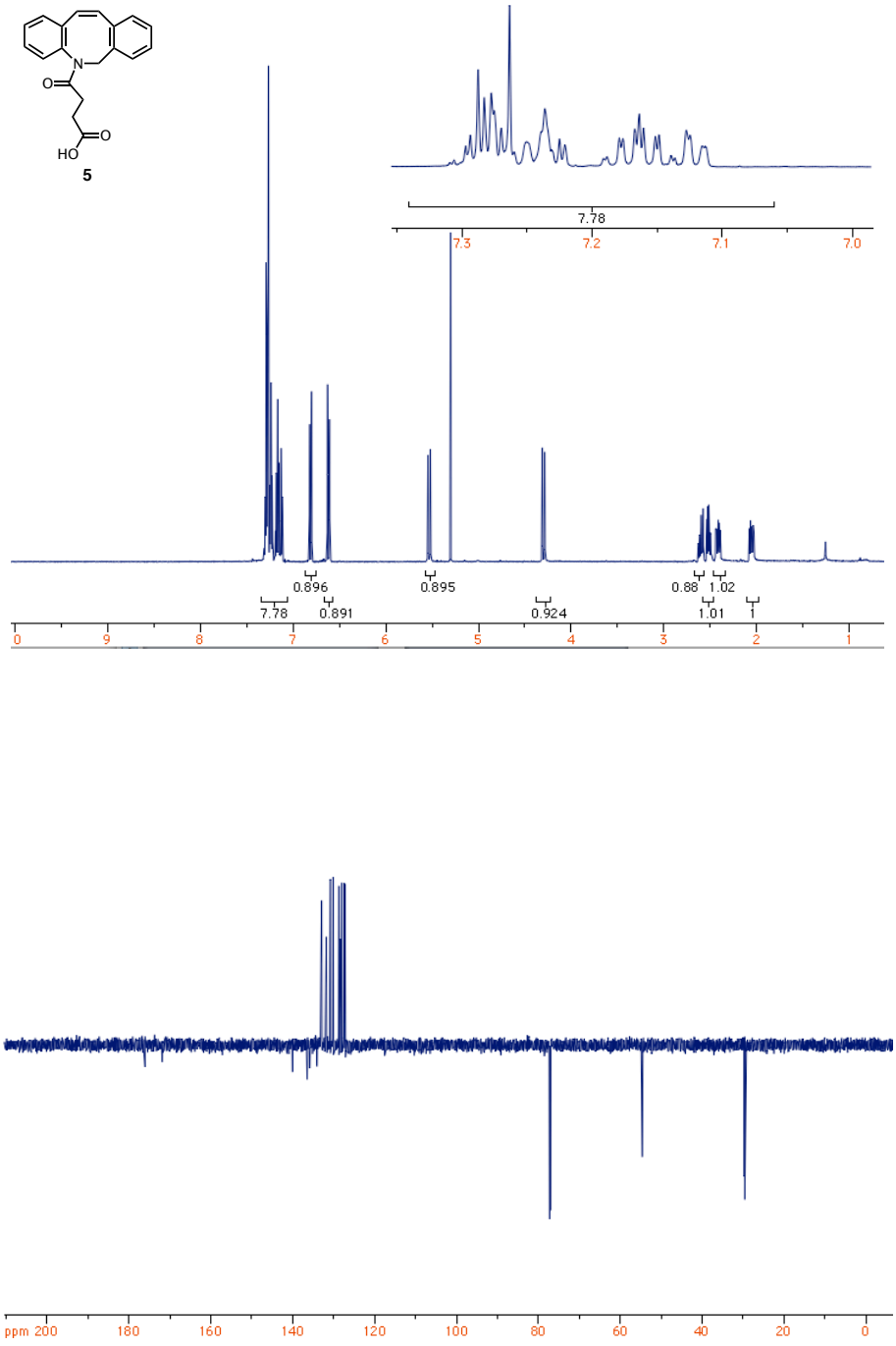

Figure 2.7. ^{1}H (top) and ^{13}C DEPT-q (bottom, CH_2 down) NMR spectra for compound **5**.

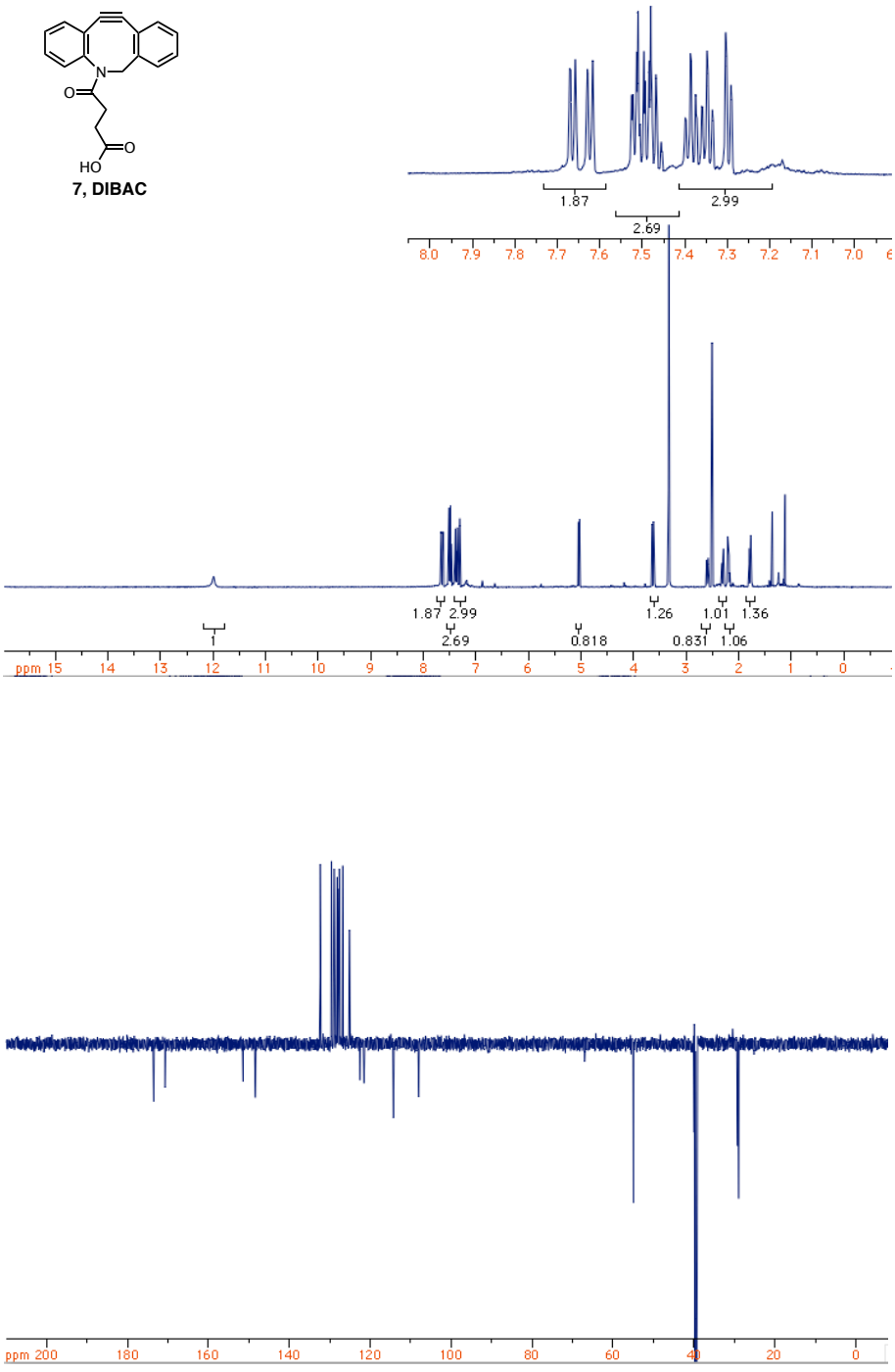

Figure 2.8. ^{1}H (top) and ^{13}C DEPT-q (bottom, CH_2 down) NMR spectra for compound **7**.

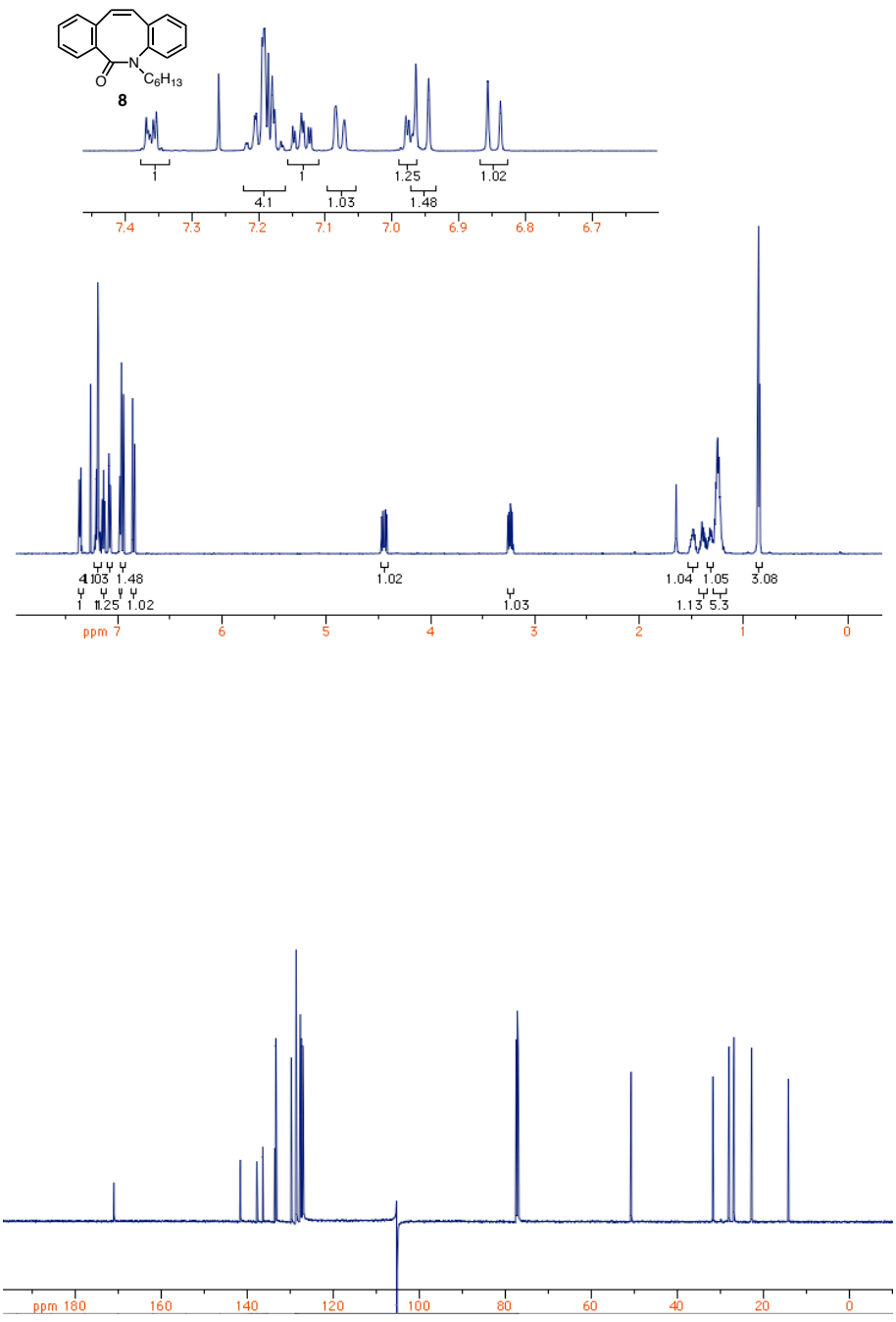

Figure 2.9. ^{1}H (top) and ^{13}C DEPT-q (bottom, CH_2 up) NMR spectra for compound **8**.

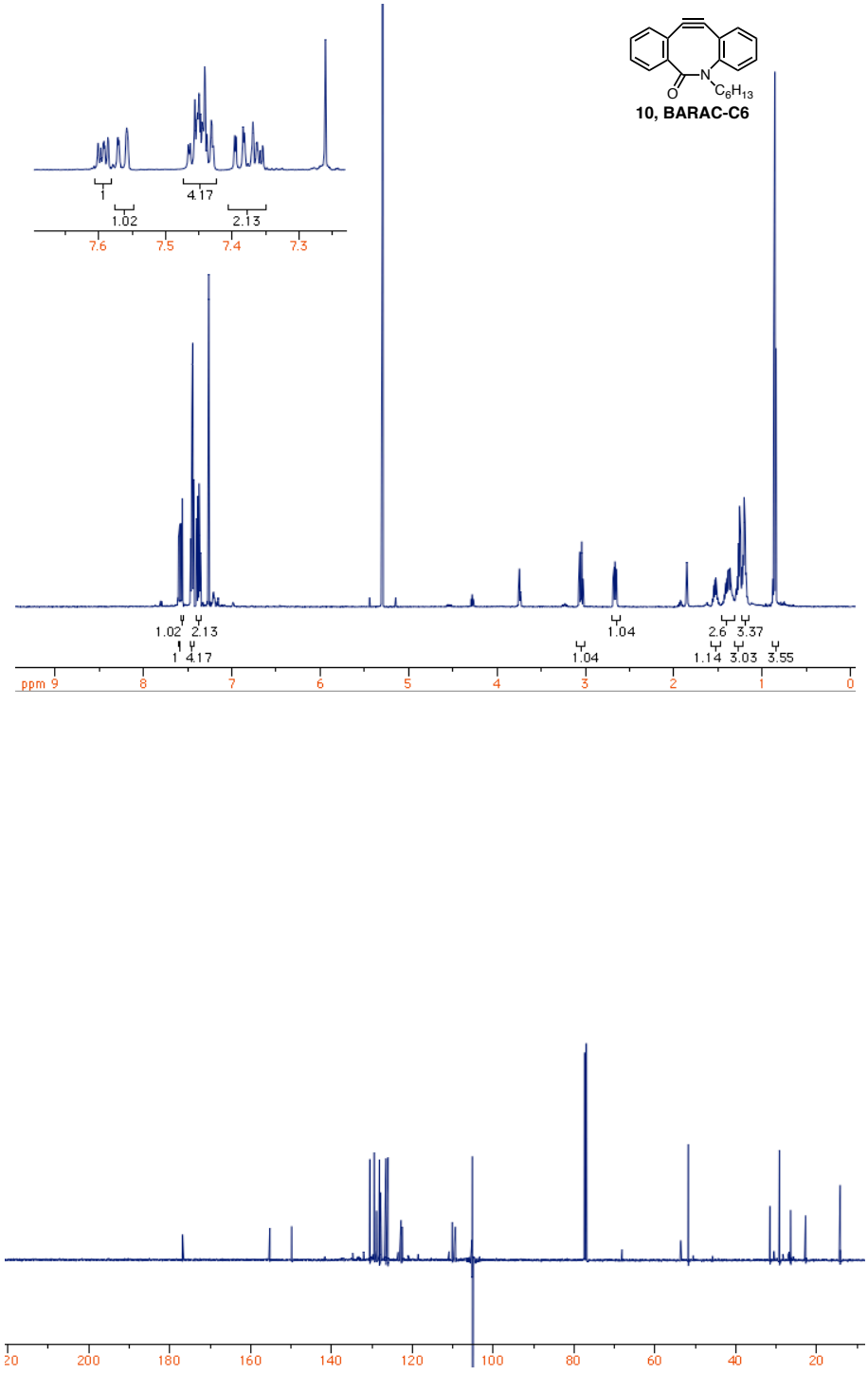

Figure 2.10. ^{1}H (top) and ^{13}C DEPT-q (bottom, CH_2 up) NMR spectra for compound **10**.

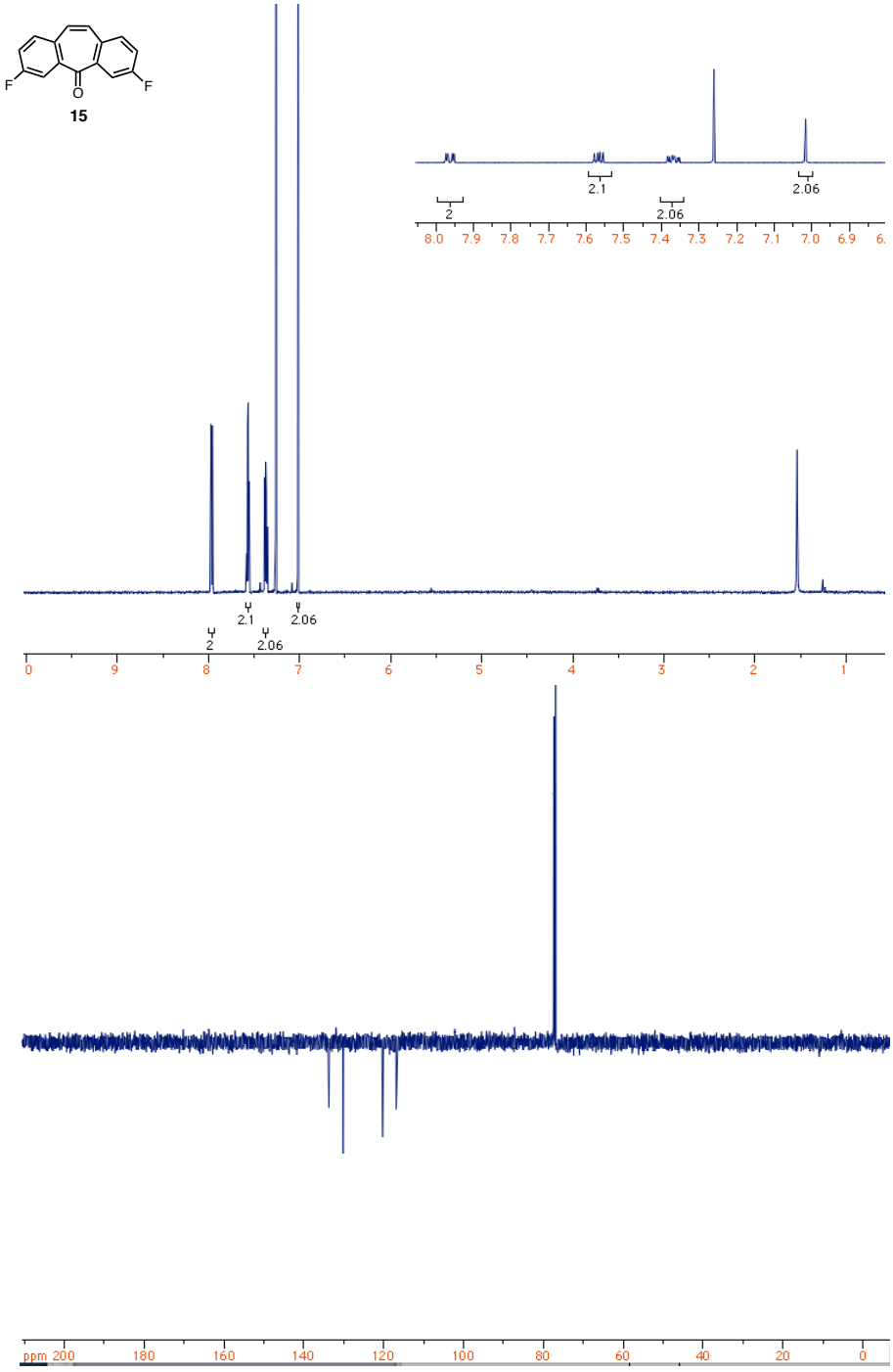

Figure 2.11. ^{1}H (top) and ^{13}C DEPT-q (bottom, CH_2 up) NMR spectra for compound **15**.

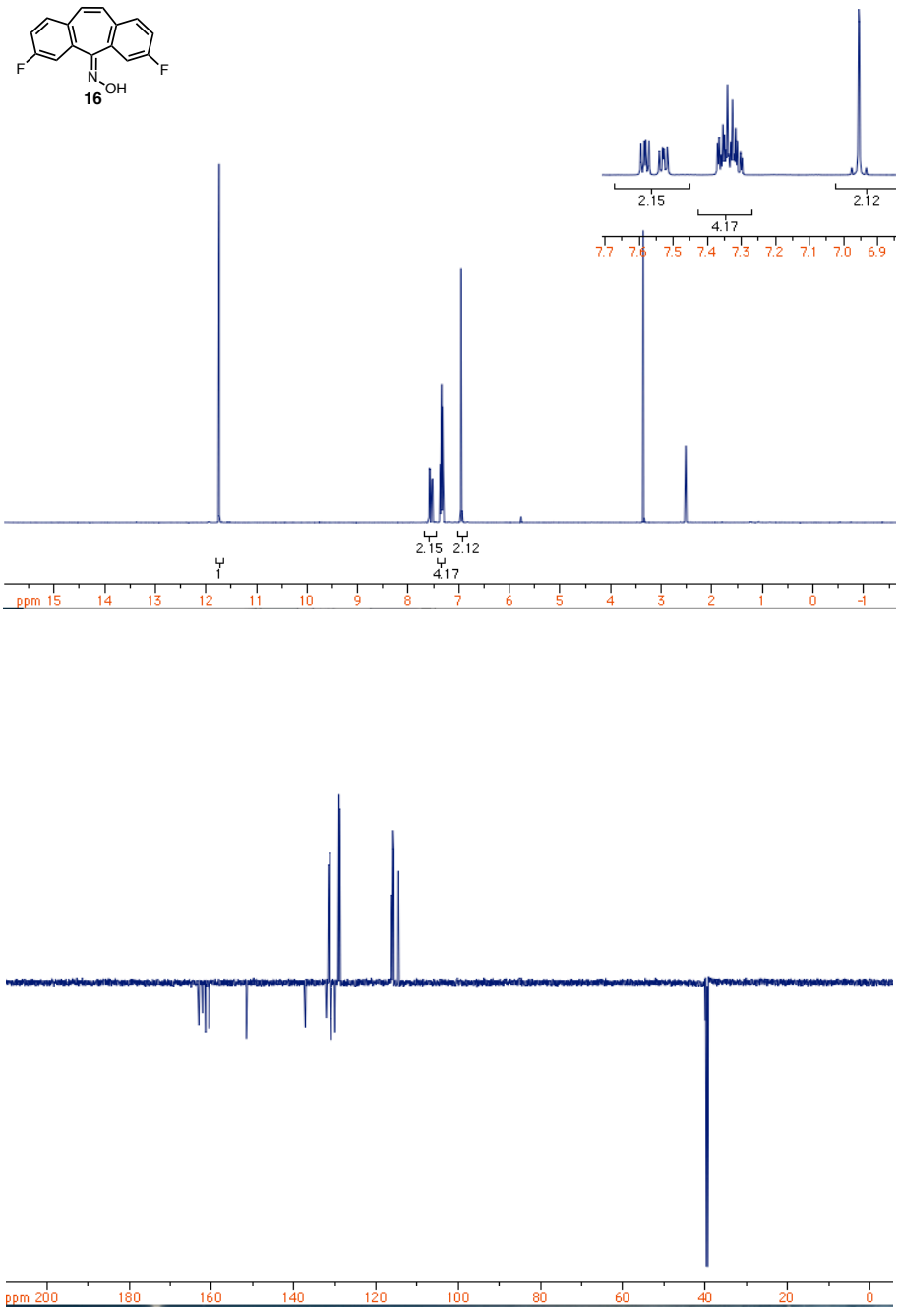

Figure 2.12. ^{1}H (top) and ^{13}C DEPT-q (bottom, CH_2 down) NMR spectra for compound **16**.

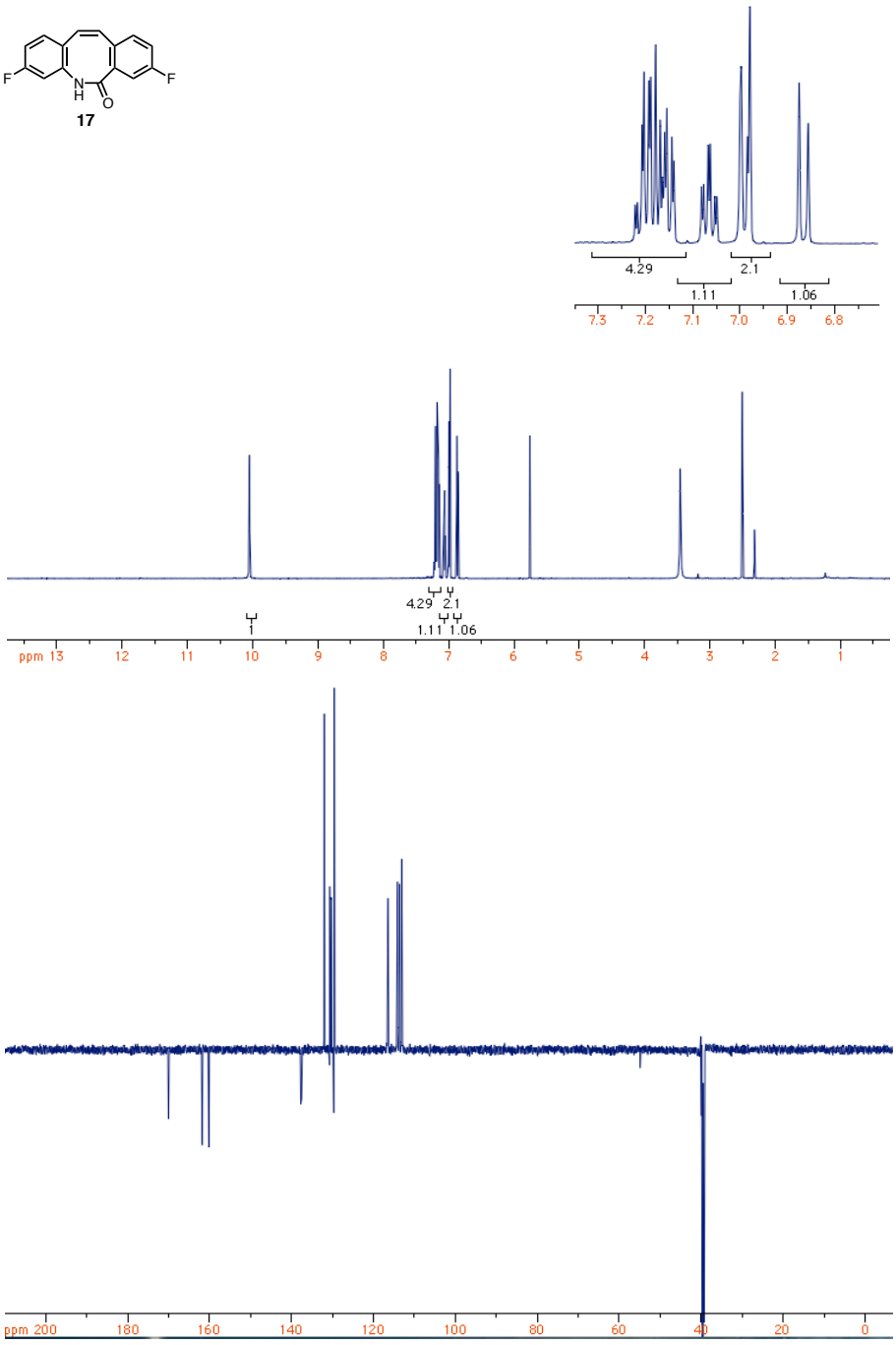

Figure 2.13. ^{1}H (top) and ^{13}C DEPT-q (bottom, CH_2 down) NMR spectra for compound **17**.

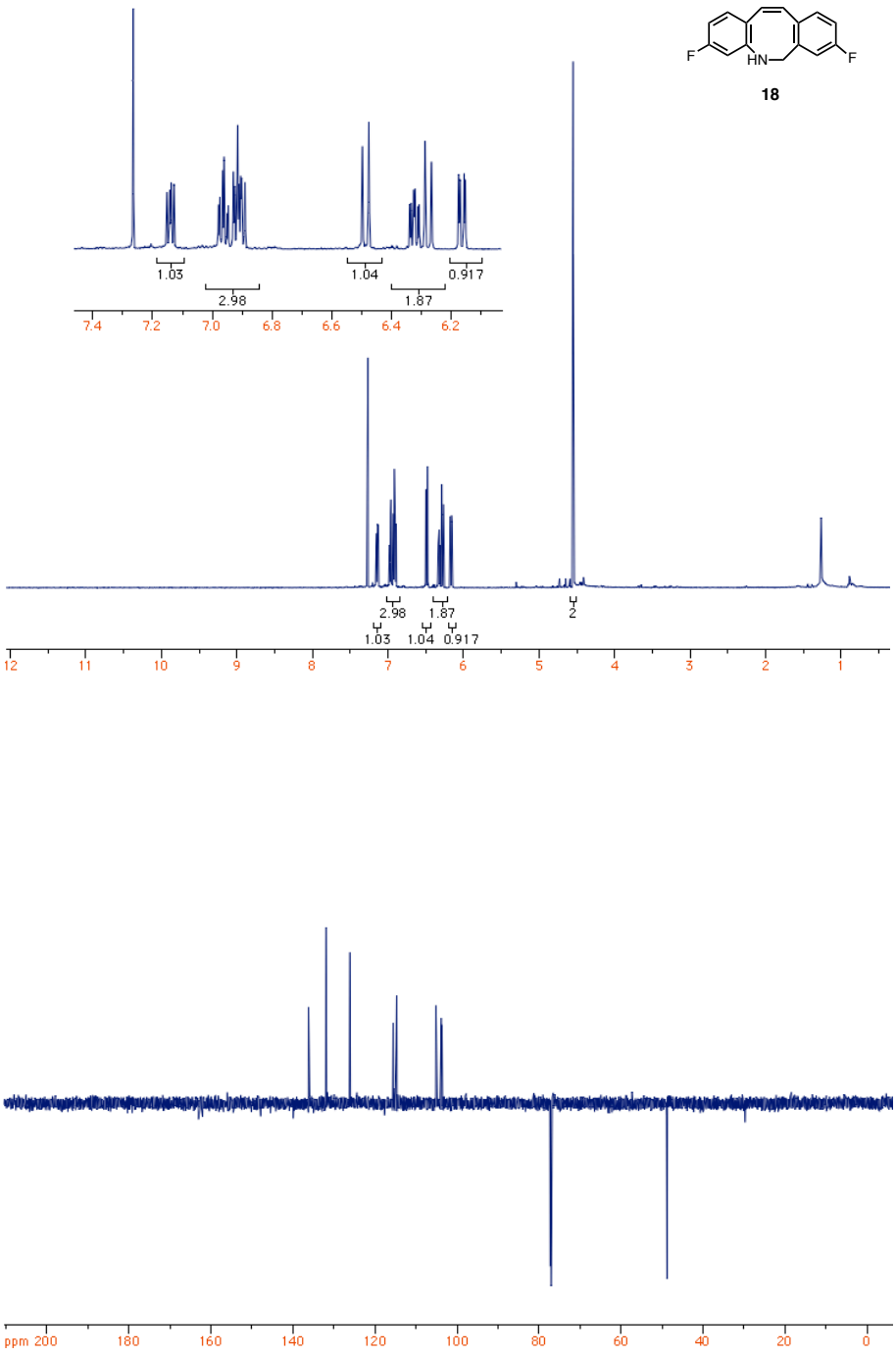

Figure 2.14. ^{1}H (top) and ^{13}C DEPT-q (bottom, CH_2 down) NMR spectra for compound **18**.

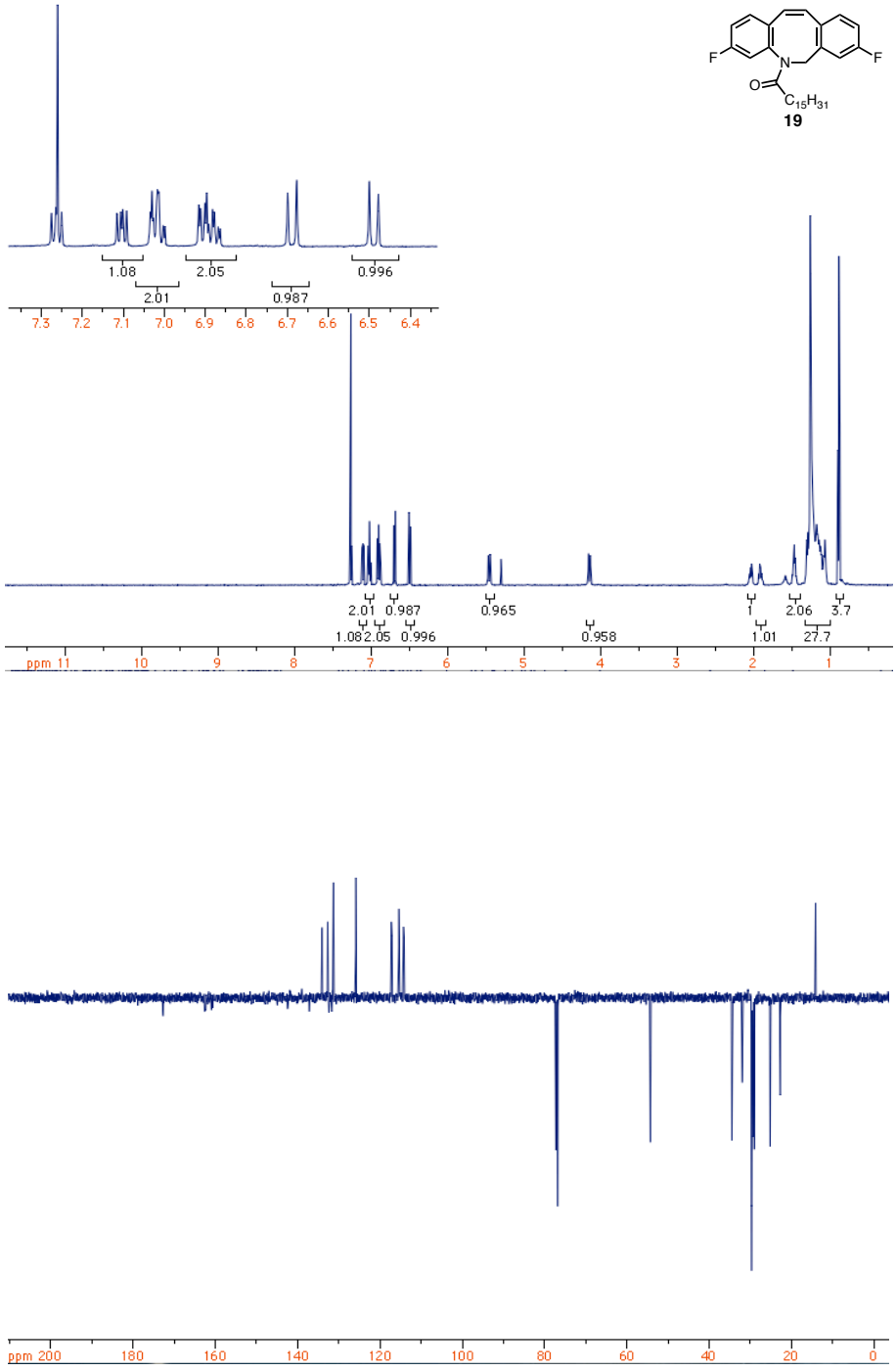

Figure 2.15. ^{1}H (top) and ^{13}C DEPT-q (bottom, CH_2 down) NMR spectra for compound **19**.

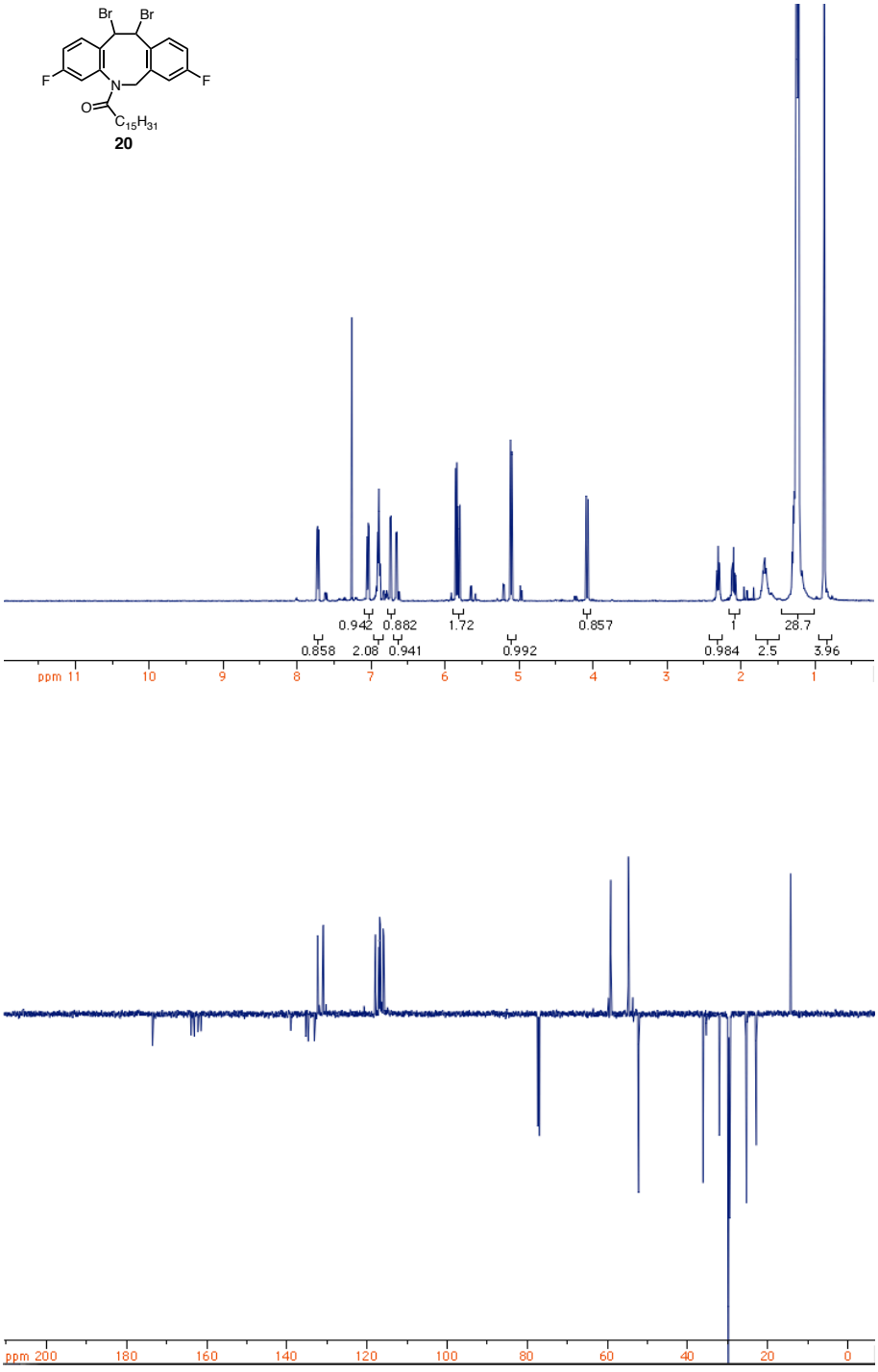

Figure 2.16. ^{1}H (top) and ^{13}C DEPT-q (bottom, CH_2 down) NMR spectra for compound **20**.

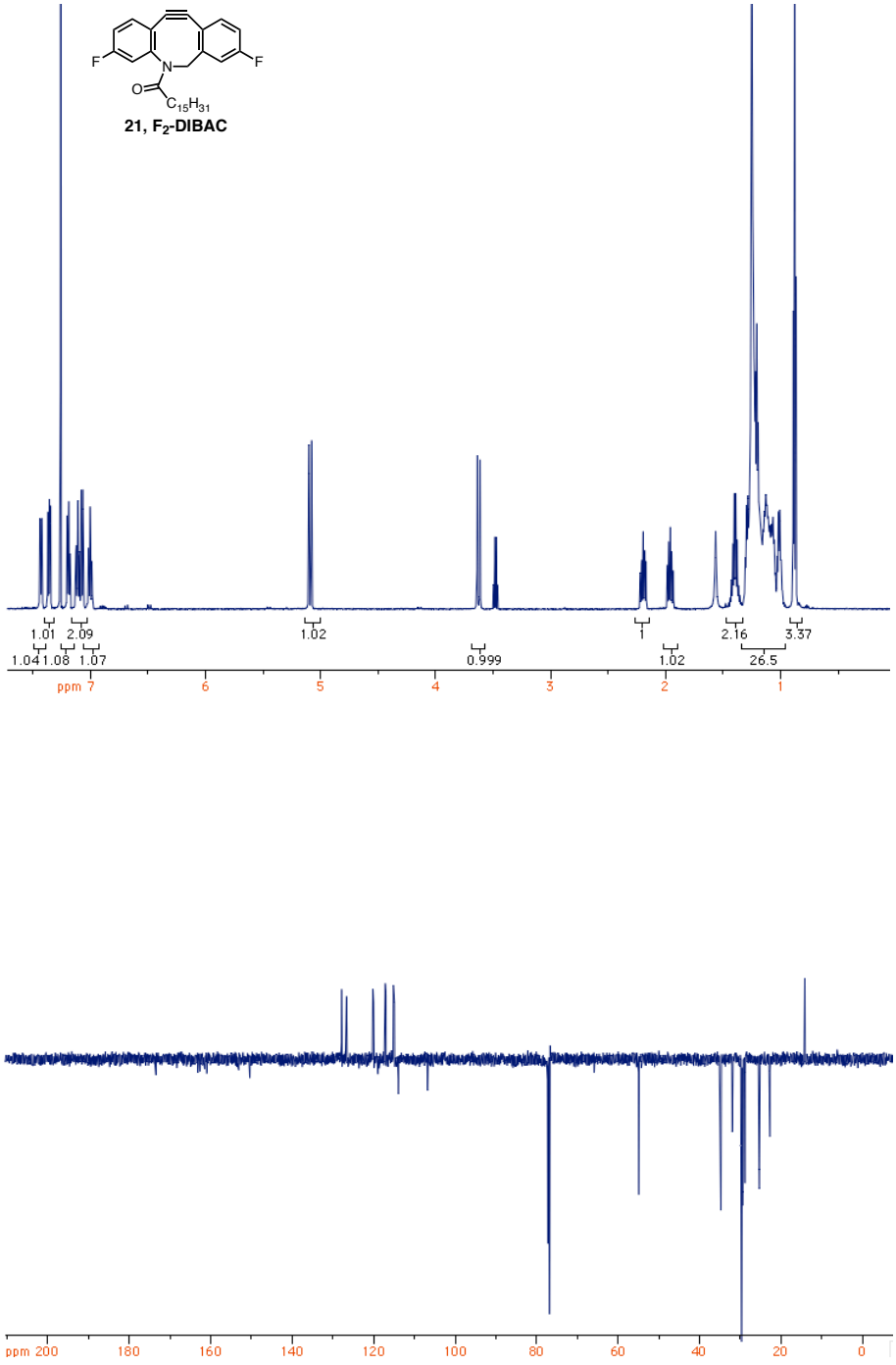

Figure 2.17. ^{1}H (top) and ^{13}C DEPT-q (bottom, CH_2 down) NMR spectra for compound **21**.

2.6. References

(1) Blomquist, A. T.; Liu, L. H. *J. Am. Chem. Soc.* **1953**, *75*, 2153.

(2) Wittig, G.; Krebs, A. *Chem. Ber.* **1961**, *94*, 3260.

(3) Debets, M. F.; van Berkel, S. S.; Dommerholt, J.; Dirks, A. T. J.; Rutjes, F. P. J. T.; van Delft, F. L. *Acc. Chem. Res.* **2011**, *44*, 805.

(4) Krebs, A.; Wilke, J. In *Wittig Chemistry*; Springer Berlin Heidelberg, 1983; Vol. 109, pp. 189–233.

(5) Krebs, A.; Kimling, H. *Tett. Lett.* **1970**, *11*, 761.

(6) Krebs, A.; Kimling, H. *Angew. Chem. Int. Ed.* **1971**, *10*, 509.

(7) Kolb, H. C.; Finn, M. G.; Sharpless, K. B. *Angew. Chem. Int. Ed.* **2001**, *40*, 2004.

(8) Agard, N. J.; Prescher, J. A.; Bertozzi, C. R. *J. Am. Chem. Soc.* **2004**, *126*, 15046.

(9) Winterfeldt, E. *Angew. Chem. Int. Ed.* **1967**, *6*, 423.

(10) de Almeida, G.; Sletten, E. M.; Nakamura, H.; Palaniappan, K. K.; Bertozzi, C. R. *Angew. Chem. Int. Ed.* **2012**, *51*, 2443.

(11) Sletten, E. M.; Bertozzi, C. R. *Acc. Chem. Res.* **2011**, *44*, 666.

(12) Garcia-Hartjes, J.; Dommerholt, J.; Wennekes, T.; van Delft, F. L.; Zuilhof, H. *Eur. J. Org. Chem.* **2013**, *2013*, 3712.

(13) Debets, M. F.; van Berkel, S. S.; Schoffelen, S.; Rutjes, F. P. J. T.; van Hest, J. C. M.; van Delft, F. L. *Chem. Commun.* **2010**, *46*, 97.

(14) Kuzmin, A.; Poloukhtine, A.; Wolfert, M. A.; Popik, V. V. *Bioconj. Chem.* **2010**, *21*, 2076.

(15) Jewett, J. C.; Sletten, E. M.; Bertozzi, C. R. *J. Am. Chem. Soc.* **2010**, *132*, 3688.

(16) Gordon, C. G.; Mackey, J. L.; Jewett, J. C.; Sletten, E. M.; Houk, K. N.; Bertozzi, C. R. *J. Am. Chem. Soc.* **2012**, *134*, 9199.

(17) Chigrinova, M.; McKay, C. S.; Beaulieu, L.-P. B.; Udachin, K. A.; Beauchemin, A. M.; Pezacki, J. P. *Org. Biomol. Chem.* **2013**, *11*, 3436.

(18) Lallana, E.; Fernandez-Trillo, F.; Sousa-Herves, A.; Riguera, R.; Fernandez-Megia, E. *Pharm. Res.* **2012**, *29*, 902.

(19) Lallana, E.; Riguera, R.; Fernandez-Megia, E. *Angew. Chem. Int. Ed.* **2011**, *50*, 8794.

(20) DeForest, C. A.; Sims, E. A.; Anseth, K. S. *Chem. Mater.* **2010**, *22*, 4783.

(21) Beckmann, E. *Chem. Ber.* **1886**, *20*, 2580.

(22) Sachin, K.; Jadhav, V. H.; Kim, E.-M.; Kim, H. L.; Lee, S. B.; Jeong, H.-J.; Lim, S. T.; Sohn, M.-H.; Kim, D. W. *Bioconj. Chem.* **2012**, *23*, 1680.

(23) Campbell-Verduyn, L. S.; Mirfeizi, L.; Schoonen, A. K.; Dierckx, R. A.; Elsinga, P. H.; Feringa, B. L. *Angew. Chem. Int. Ed.* **2011**, *50*, 11117.

(24) Eaton, P. E.; Carlson, G. R.; Lee, J. T. *J. Org. Chem* **1973**, *38*, 4071.

(25) Mücke, P.; Zabel, M.; Edge, R.; Collison, D.; Clément, S.; Záliš, S.; Winter, R. F. *J. Organomet. Chem.* **2011**, *696*, 3186.

(26) Thompson, W. J.; Anderson, P. S.; Britcher, S. F.; Lyle, T. A.; Thies, J. E.; Magill, C. A.; Varga, S. L.; Schwering, J. E.; Lyle, P. A.; Christy, M. E. *J. Med. Chem.* **1990**, *33*, 789.

(27) Schmuck, C.; Wienand, W. *Synthesis* **2002**, *2002*, 0655.

(28) Wei, Y.; Chen, C.-T. *J. Am. Chem. Soc.* **2007**, *129*, 7478.

(29) Liu, C.; Li, T.; Rosi, N. L. *J. Am. Chem. Soc.* **2012**, *134*, 18886.

Chapter 3

Properties of Poly(ethylene glycol) Hydrogels Cross-Linked via Strain Promoted Alkyne-Azide Cycloaddition (SPAAC)

This chapter has been reprinted with permission from Biomacromolecules; Sabrina M. Hodgson, Emilia Bakaic, S. Alison Stewart, Todd Hoare and Alex Adronov, **2016**, *17*, 1093-1100, DOI: 10.1021/acs.biomac.5b01711.

Sabrina Hodgson primarily planned this study. Sabrina Hodgson synthesized all of the precursor polymers and the resulting hydrogels. Sabrina Hodgson carried out the mechanical and rheological tests of the hydrogels with the help of Emilia Bakaic and S. Alison Stewart. Emilia Bakaic performed the biological assays with the hydrogels.

Abstract

A series of poly(ethylene glycol) (PEG) hydrogels was synthesized using the Strain-Promoted Alkyne-Azide Cycloaddition (SPAAC) between PEG chains terminated with either aza-dibenzocyclooctynes or azide functionalities. The gelation process was found to occur rapidly upon mixing the two components in aqueous solution without the need for external stimuli or catalysts, making the system a candidate for use as an injectable hydrogel. The mechanical and rheological properties of these hydrogels were found to be tuneable by varying the polymer molecular weight and the number of crosslinking groups per chain. The gelation times of these hydrogels ranged from 10 to 60 seconds at room temperature. The mass-based swelling ratios varied from 45 to 76 at maximum swelling (relative to the dry state) while the weight percent of polymer in these hydrogels ranged from 1.31 to 2.05 %, demonstrating the variations in amount of polymer required to maintain the structural integrity of the gel. Each hydrogel degraded at a different rate in PBS at pH = 7.4, with degradation times ranging from 1 to 35 days. By changing the composition of the two starting components, it was found that the Young's modulus of each hydrogel could be varied from 1 to 18.1 kPa. Hydrogel incubation with bovine serum albumin showed minimal protein adsorption. Finally, a cell cytotoxicity study of the precursor polymers with 3T3 fibroblasts demonstrated that the azide- and strained alkyne-functionalized PEGs are non-cytotoxic.

3.1. Introduction

Hydrogels are three-dimensional polymer networks that, once swollen in water, have the ability to house important biological therapeutics.[1] The porous scaffold of hydrogels is ideal for applications in controlled drug release,[2] cell therapy,[3] wound dressing,[4] and tissue engineering[5] (*i.e.* repairing and regenerating tissues and organs). Hydrogels closely resemble the natural extracellular matrix (ECM) of the body[6,7] and, if made using biocompatible constituents, can protect encapsulated materials from host rejection.[8] Hydrogels made of synthetic polymers pose an advantage over those made with natural polymers, largely owing to the increased amount of structural control, reproducibility of synthesis, and reduced risk of endotoxin contamination that they provide. Some examples of synthetic hydrogel precursor polymers include poly(2-hydroxyethyl methacrylate) (PHEMA),[9,10] poly(*N*-isopropylacrylamide) (PNIPAAm),[11] poly(vinyl alcohol) (PVA),[12–14] poly(oligoethylene glycol methacrylate) (POEGMA),[15] and poly(ethylene glycol) (PEG).[7,16]

PEG is an excellent choice for a hydrogel material. It has been used for numerous medical and biological applications in various fields of research,[16–20] and is commercially available as a laxative,[21] in lubricating eye drops,[22] and as an excipient in many pharmaceutical products.[23] As a surface coating, it has been shown to significantly reduce protein adsorption and thus minimize the immune response to biomaterials.[24–26] It is also used to increase circulation time for therapeutic agents, which leads to reduced toxicity, lower required drug loading, and longer dosing intervals.[27–29] These attributes have also led to extensive investigation into the use of PEG as a hydrogel material for tissue engineering and cell delivery.[30] For example, Anseth and coworkers have reported encapsulation of osteoblasts in RGD-modified PEG hydrogels for bone tissue engineering,[31] as well as chondrocytes to facilitate cartilaginous tissue production.[32] Additionally, Hubbell and coworkers have

used matrix metalloproteinase-degradable PEG hydrogels to direct differentiation of pluripotent cardioprogenitor cells.[33]

Recently, there has been great emphasis on "injectable" hydrogel delivery, which involves hydrogel compositions that crosslink and form a gel post-injection into the host via syringe.[34] The advantage to this method is the ability to simply inject the hydrogel to the target area without requiring a surgical procedure. The cross-linking reaction for an injectable system must be fast and achievable under physiological conditions (pH and temperature). Importantly, the reaction should also be bio-orthogonal and should not liberate toxic by-products. Several reactions have been explored for polymer crosslinking to make hydrogels, such as Diels-Alder,[35,36] hydrazone formation,[37] Michael Addition,[38] Copper-Catalyzed Alkyne-Azide Cycloaddition (CuAAC),[39] and the Strain-Promoted Alkyne-Azide Cycloaddition (SPAAC), but each has its limitations. Some of these limitations include requiring high temperatures,[35] long curing times,[36,37] or toxic catalysts.[40–42] Of these options, SPAAC, which involves a rapid [3 + 2] cycloaddition reaction between a strained cyclooctyne and an azide, is highly promising. SPAAC does not require any reagents, catalysts, or external stimuli (i.e., UV light), and the resulting linkage is extremely stable, as it forms an irreversible triazole ring. The reaction is fast, efficient, bio-orthogonal and does not produce any by-products, making it ideal for hydrogel cross-linking.[43] Recently, this chemistry has been used successfully for bioconjugation,[44] suggesting its compatibility with biological systems. Furthermore, several reports describing PEG hydrogels made via SPAAC have recently appeared and have demonstrated these hydrogels to be cytocompatible,[45,46] with easily modified degradation times that depend on the functional group chemistry used to connect PEG with the strained alkyne or azide.[43,47] Anseth and co-workers have additionally taken advantage of the UV-transparency of PEG to spatiotemporally regulate photocleavage in a

SPAAC crosslinked hydrogel.[48–50] However, a disadvantage of SPAAC is that production of functional cyclooctynes, such as derivatives of the relatively reactive aza-dibenzocyclooctyne (DIBAC), involves multi-step synthesis that is typically done on small scale. We have recently reported an optimized synthesis of DIBAC, enhancing its viability for large-scale production and use.[51] With a facile route to gram-quantities of DIBAC, its use in SPAAC-crosslinking of hydrogels can be extensively explored in a variety of biomaterials, drug delivery, and extracellular matrix applications. Other reports of SPAAC-crosslinked PEG hydrogels have been reported with less reactive cyclooctynes, such as the recent reports by Zhong et al.[52,53] These cyclooctynes are less reactive than DIBAC, and therefore the respective PEG hydrogels exhibit longer gelation times (several minutes). Despite the aforementioned reports of SPAAC-crosslinked PEG hydrogels, the mechanical and rheological properties of PEG hydrogels functionalized with the more reactive cyclooctyne, DIBAC, remain relatively underexplored. Herein we describe the gelation kinetics, Young's modulus (stiffness), rate of degradation, degree of swelling, effect of functional group ratio on the extent of crosslinking, as well as protein adsorption and cytotoxicity studies for a series of eight PEG hydrogels formed through the SPAAC reaction. These rheological, mechanical, and biological properties have important implications for their use in a variety of tissue engineering applications.

3.2. Materials and Methods

3.2.1. Synthetic Procedures

General

All reagents were obtained from commercial sources and were used as received without further purification, unless otherwise stated. DIBAC was

synthesized as described previously.[51,54,55] The azide monomer was synthesized according to the procedure developed by Song and coworkers.[56] ^{1}H NMR spectra were recorded on Bruker Avance 600 MHz spectrometers. Gel Permeation Chromatrography (GPC) was performed on a Waters 2695 Separations Module, equipped with a Waters 2414 refractive-index detector and a Jordi Fluorinated DVB mixed-bed column. Polystyrene standards were used for calibration, with THF as the eluent at a flow rate of 3.0 mL/min. UV-Vis spectra were measured on a Cary 5000 spectrophotometer. MALDI spectra were acquired using a Bruker Ultraflextreme spectrometer in positive ion mode using dithranol as matrix and PEG as an external standard. Samples were mixed in a ratio of 10:5:1 matrix:polymer:saturated $NaNO_3$ in THF.

$PEG_n(DIBAC)_2$, n = 4.6k, 10k, 20k

The synthetic procedure to functionalize PEG-diol with a cyclooctyne-acid via Steglich esterification was reported by Song and co-workers.[45] A slightly modified version of this procedure was used, an example of which is described for the polymer $PEG_{10k}(DIBAC)_2$: An oven-dried flask equipped with a stir bar was charged with DIBAC-acid (0.09 g, 0.3 mmol), PEG-10k diol (1.0 g, 0.1 mmol), DMAP (0.006 g, 0.05 mmol) and CH_2Cl_2 (7 mL). EDC (0.16 g, 25 mmol) was then added to the flask along with additional CH_2Cl_2 (3 mL) to wash down the sides of the flask. The reaction mixture was then stirred overnight at room temperature under an argon atmosphere. The reaction mixture was then diluted with CH_2Cl_2 (40 mL) and washed with 1M $NaHSO_4$ (3 x 50 mL), and brine (10 mL). The organic layers were collected and dried over Na_2SO_4. The solution was concentrated under reduced pressure to a volume of ca. 10 mL, followed by precipitation into diethyl ether to yield a white powder (0.94 g, 88%). ^{1}H-NMR (600 MHz, $CDCl_3$): δ = 7.66 (d, *J* = 7.2 Hz, 2 H), 7.62 (d, *J* = 7.8 Hz, 2 H), 7.52-7.46 (m, 6 H), 7.39-7.33 (m, 4 H), 7.30

(d, *J* = 7.2 Hz, 2 H), 5.03 (d, *J* = 13.8 Hz, 2 H), 4.03-3.99 (m, 2 H), 3.95-3.91 (m, 2 H), 3.57-3.43 (m, 923 H), 2.32-2.27 (m, 2 H), 1.84-1.79 (m, 2 H).

$PEG_{10k}(N_3)_m$, m = 6, 9, 12

The synthetic procedure describing the ring-opening polymerization of 5,5-bis(azidomethyl)-1,3-dioxan-2-one, an azido-functionalized cyclic carbonate monomer, was previously outlined by Song and co-workers.[45,56] A representative procedure for $PEG_{10k}(N_3)_9$ is as follows: An oven-dried flask equipped with a magnetic stir bar was charged with 5,5-bis(azidomethyl)-1,3-dioxan-2-one (0.16 g, 0.75 mmol) and PEG-10k diol (1.5 g, 0.15 mmol). The flask was opened to argon atmosphere, and dry CH_2Cl_2 (10 mL) was added via syringe. Subsequently, DBU (0.009 mL, 0.06 mmol) was added to initiate the ring-opening oligomerization. After stirring for 4 h, benzoic acid (0.018 g, 0.12 mmol) was added to neutralize the DBU. After stirring for 10 min, the polymer was isolated by precipitation into diethyl ether to yield a white powder (1.56 g, 96%). ^{1}H-NMR (600 MHz, $CDCl_3$): δ = 4.29-4.27 (m, 4 H), 4.10 (s, 9 H), 4.08 (s, 4 H), 3.71-3.69 (m, 6 H), 3.67-3.56 (m, 1160 H), 3.44 (s, 10 H), 3.41-3.38 (m, 8 H). GPC: $PEG_{10k}(N_3)_6$, M_n = 11272, PDI = 1.153; $PEG_{10k}(N_3)_9$, M_n = 11620, PDI = 1.159; $PEG_{10k}(N_3)_{12}$, M_n = 12119, PDI = 1.181. MALDI: $PEG_{10k}(N_3)_6$, M_n = 11070, PDI = 1.0025; $PEG_{10k}(N_3)_9$, M_n = 11194, PDI = 1.0013; $PEG_{10k}(N_3)_{12}$, M_n = 11142, PDI = 1.0014.

Fluorescein Isothiocyanate-Labeled Proteins[57,58]

Fluorescein isothiocyanate (FITC)-labeled bovine serum albumin (BSA-FITC) was prepared by dissolving 50 mg of BSA in a 100 mL 0.1 M carbonate buffer at pH = 9.0. Subsequently, FITC (1 mg) was added, and the solution was incubated at room temperature for a minimum of 12 h while stirring. The FITC-labeled protein was then dialyzed using 1,000 Da MWCO tubing against distilled deionized water and lyophilized to dryness. The isolated

protein conjugates were stored at -20 °C in the dark. A calibration curve was prepared for BSA-FITC by relating the protein concentration to the fluorescence signal (in PBS) at 495 nm and 519 nm for excitation and emission wavelengths. The linear concentration range determined from the calibration curve for BSA-FITC is 1 – 100 μg/mL (R^2 = 0.999).

3.2.2. Hydrogel Preparation

Functionalized PEG hydrogels were prepared through the rapid mixing of complementary strained alkyne ($PEG_n(DIBAC)_2$, n = 4.6, 10, or 20 kDa) and azide-functionalized ($PEG_{10k}(N_3)_m$, m = 6, 9, or 12) PEG polymers. Complete mixing of the functionalized precursor polymers was achieved by co-extrusion using a double barrel syringe (Medmix, L-System, 2.5 mL) with a static mixer at the outlet of the syringe. Each barrel of the syringe was loaded with a complementary precursor polymer dissolved in 10 mM PBS. In all hydrogels, the functional group ratio of strained alkynes to azides remained 1:2, respectively. Considering that the number of strained alkynes or azides present *per polymer chain* is controlled as a result of the chain-end functionalization method, it was possible to maintain the 1:2 strained alkyne:azide ratio by preparing each precursor polymer solution at the appropriate mass concentration (see Table 3.1).

Table 3.1. Precursor Polymer and Functional Group Concentrations Used to Maintain 1:2 Strained Alkyne:Azide Functional Group Ratio Across All Tested Hydrogels.

Polymer	Polymer Concentration (wt%)	Functional Group Concentration (mol/mL)
$PEG_{4.6k}(DIBAC)_2$	4.6	$2x10^{-5}$
$PEG_{10k}(DIBAC)_2$	10	$2x10^{-5}$
$PEG_{20k}(DIBAC)_2$	20	$2x10^{-5}$
$PEG_{10k}(N_3)_6$	6.7	$4x10^{-5}$
$PEG_{10k}(N_3)_9$	4.4	$4x10^{-5}$
$PEG_{10k}(N_3)_{12}$	3.3	$4x10^{-5}$

Hydrogel disks used for swelling, degradation, and rheology experiments were prepared through extrusion of the reactive polymer precursors into cylindrical silicone rubber molds (diameter = 7 mm, volume = 300 μL). Unless stated otherwise, gels were incubated at room temperature for at least 2 h to ensure complete gelation prior to testing. Each of the hydrogels composed of $PEG_n(DIBAC)_2$ and $PEG_{10k}(N_3)_m$ was named using the code $n(D)_2$-10k$(N)_m$, where n is the molecular weight of PEG on the strained alkyne polymer, D denotes DIBAC, N denotes azide, and m is the number of azide groups on the azide-decorated polymer.

3.2.3. Characterization

3.2.3.1. UV-Vis Data

All spectrophotometric absorption measurements were performed on a Cary 5000 spectrometer operating in dual beam mode. Sample preparation involved sandwiching the PEG hydrogels between two quartz slides. To maintain a constant hydrogel thickness, Scotch tape (thickness = 0.0625 mm) was adhered to the top and bottom ends of one of the quartz slides,

approximately 0.5 cm in length from the edge of the slide. For this experiment, solutions of only two polymers, $PEG_{4.6k}(DIBAC)_2$ and $PEG_{10k}(N_3)_9$, were prepared at various DIBAC:azide ratios. To vary the functional group ratio, the concentration of $PEG_{4.6k}(DIBAC)_2$ was kept constant at 4.6 wt%, while the concentration of $PEG_{10k}(N_3)_9$ was varied based on the desired strained alkyne to azide functional group ratio: 1.1 wt% (strained alkyne to azide ratio = 1 : 0.5), 2.2 wt% (1 : 1), 3.3 wt% (1 : 1.5), 4.4 wt% (1 : 2), and 5.5 wt% (1 : 2.5). Control samples containing either just $PEG_{4.6k}(DIBAC)_2$ or just $PEG_{10k}(N_3)_9$ (the 1 : 0 and 0 : 1 strained alkyne to azide ratios, respectively) were prepared by replacing the missing polymer (azide- or strained alkyne-decorated PEG) with PBS. 50 μL of each corresponding polymer solution was pipetted into a snap-cap vial and the solutions were quickly mixed through aspiration with a pipette. This was followed by placing 2-3 drops of the mixture onto the middle of the taped quartz slide and subsequently compressing the gelation mixture with the second slide. A small clamp was used to hold the slides together during the measurement process. The hydrogel was allowed to fully react, and any excess hydrogel was cleaned off the sides prior to acquiring the UV-Vis spectra.

3.2.3.2. Swelling and Degradation Kinetics

Swelling kinetics of the PEG hydrogels were measured at room temperature in 10 mM PBS at pH 7.4. Hydrogel disks were placed into cell culture inserts that were subsequently placed in a 12-well cell culture plate and completely submerged in 10 mM PBS (4 mL/well). At predetermined time intervals, the cell culture inserts with hydrogels were removed from the wells, the PBS drained, and the hydrogel gently dabbed with paper towel to wick off any non-absorbed PBS prior to gravimetric analysis. PEG hydrogels were then re-submerged in a fresh 4 mL aliquot of PBS solution. This process

was repeated until maximum swelling of the gel was reached, or the hydrogel stopped increasing in weight. The hydrogel mass-based swelling ratio is defined as: swelling ratio = $(W_s - W_d)/W_d$, where W_s is the weight of the hydrogel at maximum swelling (*i.e.* the last measurement taken prior to degradation) and W_d is the weight of the dried polymer in the hydrogel (extrapolated based on initial hydrogel mass and concentration of polymer).[57] Degradation kinetics were subsequently evaluated by continuing the swelling experiment until no separate phase was observed between the hydrogel and the PBS solution.

3.2.3.3. Hydrogel Mechanics

Mechanical properties of the hydrogels were determined using a home-built apparatus that measures the contact mechanics between a glass hemisphere and an elastic hydrogel. This relationship is described by the Hertzian theory as

$$F = \frac{4ER^{1/2}}{3(1-\nu^2)} d^{3/2} \quad (3.1)$$

where F is the force, d is the deformation, R is the radius of the glass hemispherical indenter, ν is the Poisson's ratio and E is the Young's modulus of the elastic substrate.[59] Each hydrogel was investigated using a compression method with a hemispherical indenter consisting of a glass melting point tube (VWR) with a hemispherical end (r = 0.83 mm) attached to a force transducer (Transducer Techniques, GSO series, 10 g full scale). After complete gelation of PEG hydrogel disks within the silicone rubber mold, 2 drops of silicone oil were added to the top of each hydrogel to prevent water evaporation, and then hydrogels were placed on an inverted microscope. The vertical position of the glass indenter was controlled with a servo motor, programmed to move the rounded end of the indenter to a

maximum depth of 10 % of gel thickness. The indenter contacts the gel at a constant speed, the exact value of which is not required to calculate the Young's modulus. The force transducer measures the force relative to time and vertical position of the indenter. This was repeated in triplicate at different positions for each gel. The Young's modulus (YM) was obtained using the equation described by the Hertzian theory, rearranged to isolate YM as the slope, when plotting the measured force (F) as a function of deformation (d):

$$F = E\frac{4R^{1/2}d^{3/2}}{3(1-\nu^2)} \quad (3.2)$$

The Poisson's ratio is assumed to be ν = 0.5 based on hydrogels having similar mechanical properties to elastic, rubber-like materials.[60]

3.2.4. Biological Evaluation

3.2.4.1. Protein Adsorption

Adsorption of bovine serum albumin to hydrogels was investigated using a reported technique.[57] Briefly, PEG hydrogels were formed inside the wells of a 96-well plate. All functionalized PEG precursors were sterilized via filtration through a 0.2 μm filter before aliquots of 30 μL of each precursor solution were extruded into each well and left overnight to ensure complete gelation. Once gelation was complete, 180 μL of 10 mM PBS was added to each well, and hydrogels were allowed to swell to equilibrium prior to protein addition (greater than 30 h as determined by swelling tests). Once equilibrium swelling was achieved, excess PBS was removed from the top of the gels and 60 μL of BSA-FITC solution (125, 250, 500 or 1000 μg/mL in PBS) was added. After 2 h of incubation at 37°C, the PEG hydrogels were rinsed to remove any free protein, and a fluorescence signal was measured

using a VICTOR 3 multi-label microplate reader and compared to the stock BSA-FITC solution controls. Each experiment was done in five replicates.

3.2.4.2. Cell Cytotoxicity

To determine the effects of the polymers on cells, an *in vitro* thiazolyl blue tetrazolium bromide (MTT) assay was used.[61] NIH 3T3 mouse fibroblasts were plated at a cell density of 1.0×10^4 cells per well in a 24-well plate of DMEM media supplemented with 10% calf bovine serum (CBS) and 1% penicillin. After 24 h of culture, the 3T3 mouse fibroblasts were exposed to PEG polymer concentrations ranging from 100 to 1000 μg/mL. Cell viability was then characterized after 24 h of polymer exposure by reading the absorbance of the MTT solution using a VICTOR 3 multi-label microplate reader operating at 570 nm and normalized against a 630 nm baseline to account for any non-specific scattering. All experiments were done in replicates of 4.

3.3. Results and Discussion

3.3.1. Preparation of Polymers and Hydrogels

Following our previously reported procedures,[51] we prepared DIBAC on multi-gram scale and used it to functionalize the ends of various molecular weight poly(ethylene glycol) (PEG) chains according to literature protocols (Scheme 3.1).[45] The three PEG chains, with molecular weights of 4.6, 10 and 20 kDa, were chosen to assess the effect of chain length on hydrogel properties. ^{1}H-NMR spectroscopy was used to confirm complete esterification between PEG-diol and two DIBAC-acid groups, as indicated by the disappearance of the PEG-O<u>H</u> resonance at 4.6 ppm (Figure 3.1). The appearance of peaks corresponding to the aromatic groups of DIBAC

between 7.3 and 7.7 ppm was also observed and corroborated the complete functionalization.

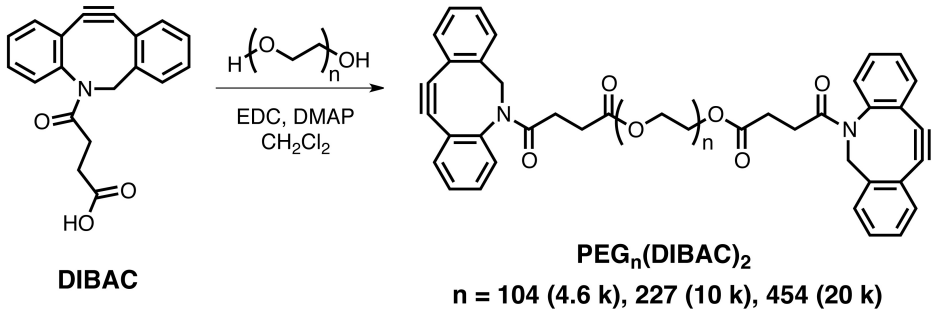

Scheme 3.1. Synthetic scheme for the synthesis of $PEG_n(DIBAC)_2$ from DIBAC.

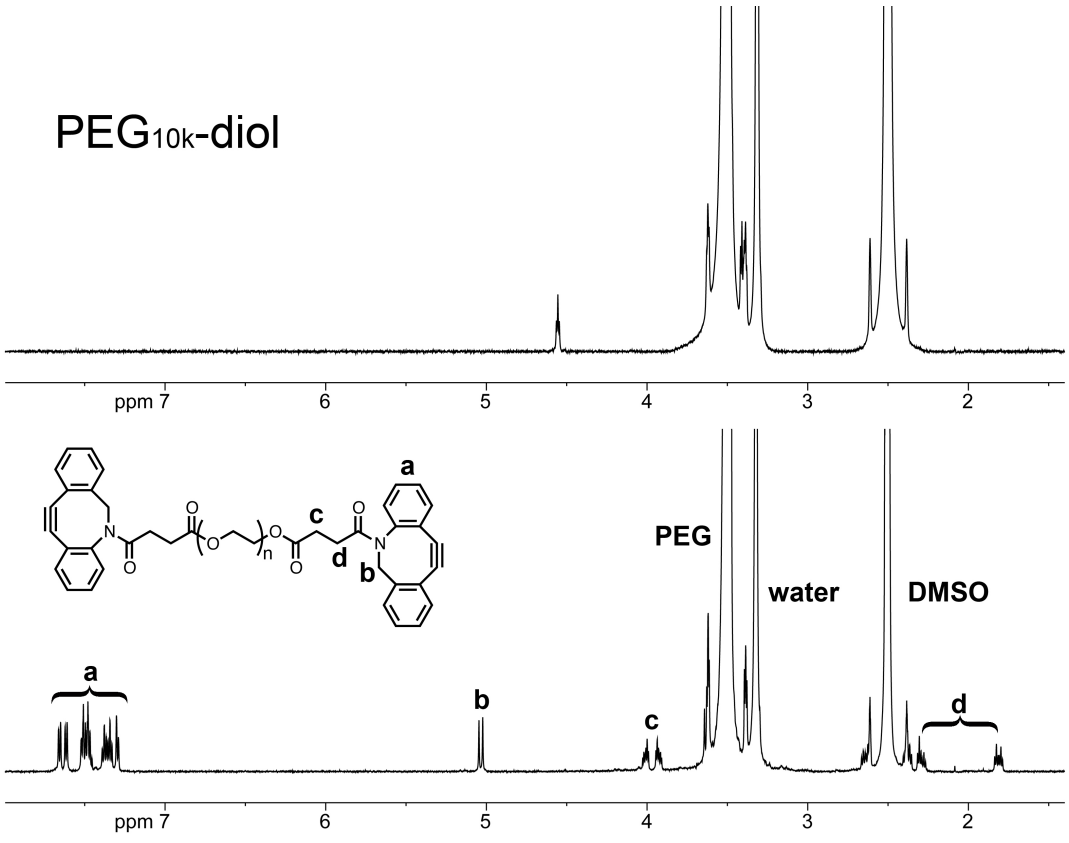

Figure 3.1. ^1H NMR spectra in DMSO-d_6 of PEG_{10k}-diol (top) and $PEG_{10k}(DIBAC)_2$ (bottom).

Preparation of the $PEG_{10k}(N_3)_m$ polymers was carried out by the ring-opening polymerization of a cyclic azide-functionalized monomer according to the procedures of Song and co-workers (Scheme 3.2).[45,56] Synthesis of the cyclic azide-functionalized monomer was first reported by Zhuo and coworkers.[62] The number of azido groups per PEG chain was controlled by adding specific amounts of the azide monomer to the reaction mixture relative to PEG. Three batches of $PEG_{10k}(N_3)_m$ polymer were prepared with varying average numbers of azide groups *m*, where *m* = 6, 9, and 12. It was found that polymer chains with greater than 12 azide groups were not water soluble; thus, 12 was the upper limit for azide incorporation. ^{1}H NMR was used to determine the degree of polymerization of each product (Figure 3.2). This was accomplished by comparing the integration of the signal at 4.3 ppm, corresponding to the methylene protons at each terminus of the PEG block, to the integration of the signals between 3.40 ppm and 3.45 ppm, corresponding to the methylene protons adjacent to each azide. Several signals are observed for these methylene protons as each unit is in a slightly different environment. Two separate signals are also observed for the methylene protons adjacent to carbonate groups on the polymer backbone (at 4.09 ppm and 4.11 ppm) which integrate to 16 protons for the internal portion of the polymer block and 4 protons for the outermost carbonate protons in the case of $PEG_{10k}(N_3)_{12}$.

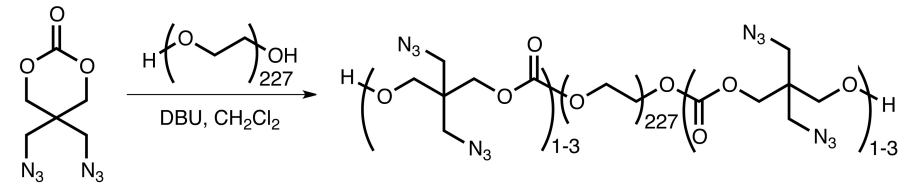

Azide Monomer

$PEG_{10k}(N_3)_m$ m = 6, 9, 12

Scheme 3.2. Synthetic scheme for $PEG_{10k}(N_3)_m$ from 5,5-bis(azidomethyl)-1,3-dioxan-2-one (azide monomer).

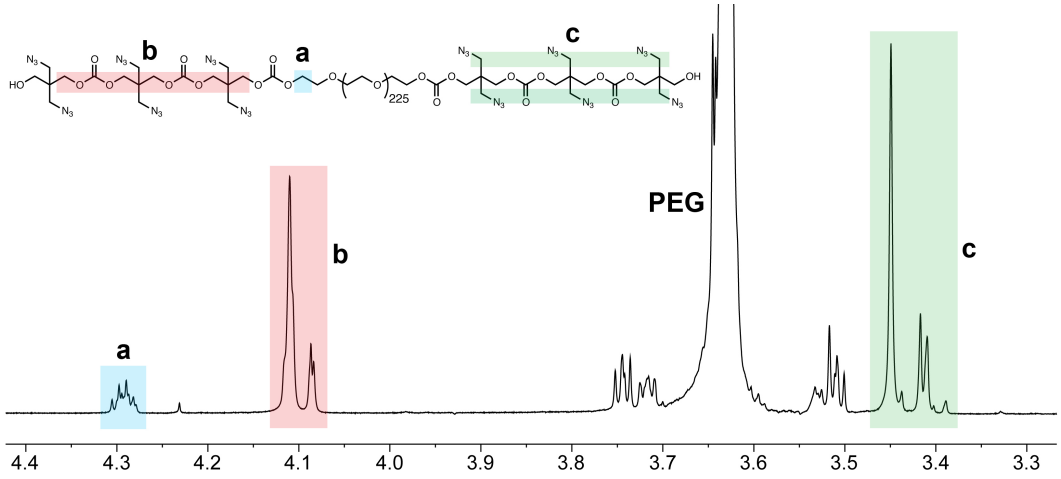

Figure 3.2. ^{1}H NMR spectrum in $CDCl_3$ of $PEG_{10k}(N_3)_{12}$.

3.3.2. Hydrogel Formation and Gelation Time

Formation of PEG hydrogels was achieved using a double-barrel syringe, with one barrel filled with a solution of one of the three $PEG_n(DIBAC)_2$ polymers in PBS and the other barrel filled with a solution of one of the three $PEG_{10k}(N_3)_m$ polymers in PBS, both at the concentrations indicated in Table 3.1. To maintain constant relative volumes of strained alkyne polymer and azide polymer solutions (as required for "injectable" gelation through the double-barrel syringe) while maintaining a constant functional group ratio and functional group concentration, the mass fraction of polymer in each hydrogel composition was varied. The polymers were combined in a mixing channel prior to extrusion into a silicone rubber mold, where they quickly reacted to form a hydrogel without the need for external stimuli or catalysts (Figure 3.3).

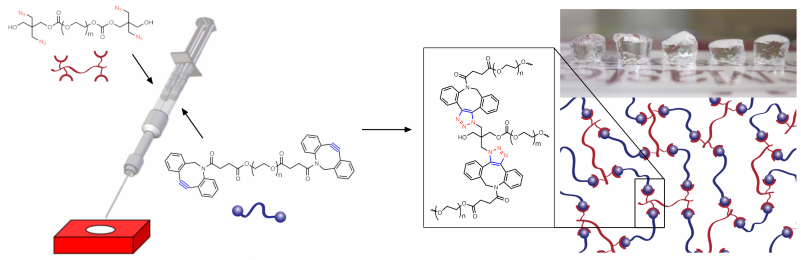

Figure 3.3. Graphical representation of hydrogel formation between $PEG_n(DIBAC)_2$ (blue polymer) and $PEG_{10k}(N_3)_m$ (red polymer) using a double barrel syringe (left). The photograph (top right) shows actual hydrogel disks produced, with a visual representation of an idealized hydrogel network formed between the strained alkyne (blue) and azide (red) polymers shown below.

Table 3.2. Functional Group and Polymer Concentrations Post-Gelation.

Hydrogel Composition (Ratio = 1:2 Strained Alkyne/Azide)	Total Functional Group Concentration (mol/mL)	Total PEG Concentration (wt%)	Gelation Time (s)
4.6k$(D)_2$-10k$(N)_6$	$3x10^{-5}$	5.65	60
4.6k$(D)_2$-10k$(N)_9$	$3x10^{-5}$	4.50	15
4.6k$(D)_2$-10k$(N)_{12}$	$3x10^{-5}$	3.95	15
10k$(D)_2$-10k$(N)_6$	$3x10^{-5}$	8.35	35
10k$(D)_2$-10k$(N)_9$	$3x10^{-5}$	7.20	10
10k$(D)_2$-10k$(N)_{12}$	$3x10^{-5}$	6.65	10
20k$(D)_2$-10k$(N)_6$	$3x10^{-5}$	13.35	**NO GELATION**
20k$(D)_2$-10k$(N)_9$	$3x10^{-5}$	12.20	40
20k$(D)_2$-10k$(N)_{12}$	$3x10^{-5}$	11.65	30

Table 3.2 outlines the final concentrations and gelation times for each of the hydrogel compositions. The functional group ratio of strained alkyne to azide for each polymer combination was maintained at 1:2, while the total functional group concentration was maintained at $3x10^{-5}$ mol/mL. Formation

of gels using a strained alkyne:azide ratio of 1:1 was also attempted but resulted in gelation for only 2 out of the 9 combinations, namely 10k$(D)_2$-10k$(N)_9$ and 10k$(D)_2$-10k$(N)_{12}$. Conversely, at a strained alkyne:azide ratio of 1:2, gelation occurred in 8 out of the 9 polymer combinations, as indicated in Table 3.2. The single combination that did not result in gelation at a 1:2 strained alkyne:azide ratio was 20k$(D)_2$-10k$(N)_6$, even though it had the highest polymer concentration. We hypothesize that this was the result of the low number of azide groups per PEG-azide and the high PEG-strained alkyne chain length separating reactive functionalities in this polymer combination, both leading to a low crosslink density even at the higher overall polymer weight fraction. For all other polymer combinations, rapid gelation was observed, with the fastest gelation occurring for the 10k$(D)_2$-10k$(N)_{12}$ and 10k$(D)_2$-10k$(N)_9$ compositions, both of which gelled in 10 seconds. The slowest gelation occurred with 4.6k$(D)_2$-10k$(N)_6$ and 20k$(D)_2$-10k$(N)_9$, with gelation times of 60 and 40 seconds, respectively. These gelation time differences result from the structural variations within each polymer combination, which impact the efficiency with which the alkyne- and azide-functionalized polymers react. However, the difference in gelation time among the various polymer combinations is small, with even the slowest hydrogel forming in under a minute. The fast gelation times are due to the fast reaction kinetics that comes from using DIBAC as the strained cyclooctyne, since it is one of the more reactive cyclooctynes (k = 0.31 $M^{-1}s^{-1}$). Comparatively, most other cyclooctynes are an order or magnitude slower, or more, such as the commonly used ALO (k = 0.0013 $M^{-1}s^{-1}$) DIBO (k = 0.057 $M^{-1}s^{-1}$) or DIFO (k = 0.076 $M^{-1}s^{-1}$).[63] This demonstrates the efficient nature of the SPAAC reaction with DIBAC, making it an ideal crosslinking reaction for injectable hydrogels.

3.3.3. UV-Vis Analysis of Cross-Linking

To understand why a 1:2, rather than a 1:1 strained alkyne:azide ratio was required to achieve efficient gelation, UV-Vis absorption measurements were carried out. The specific hydrogel investigated was the 4.6k$(D)_2$-10k$(N)_9$ composition, since this was a combination that gelled at a functional group ratio of 1:2, but not at 1:1. Absorption measurements were made for gelation attempts with different ratios of strained alkyne to azide, ranging from 1:0 to 1:2.5 (Figure 3.4). For the 1:0 ratio (only strained alkyne-decorated polymer), intense absorption peaks at approximately 290 and 310 nm were observed, attributable to the DIBAC terminal units of the polymer. Upon increasing the strained alkyne:azide ratio to 1:0.5 and 1:1, the UV-Vis data shows the expected decrease in the absorption attributed to DIBAC. Surprisingly, at a 1:1 ratio, all the DIBAC is not consumed, as significant absorption from unreacted strained alkyne is present (Figure 3.4). At 1:1.5, very little strained alkyne remains, but all DIBAC units are not consumed until a ratio of 1:2 is reached. Increasing the ratio to 1:2.5 resulted in no significant change beyond the 1:2 ratio. Note that the absorption spectrum of the azide polymer alone (functional group ratio of 0:1) showed no appreciable absorption across the entire spectral window. Overall, this data indicates that, at a 1:1 strained alkyne:azide ratio, the bulky DIBAC units might not be able to access all of the azide groups, likely due to steric hindrance imparted by the bulky DIBAC units relative to the spacing between the azide groups at the polymer chain ends. It is only when the number of azide groups is doubled that they are able to consume all the strained alkyne functionality. This explains why so few polymer combinations formed hydrogels at a 1:1 strained alkyne:azide ratio.

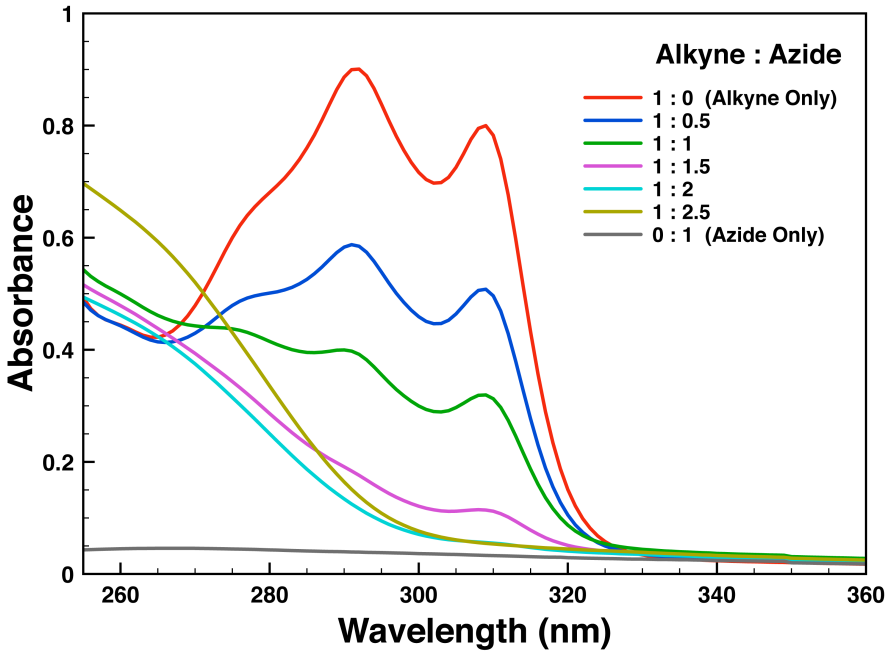

Figure 3.4. UV-Vis spectra of hydrogels made between $PEG_{4.6k}(DIBAC)_2$ and $PEG_{10k}(N_3)_9$ with varying functional group ratios of strained alkyne to azide.

3.3.4. Swelling and Degradation

The swelling and degradation profiles of each hydrogel composition were measured sequentially by weighing the hydrogels at pre-determined time intervals as they swelled and degraded in 10 mM PBS. The mass-based swelling ratios were calculated from the weight of the swollen hydrogel at the onset of degradation (defined as the initial time point at which a reduction in mass was observed) compared to the dry mass of the polymer used (Figure 3.5). The hydrogels with the highest swelling ratios (i.e., ability to retain the most water before losing mass), were $4.6k(D)_2$-$10k(N)_6$ and $10k(D)_2$-$10k(N)_6$, with average swelling ratios of 76 ± 9 and 69 ± 1 respectively. Each of these polymers degraded within 4 days (Table 3.3). Conversely, the lowest swelling ratios were observed for $10k(D)_2$-$10k(N)_{12}$ and $10k(D)_2$-$10k(N)_9$ (45 ± 1 and 49 ± 3), but these polymers took 35 and 27 days to degrade, respectively. This data seems to indicate that the use of

polymers bearing a larger number of azide end-groups results in a larger extent of crosslinking, and this leads to stronger gels that degrade more slowly. However, these gels also don't swell to a large extent. Conversely, gels composed of polymers with fewer azide end-groups are more loosely crosslinked, leading to weaker gels that likely undergo simultaneous swelling and degradation, and consequently reach higher swelling ratios. The mechanism of degradation is believed to primarily involve hydrolysis of the ester linkages that connect DIBAC to the PEG polymer chain, as these are the most hydrolytically labile bonds present in the hydrogel system. Therefore, polymers with fewer azides and, consequently, fewer crosslinks, have a higher probability of degradation via the ester linkages. The ability of each hydrogel composition to retain water is also reported as polymer weight percent at maximum swelling (Table 3.3).

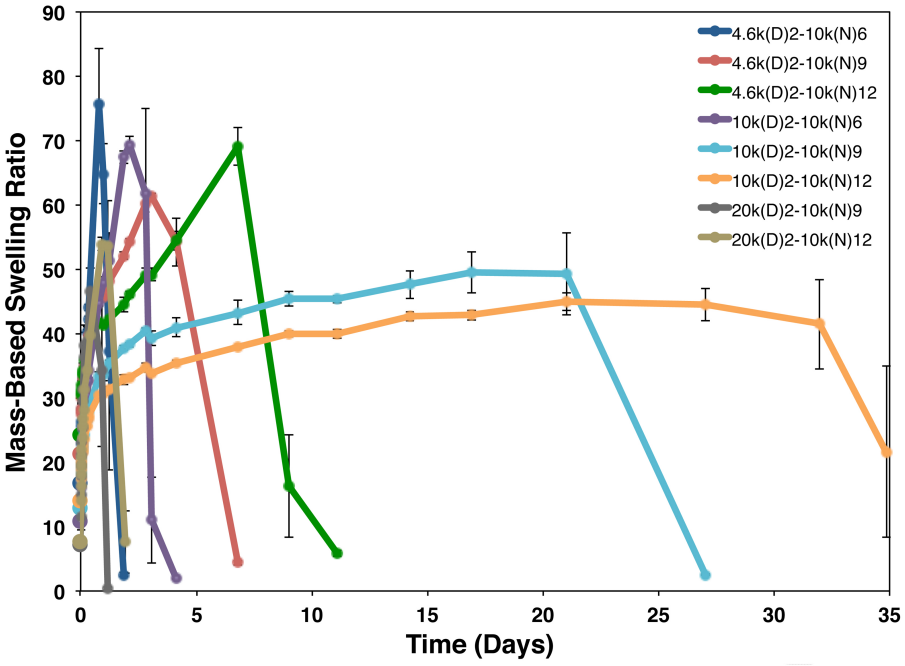

Figure 3.5. Mass-based swelling ratio of each hydrogel composition over time. Each measurement is represented as the mean ± standard error of the mean (s.e.m.) from triplicate experiments.

Table 3.3. Summary of Hydrogel Swelling, Degradation, and Young's Moduli.

Hydrogel Composition	Polymer Weight Percent at Max. Swelling (%)	Degradation Time (days)	Young's Modulus (kPa)
4.6k(D)$_2$-10k(N)$_6$	1.31 ± 0.12	2	1.6 ± 0.1
4.6k(D)$_2$-10k(N)$_9$	1.60 ± 0.01	7	2.1 ± 0.1
4.6k(D)$_2$-10k(N)$_{12}$	1.43 ± 0.06	10	2.6 ± 0.1
10k(D)$_2$-10k(N)$_6$	1.36 ± 0.04	3	6.0 ± 0.1
10k(D)$_2$-10k(N)$_9$	1.95 ± 0.11	27	14.5 ± 0.2
10k(D)$_2$-10k(N)$_{12}$	1.97 ± 0.08	35	18.1 ± 2.9
20k(D)$_2$-10k(N)$_9$	2.05 ± 0.22	1	1.0 ± 0.1
20k(D)$_2$-10k(N)$_{12}$	1.67 ± 0.05	2	1.9 ± 0.1

3.3.5. Young's Modulus Measurements

The stiffness of each hydrogel composition was measured using a home-built mechanical force analyzer from which the Young's modulus (YM) was calculated. The eight hydrogels tested ranged in YM values from 1.0 ± 0.1 kPa to 18.1 ± 2.9 kPa (Table 3.3). For each group of hydrogel compositions having the same $PEG_n(DIBAC)_2$ length, there is a direct correlation between the number of chain-end azides in $PEG_{10k}(N_3)_m$ and the YM of the resulting gel. This again indicates that increasing the number of azides results in a higher crosslink density in the hydrogel. Furthermore, in the cases where the two polymeric reaction partners ($PEG_n(DIBAC)_2$ and $PEG_{10k}(N_3)_m$) have the same molecular weight, the observed Young's moduli are higher, irrespective of the number of azides, than when the polymer molecular weights are mismatched. While it is difficult to definitively determine the reason for this observation, it seems that PEG lengths of 10 kDa provide the right balance between chain-end reactivity and inter-crosslink distance to result in more efficient crosslinking within the final gel, relative to the case where the $PEG_n(DIBAC)_2$ polymer is shorter or longer. Not surprisingly, as YM increases in this series of gels, the degradation time also increases, which is again indicative of the larger number of crosslinks formed in the stiffer gels.

The observed YM values are comparable to a variety of natural tissues, allowing each hydrogel's mechanical properties to be matched to specific target tissues in their application.[64] The hydrogels with the lowest YM were the 20k$(D)_2$-10k$(N)_9$, 20k$(D)_2$-10k$(N)_{12}$ and 4.6k$(D)_2$-10k$(N)_6$ compositions, which had modulus values of 1.0 ± 0.1, 1.9 ± 0.1, and 1.6 ± 0.1 kPa, respectively. These hydrogels most closely mimic breast,[65] liver, and kidney tissue.[66,67] The hydrogel compositions 4.6k$(D)_2$-10k$(N)_9$, 4.6k$(D)_2$-10k$(N)_{12}$ and 10k$(D)_2$-10k$(N)_6$ had YM values of 2.1 ± 0.1, 2.6 ± 0.1, and 6.0 ± 0.1 kPa, respectively, which most closely mimic soft muscle tissue.[66] The most rigid hydrogel compositions, 10k$(D)_2$-10k$(N)_9$ and 10k$(D)_2$-10k$(N)_{12}$ could be used for applications in collagen-rich regions of vascular tissue[68] or corneal anterior basement membranes,[69] with values of 14.5 ± 0.2 kPa and 18.1 ± 2.9 kPa, respectively.

3.3.6. Protein Adsorption Study (BSA)

Protein adsorption to the PEG hydrogels was evaluated using a model protein, bovine serum albumin (BSA).[70] BSA is commonly used to assess protein binding, as it provides an analogue to human serum albumin (HSA), which is the most abundant protein in human plasma. HSA has a typical blood concentration of 50 mg/mL and can adsorb onto surfaces within seconds to minutes.[57,71] BSA adsorption was tested on three model hydrogel compositions, 4.6k$(D)_2$-10k$(N)_{12}$, 10k$(D)_2$-10k$(N)_9$ and 10k$(D)_2$-10k$(N)_{12}$, which were chosen based on their YM values to enable evaluation of BSA adsorption on a soft, a medium, and a stiff hydrogel. As expected, BSA adsorption increased with increasing protein concentration from approximately 10 ng/cm^2 to 80 ng/cm^2 over the range of concentrations tested (125 to 1000 μg/mL) (Figure 3.6). Furthermore, BSA adsorption for the 10k$(D)_2$-10k$(N)_{12}$ composition (the "stiff" hydrogel tested) was

consistently the highest at each concentration. For example, at 1000 µg/mL, the BSA adsorption was 77.8 ± 10.4 ng/cm^2 for 10k(D)$_2$-10k(N)$_{12}$, compared to 39.7 ± 6.9 ng/cm^2 for the 10k(D)$_2$-10k(N)$_9$ composition (the "medium" hydrogel tested), and 10.7 ± 9.4 ng/cm^2 for the 4.6k(D)$_2$-10k(N)$_{12}$ composition (the "soft" hydrogel tested). Thus, as the YM increases, increased protein adsorption is also observed. However, it should be emphasized that the total protein adsorption in all these samples is extremely low relative to most biomaterials and at least on par with other PEG-based hydrogel compositions.[57,58,72]

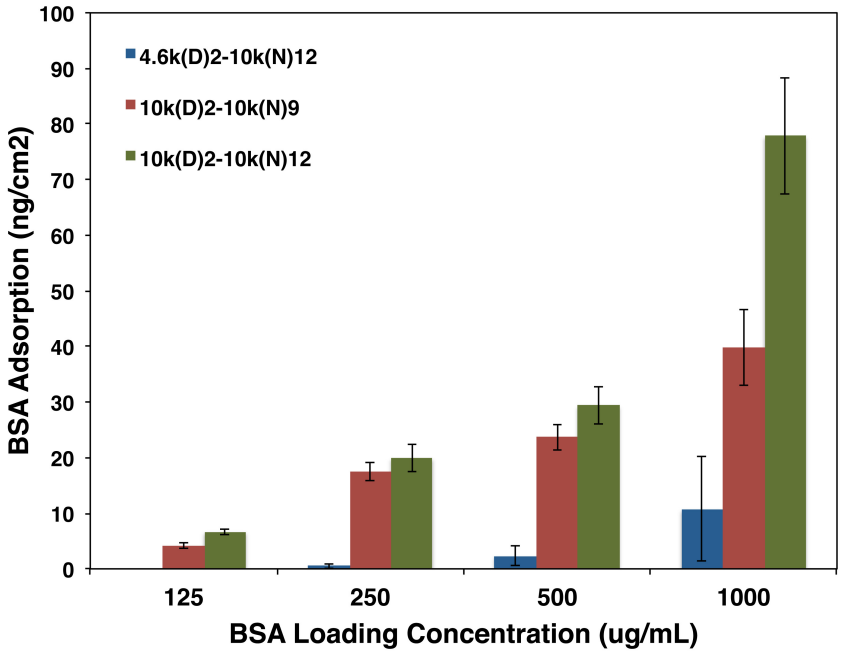

Figure 3.6. Bovine serum albumin (BSA) adsorption onto hydrogel compositions 4.6k(D)$_2$-10k(N)$_{12}$, 10k(D)$_2$-10k(N)$_9$, and 10k(D)$_2$-10k(N)$_{12}$ at 37°C as a function of the protein concentration in the loading solution. Error bars represent one standard deviation of five replicates.

3.3.7. MTT Assay

We carried out an MTT assay to determine whether the DIBAC- and azide-functionalized PEG structures that make up the hydrogels impart any

cytotoxicity. The polymers used for this assay were $PEG_{4.6k}(DIBAC)_2$ and $PEG_{10k}(N_3)_{12}$, as these polymers have the highest ratio of functional group to PEG and therefore the greatest chance of causing any potential cytotoxicity. The cytotoxicity of the polymer precursors was tested using an MTT assay on NIH 3T3 mouse fibroblasts (Figure 3.7). Results of the MTT assay demonstrate that neither the strained alkyne nor azide functionalized precursors show substantial cytotoxicity up to 1000 μg/mL (a typical upper limit of polymer concentration for *in vitro* screening[61,73]) after one day of incubation. It was especially important that the azide polymer did not elicit a cytotoxic response due to the fact that there was a known excess of azide groups in all hydrogel compositions.

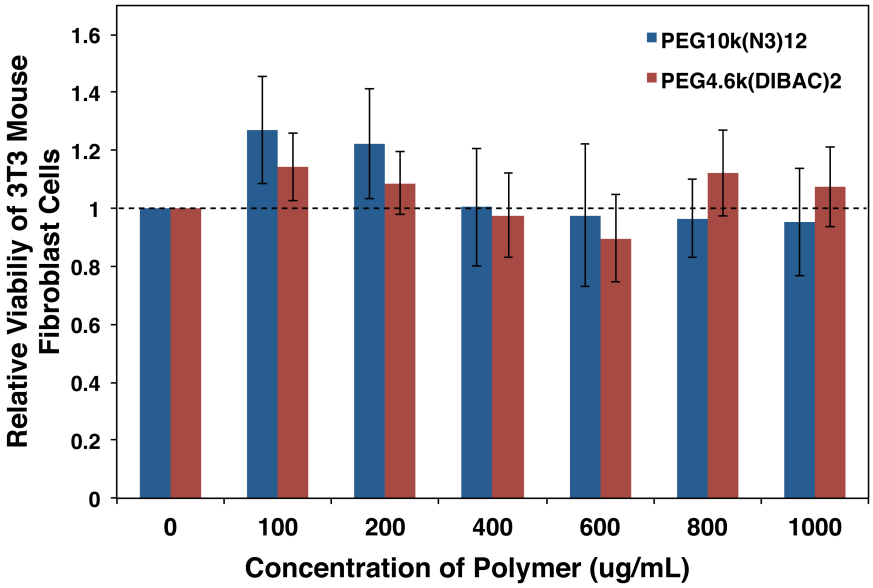

Figure 3.7. Cytotoxicity of $PEG_{4.6k}(DIBAC)_2$ (blue) and $PEG_{10k}(N_3)_{12}$ (red) polymer precursors via an MTT assay on NIH 3T3 fibroblasts relative to a cell-only control. Dotted line indicates relative viability = 1. Error bars represent one standard deviation of four replicates.

3.4. Conclusions

PEG hydrogels cross-linked via strain-promoted alkyne/azide cycloaddition (SPAAC) can be prepared with a wide range of mechanical and rheological properties suitable for biomedical applications. These hydrogels exhibited fast gelation times of 10 – 60 seconds, the ability to retain approximately 45 – 76 times their dry weight in water, varying degradation rates from 1 to 35 days, and Young's modulus values of 1 – 18 kPa. These PEG hydrogels show minimal BSA protein adsorption and the original polymer precursors had no significant cytotoxicity to 3T3 fibroblast cells. In particular, this series of eight PEG hydrogels with various mechanical and rheological properties may have potential applications in tissue engineering of a wide range of tissues, from soft liver tissue to more rigid collagen-rich regions of vascular tissue.

3.5. References

(1) Peppas, N. A.; Hilt, J. Z.; Khademhosseini, A.; Langer, R. *Adv. Mater.* **2006**, *18*, 1345–1360.

(2) Hoare, T. R.; Kohane, D. S. *Polymer* **2008**, *49*, 1993–2007.

(3) Schmidt, J. J.; Rowley, J.; Kong, H. J. *J. Biomed. Mater. Res. Part A* **2008**, *87*, 1113–1122.

(4) Balakrishnan, B.; Mohanty, M.; Umashankar, P. R.; Jayakrishnan, A. *Biomaterials* **2005**, *26*, 6335–6342.

(5) Hoffman, A. S. *Adv. Drug Deliv. Rev.* **2002**, *43*, 3–12.

(6) Tibbitt, M. W.; Anseth, K. S. *Biotechnol. Bioeng.* **2009**, *103*, 655–663.

(7) Lee, K. Y.; Mooney, D. J. *Chem. Rev.* **2001**, *101*, 1869–1879.

(8) Babensee, J. E.; Anderson, J. M.; McIntire, L. V.; Mikos, A. G. *Adv. Drug*

Deliv. Rev. **1998**, *33*, 111–139.

(9) Gulsen, D.; Chauhan, A. *Int. J. Pharm.* **2005**, *292*, 95–117.

(10) Karlgard, C. C. S.; Wong, N. S.; Jones, L. W.; Moresoli, C. *Int. J. Pharm.* **2003**, *257*, 141–151.

(11) Zhang, X.-Z.; Wu, D.-Q.; Chu, C.-C. *Biomaterials* **2004**, *25*, 3793–3805.

(12) Hyon, S.-H.; Cha, W.-I.; Ikada, Y. *Polym. Bull.* **1989**, *22*, 119–122.

(13) Kokabi, M.; Sirousazar, M.; Hassan, Z. M. *Eur. Polym. J.* **2007**, *43*, 773–781.

(14) Stammen, J. A.; Williams, S.; Ku, D. N.; Guldberg, R. E. *Biomaterials* **2001**, *22*, 799–806.

(15) Lutz, J.-F. *J. Polym. Sci. Part A Polym. Chem.* **2008**, *46*, 3459–3470.

(16) Bakaic, E.; Smeets, N. M. B.; Hoare, T. *RSC Adv.* **2015**, *5*, 35469–35486.

(17) Wu, Y.; Ng, D. Y. W.; Kuan, S. L.; Weil, T. *Biomater. Sci.* **2015**, *3*, 214–230.

(18) Lowe, S.; O'Brien-Simpson, N. M.; Connal, L. A. *Polym. Chem.* **2015**, *6*, 198–212.

(19) Kolate, A.; Baradia, D.; Patil, S.; Vhora, I.; Kore, G.; Misra, A. *J. Control. Release* **2014**, *192*, 67–81.

(20) Hamley, I. W. *Biomacromolecules* **2014**, *15*, 1543–1559.

(21) DiPalma, J. A.; DeRidder, P. H.; Orlando, R. C.; Kolts, B. E.; Cleveland, M. vB. *Am. J. Gastroenterol.* **2000**, *95*, 446–450.

(22) Foulks, G. N. *Drugs Today* **2007**, *43*, 887.

(23) Strickley, R. G. *Pharm. Res.* **2004**, *21*, 201–230.

(24) Liu, X.; Yuan, L.; Li, D.; Tang, Z.; Wang, Y.; Chen, G.; Chen, H.; Brash, J. L. *J. Mater. Chem. B* **2014**, *2*, 5718–5738.

(25) Unsworth, L. D.; Sheardown, H.; Brash, J. L. *Langmuir* **2005**, *21*, 1036–

1041.

(26) Unsworth, L. D.; Sheardown, H.; Brash, J. L. *Biomaterials* **2005**, *26*, 5927–5933.

(27) Jokerst, J. V.; Lobovkina, T.; Zare, R. N.; Gambhir, S. S. *Nanomedicine* **2011**, *6*, 715–728.

(28) van Vlerken, L. E.; Vyas, T. K.; Amiji, M. M. *Pharm. Res.* **2007**, *24*, 1405–1414.

(29) Veronese, F. M.; Pasut, G. *Drug Discov. Today* **2005**, *10*, 1451–1458.

(30) Lin, C.-C.; Anseth, K. S. *Pharm. Res.* **2009**, *26*, 631–643.

(31) Burdick, J. A.; Anseth, K. S. *Biomaterials* **2002**, *23*, 4315–4323.

(32) Bryant, S. J.; Bender, R. J.; Durand, K. L.; Anseth, K. S. *Biotechnol. Bioeng.* **2004**, *86*, 747–755.

(33) Kraehenbuehl, T. P.; Zammaretti, P.; Van der Vlies, A. J.; Schoenmakers, R. G.; Lutolf, M. P.; Jaconi, M. E.; Hubbell, J. A. *Biomaterials* **2008**, *29*, 2757–2766.

(34) Tan, H.; Marra, K. G. *Materials* **2010**, *3*, 1746–1767.

(35) Liu, Y.-L.; Hsieh, C.-Y.; Chen, Y.-W. *Polymer* **2006**, *47*, 2581–2586.

(36) Wei, H.-L.; Yang, Z.; Zheng, L.-M.; Shen, Y.-M. *Polymer* **2009**, *50*, 2836–2840.

(37) Vetrík, M.; Přádný, M.; Hrubý, M.; Michálek, J. *Polym. Degrad. Stab.* **2011**, *96*, 756–759.

(38) Jin, R.; Moreira Teixeira, L. S.; Krouwels, A.; Dijkstra, P. J.; van Blitterswijk, C. A.; Karperien, M.; Feijen, J. *Acta Biomater.* **2010**, *6*, 1968–1977.

(39) Uliniuc, A.; Popa, M.; Hamaide, T.; Dobromir, M. *Cellul. Chem. Technol.* **2012**, *46*, 1–11.

(40) Link, A. J.; Vink, M. K. S.; Agard, N. J.; Prescher, J. A.; Bertozzi, C. R.; Tirrell, D. A. *Proc. Natl. Acad. Sci. U. S. A.* **2006**, *103*, 10180–10185.

(41) Samuni, A.; Aronovitch, J.; Godinger, D.; Chevion, M.; Czapski, G. *Eur. J. Biochem.* **1983**, *137*, 119–124.

(42) Gaetke, L. M.; Chow, C. K. *Toxicology* **2003**, *189*, 147–163.

(43) Steinhilber, D.; Rossow, T.; Wedepohl, S.; Paulus, F.; Seiffert, S.; Haag, R. *Angew. Chemie - Int. Ed.* **2013**, *52*, 13538–13543.

(44) Debets, M. F.; van Berkel, S. S.; Dommerholt, J.; Dirks, A. T. J.; Rutjes, F. P. J. T.; van Delft, F. L. *Acc. Chem. Res.* **2011**, *44*, 805–815.

(45) Xu, J.; Filion, T. M.; Prifti, F.; Song, J. *Chem. Asian J.* **2011**, *6*, 2730–2737.

(46) Zheng, J.; Smith Callahan, L. A.; Hao, J.; Guo, K.; Wesdemiotis, C.; Weiss, R. A.; Becker, M. L. *ACS Macro Lett.* **2012**, *1*, 1071–1073.

(47) Xu, J.; Feng, E.; Song, J. *J. Am. Chem. Soc.* **2014**, *136*, 4105–4108.

(48) DeForest, C. A.; Sims, E. A.; Anseth, K. S. *Chem. Mater.* **2010**, *22*, 4783–4790.

(49) DeForest, C. A.; Anseth, K. S. *Nat. Chem.* **2011**, *3*, 925–931.

(50) McKinnon, D. D.; Brown, T. E.; Kyburz, K. A.; Kiyotake, E.; Anseth, K. S. *Biomacromolecules* **2014**, *15*, 2808–2816.

(51) Chadwick, R. C.; Van Gyzen, S.; Liogier, S.; Adronov, A. *Synthesis* **2014**, *46*, 669–677.

(52) Su, X.; Bu, L.; Dong, H.; Fu, S.; Zhuo, R.; Zhong, Z. *RSC Adv.* **2016**, *6*, 2904–2909.

(53) Jiang, H.; Qin, S.; Dong, H.; Lei, Q.; Su, X.; Zhuo, R.; Zhong, Z. *Soft Matter* **2015**, *11*, 6029–6036.

(54) Campbell-Verduyn, L. S.; Mirfeizi, L.; Schoonen, A. K.; Dierckx, R. A.; Elsinga, P. H.; Feringa, B. L. *Angew. Chemie Int. Ed.* **2011**, *50*, 11117–

11120.

(55) Kuzmin, A.; Poloukhtine, A.; Wolfert, M. A.; Popik, V. V. *Bioconjug. Chem.* **2010**, *21*, 2076–2085.

(56) Xu, J.; Prifti, F.; Song, J. *Macromolecules* **2011**, *44*, 2660–2667.

(57) Hou, Y.; Schoener, C. A.; Regan, K. R.; Munoz-Pinto, D.; Hahn, M. S.; Grunlan, M. A. *Biomacromolecules* **2010**, *11*, 648–656.

(58) Smeets, N. M. B.; Bakaic, E.; Patenaude, M.; Hoare, T. *Chem. Commun.* **2014**, *50*, 3306–3309.

(59) Long, R.; Hall, M. S.; Wu, M.; Hui, C.-Y. *Biophys. J.* **2011**, *101*, 643–650.

(60) Anseth, K. S.; Bowman, C. N.; Brannon-Peppas, L. *Biomaterials* **1996**, *17*, 1647–1657.

(61) Pawlikowska, P.; Gajkowska, B.; Orzechowski, A. *Cell Tissue Res.* **2007**, *327*, 571–581.

(62) Zhang, X.; Zhong, Z.; Zhuo, R. *Macromolecules* **2011**, *44*, 1755–1759.

(63) Sletten, E. M.; Bertozzi, C. R. *Acc. Chem. Res.* **2011**, *44*, 666–676.

(64) McKee, C. T.; Last, J. A.; Russell, P.; Murphy, C. J. *Tissue Eng. Part B* **2011**, *17*, 155–164.

(65) Samani, A.; Bishop, J.; Luginbuhl, C.; Plewes, D. B. *Phys. Med. Biol.* **2003**, *48*, 2183–2198.

(66) Chen, E. J.; Novakofski, J.; Jenkins, W. K.; O'Brien, Jr, W. D. *IEEE Trans. Ultrason. Ferroelectr. Freq. Control* **1996**, *43*, 191–194.

(67) Barnes, S. L.; Lyshchik, A.; Washington, M. K.; Gore, J. C.; Miga, M. I. *Med. Phys.* **2007**, *34*, 4439–4450.

(68) Oie, T.; Murayama, Y.; Fukuda, T.; Nagai, C.; Omata, S.; Kanda, K.; Yaku, H.; Nakayama, Y. *J. Artif. Organs* **2009**, *12*, 40–46.

(69) Last, J. A.; Liliensiek, S. J.; Nealey, P. F.; Murphy, C. J. *J. Struct. Biol.* **2009**, *167*, 19–24.

(70) Raeber, G. P.; Lutolf, M. P.; Hubbell, J. A. *Biophys. J.* **2005**, *89*, 1374–1388.

(71) Sugio, S.; Kashima, A.; Mochizuki, S.; Noda, M.; Kobayashi, K. *Protein Eng.* **1999**, *12*, 439–446.

(72) Du, H.; Chandaroy, P.; Hui, S. W. *Biochim. Biophys. Acta* **1997**, *1326*, 236–248.

(73) Hoare, T.; Bellas, E.; Zurakowski, D.; Kohane, D. S. *J. Biomed. Mater. Res. Part A* **2010**, *92*, 586–595.

Chapter 4

Reproducible Dendronized PEG Hydrogels via SPAAC Cross-Linking

The following manuscript was submitted to Biomacromolecules on June 22, 2017, ID: bm-2017-00879j. The authors on this work are: Sabrina M. Hodgson, Stuart A. McNelles, Leonora Abdullahu, Ian A. Marozas, Kristi S. Anseth and Alex Adronov.

Sabrina Hodgson planned this study. Sabrina Hodgson, Stuart McNelles and Leonora Abdullahu synthesized the precursor polymers. Sabrina Hodgson performed all hydrogel formation and characterization. Sabrina Hodgson and Ian Marozas conducted the cell studies.

Abstract

A common issue with hydrogel formulations is batch-to-batch irreproducibility, originating from poorly-defined polymer precursors. Here, we report the use of dendritic polymer end-groups to address this issue and maintain reproducibility between batches of poly(ethylene glycol) (PEG) hydrogels. Specifically, we synthesized two end-functionalized PEG chains, one with azide-terminated first- and second-generation dendrons, and the other with strained cyclooctynes. The two complementary azide and alkyne polymers react via the Strain-Promoted Alkyne-Azide Cycloaddition (SPAAC) to produce hydrogels quickly in the absence of additional reagents or catalyst, at low polymer concentrations. Hydrogels made with first-generation dendrons gelled in minutes and exhibited a small degree of swelling when incubated in PBS buffer at 37ºC, while hydrogels made from second-generation dendrons gelled in seconds with almost no swelling upon incubation at 37ºC. In both cases, the hydrogels proved reproducible, resulting in identical Young's Modulus (YM) values from different batches. The hydrogels prepared with second-generation dendrons were seeded with human mesenchymal stem cells (hMSCs), and showed high cell viability, as well as cell spreading over a two-week timeframe. These studies show that the SPAAC hydrogels are non-cytotoxic, and are capable of supporting cell growth.

4.1. Introduction

Hydrogels are lightly cross-linked polymer networks that swell in water.[1–3] Hydrophilic polymers comprise the three-dimensional networks, and can be made of a number of different precursor structures, depending on the desired properties and applications. For biomedical applications, biocompatible polymers and bio-orthogonal crosslinking reactions are often required, especially if the hydrogel is formed *in-situ*.[4,5] Commonly, the synthetic polymers used to produce hydrogels are prepared via standard polymerization chemistry, which results in polymer molecular weights and dispersities that cannot easily be reproduced from batch to batch.[6,7] The resulting variation in molecular weight and, often, functional group density, makes it difficult to reproduce desirable hydrogel properties when using polymers from different rounds of synthesis.[1,8] An ideal hydrogel system would be one that produces identical polymers at each synthetic attempt, enabling the resulting hydrogel to have the same properties, no matter which polymer batch is used. To obtain the same number of functional groups each time the polymer is synthesized, a method that is more controlled than standard polymerization is required. Specifically, introduction of a well-defined polyfunctional unit at the chain ends of a polymer is desirable. Dendritic macromolecules are well known for their structural perfection and well-defined number of end groups at their periphery.[9,10] A major advantage to utilizing dendrimers for the formation of hydrogels is the complete structural control they provide, while also affording multiple cross-linking sites at their periphery.[11] It is unsurprising that, over the past two decades, there has been increasing interest in the use of dendrimers within hydrogels.[11–15] Many of the reports to date involve cross-linking between polyamidoamine (PAMAM) dendrimers and another polymer such as poly(vinyl alcohol) (PVA),[16] poly(methacrylic acid) (PMAA),[17] or poly(ethylene glycol) (PEG).[12,14,18–21] PEG is by far the most commonly used

polymer in making dendrimer-based hydrogels, as it is biocompatible, hydrophilic, and easily functionalized at its chain ends.[22–24] One of the first accounts of dendrimer-based hydrogels incorporated PEG, and was reported by Grinstaff and co-workers in 2002.[25] This report explored the use of a hydrogel composed of poly(glycerol-succinic acid)-poly(ethylene glycol) hybrid dendritic-linear copolymers. The dendritic-linear-dendritic (DLD) structure formed a gel through photopolymerization in 10-30 seconds and has potential as an ophthalmic adhesive.[26–28] The same group made similar hydrogels using B-alanine instead of succinic acid, creating carbamate linkages that are more stable than esters *in vivo*.[13] Photo-crosslinking was still necessary for hydrogel formation, but the resulting carbamate gels had higher mechanical stability, and lower swelling ratios than the previous ester-linked gels. PEG has been used in the synthesis of many other dendrimer-based hydrogels, such as with poly(benzyl ether) dendrimers,[29] lysine-based peptide dendrons,[30] and heterofunctional dendritic scaffolds.[31]

Of all the reports of dendrimer-based hydrogels, very few have exploited "click" reactions as the cross-linking chemistry. Sanyal and coworkers used the Copper-catalyzed Alkyne-Azide Cycloaddition (CuAAC) to form hydrogel scaffolds that could be further functionalized post gelation.[32] Malkoch and co-workers created bifunctional PEG-dendrimer hydrogels that were formed through thiol-ene chemistry, that also contained azides to allow for chemoselective modification with biorelevant moieties via the CuAAC click reaction.[33] Grinstaff and co-workers reacted aldehyde-functionalized PEG with a peptide-based dendrimer containing thiols to form hydrogels through thiazolidine bonds.[23,34] To our knowledge, there are no examples in the literature of reproducible dendrimer hydrogels made using the Strain-Promoted Alkyne-Azide Cycloaddition (SPAAC). Most of these reports use cross-linking chemistry that is cytotoxic and therefore not suitable for cell encapsulation studies. By using SPAAC, we were able to develop a hydrogel

formulation that is not only reproducible, but also non-cytotoxic and bioorthogonal.[35] Previous reports have paved the way for this work by demonstrating the potential for stem cell growth on hydrogels. Particularly, when the adhesion tripeptide RGD (arginine – glycine – aspartic acid) is incorporated into PEG hydrogels, hMSCs show high viability.[36] Reports have even demonstrated improved hMSC viability through spreading and migration in PEG hydrogels that degrade post-gelation, either through photodegradation[37,38] or cell-mediated degradation.[39]

Herein we report a novel and reproducible DLD-type PEG hydrogel that is cross-linked via SPAAC. We show that hMSCs remain viable within this hydrogel system for over two weeks, and that the hMSCs show signs of material interactions and remodeling, as visible by their spreading throughout the hydrogel matrix.

4.2. Materials and Methods

4.2.1. Hydrogel Formation

The synthesis of all polymer precursors and dendrons is described in the supporting information. PEG hydrogels were prepared by rapidly mixing complementary strained alkyne and azide-functionalized PEG macromolecules. Complete mixing of the functionalized precursor PEGs was achieved by co-extrusion using a double barrel syringe (Medmix, L-System, 2.5 mL) with a static mixer at the outlet of the syringe. Each barrel of the syringe was loaded with a complementary precursor polymer dissolved in 10 mM PBS. In all hydrogels, the functional group ratio of strained alkynes to azides remained 1:1. The hydrogels had total concentrations of either 2.5 wt% or 5 wt%.

4.2.2. Hydrogel Characterization

4.2.2.1. Gelation Time

Gelation time measurements were obtained by quickly placing 200 μL of each precursor polymer solution into a snap-cap vial (2 mL), vortex mixing for 5 seconds and then inverting the mixture every 5 seconds. Gelation time measurement began immediately following vortex mixing and was defined as the time when the hydrogel no longer moved upon inversion of the vial.

4.2.2.2. Swelling Kinetics (at 37°C)

Swelling kinetics of the PEG hydrogels were measured at 37°C to mimic physiological environments, in 10 mM PBS at pH 7.4. Hydrogel disks were placed into cell culture inserts that were subsequently placed in a 12-well cell culture plate and completely submerged in 10 mM PBS (4 mL/well). The plates were placed in an incubator that maintained a constant temperature of 37°C. At predetermined time intervals, the cell culture inserts with hydrogels were removed from the wells, the PBS drained, and the hydrogel gently blotted with paper towel to wick off any surface water prior to gravimetric analysis. PEG hydrogels were then resubmerged in a fresh 4 mL aliquot of PBS solution.

4.2.2.3. Hydrogel Mechanics

Mechanical properties of the hydrogels were measured using a home-built apparatus, as previously described.[40] These measurements rely on Hertzian theory, in which force applied to the gel is related to deformation by the equation:

$$F = \frac{4ER^{1/2}}{3(1-\nu^2)} d^{3/2} \quad (1)$$

where F is the force, d is the deformation, R is the radius of the glass hemispherical indenter, ν is the Poisson's ratio (assumed to have a value of 0.5 based on the similarity between hydrogels and rubbery materials),[41] and E is the Young's Modulus (YM) of the elastic substrate.[42] The YM of each hydrogel was determined by compression with a hemispherical indenter (R = 0.83 mm) attached to a force transducer (Transducer Techniques, GSO series, 10 g full scale). The vertical position of the indenter was controlled with a servo motor, programmed to move to a maximum depth of 10 % at a constant speed. The force transducer then measures the force relative to time and position. Measurements were repeated in triplicate at different positions for each gel, and the YM was obtained using equation 1, rearranged to isolate YM as the slope when plotting force (F) as a function of deformation (d).

4.2.2.4. Cell Culture

Primary human mesenchymal stem cells (hMSCs) were isolated from bone marrow aspirates (Lonza) as previously described.[1] For all experiments, hMSCs were thawed and passaged at 70-80 % confluence with medium changes every 2-3 days. hMSCs from passages two through four were used in all studies and were cultured in growth medium (low glucose DMEM supplemented with 10 % FBS, 50 U/mL of penicillin and streptomycin, 1 μg/mL Fungizone, and 1 ng/mL basic Fibroblast Growth Factor-2) at 37ºC and 5 % CO_2.

4.2.2.5. Cell Encapsulation and Live/Dead Assay

hMSCs were encapsulated at 3 x 10^6 cells/mL in 30μL of 4.8, 7.2 or 9.6 wt% PEG hydrogels functionalized with 37 mM RGD-azide to promote cell adhesion. Solutions of PEG-$(DIBAC)_2$ and RGD-azide were first mixed and allowed to react for 2 minutes, followed by addition of cells and PBS to reach

the appropriate concentration. This solution was transferred to a syringe barrel followed by the final addition and mixing of PEG-azide. The solution was allowed to reach complete gelation, and then the hydrogel disks were transferred to a 24-well plate containing 1 mL phenol red free low glucose DMEM media. Viability was assessed via Calcein AM (green, live cells) and ethidium homodimer (red, dead cells) staining 4, 8 and 15 days post-encapsulation. The stained hMSCs were imaged at 10x magnification through a water immersion lens on a Zeiss NLO confocal laser scanning microscope. Cell viability was quantified using ImageJ.

4.3. Results and Discussion

4.3.1. Preparation of Polymers

2,2-Bis(hydroxymethyl)propanoic acid (bis-MPA) dendrimers were synthesized as previously reported by our group.[43] To incorporate azides at the periphery of the bis-MPA dendrons **1** and **3,** the free hydroxyl groups were activated with *p*-nitrophenyl chloroformate,[44] followed by reaction with 3-azidopropylamine (see Supporting Information).

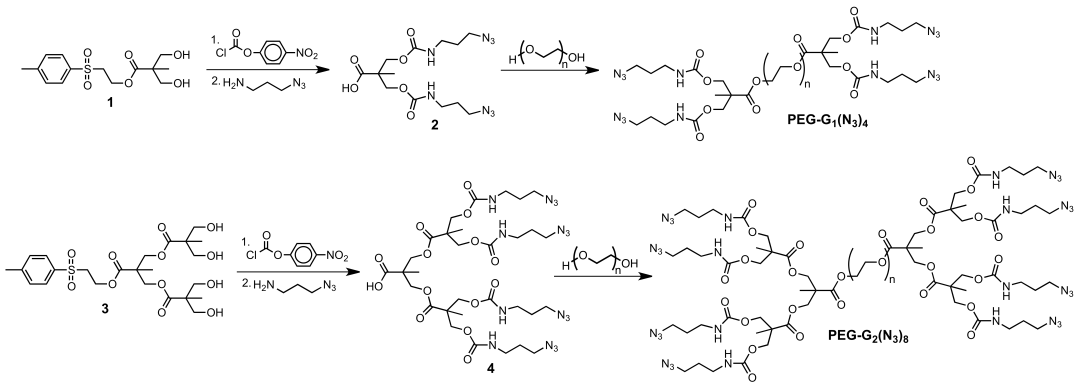

Scheme 4.1. Synthesis of PEG-G1-$(N_3)_4$ (top) and PEG-G2-$(N_3)_8$ (bottom) starting with the corresponding bis-MPA dendrons **1** and **3**.

Once the periphery was decorated with azides, the core was deprotected to liberate a carboxylic acid moiety, which was then installed on either end of a 10 kDa PEG chain via carbodiimide-mediated esterification using HOBt/EDC. Scheme 4.1 outlines the complete synthetic pathway from the first- and second-generation bis-MPA dendrons (G1 and G2, respectively) to the azide-functionalized PEG chains. ^{1}H NMR in DMSO-d6 was used to monitor the final step in the synthesis, and the reaction was complete once the terminal hydroxyl protons on PEG disappeared (Figure 4.5).

The other precursor polymer, PEG-$(DIBAC)_2$, was synthesized as previously described by our group.[40] The synthesis relies on an optimized procedure to make the carboxylic acid derivative of aza-dibenzocyclooctyne (DIBAC) (Scheme 4.2).[45] The DIBAC acid was introduced on both ends of a 10 kDa PEG chain using EDC-mediated esterification.

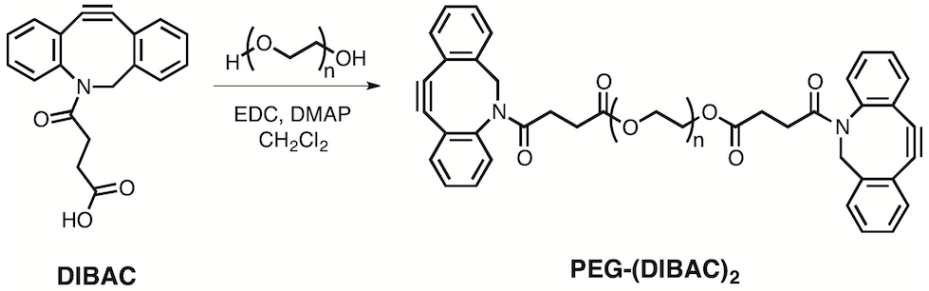

Scheme 4.2. Synthesis of PEG-$(DIBAC)_2$ from DIBAC.

4.3.2. Hydrogel Formation and Gelation Time

PEG-dendron hydrogels were prepared by rapidly mixing of PEG-$(DIBAC)_2$ with either PEG-G1-$(N_3)_4$ or PEG-G2-$(N_3)_8$. In all hydrogel formulations, the functional group ratio of strained cyclooctynes to azides remained 1:1. Hydrogels were prepared from two different concentrations, 2.5 wt% and 5 wt%, of the G1 and G2 dendrons. and the gelation times can be found in Table 4.1. Unsurprisingly, the gelation times are much faster for the 5 wt% gels

than the 2.5 wt% gels. There is also a remarkable difference in the gelation times for the G2 gels compared to G1, which can be explained by the increased density of reactive groups in the G2 hydrogel system, which enables gelation to occur at lower conversion. The 2.5 wt% G1 and G2 dendron hydrogels (two of each), created in a silicone mold, are displayed in Figure 4.1. It is evident from this image that the resulting hydrogels are clear, colourless, and transparent. Qualitatively, the more highly crosslinked G2 hydrogels are more structurally stable, allowing them to retain their shape and be released from their molds without defects than the comparable G1 gels.

Table 4.1. Gelation times for linear, G1 and G2 Systems.

Wt %	G1	G2	Linear
2.5	3 min 25 sec	25 sec	5 min 50 sec
5	1 min 15 sec	10 sec	45 sec

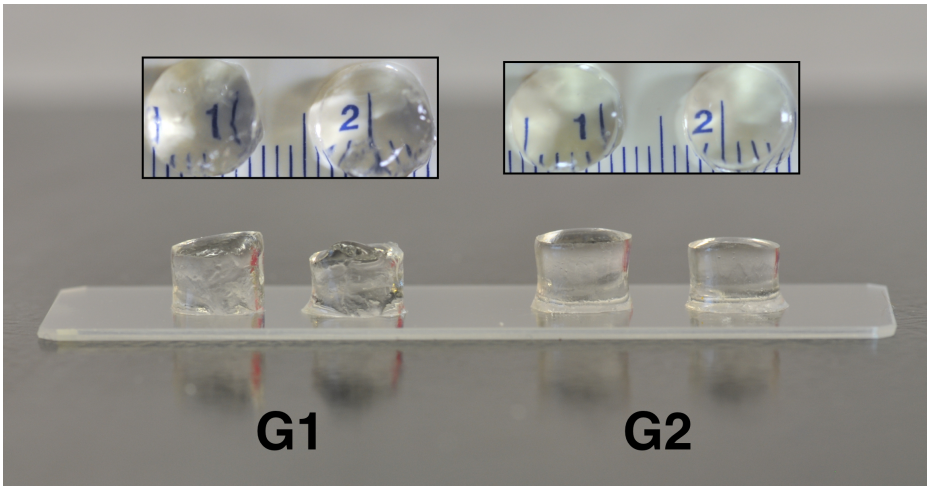

Figure 4.1. Photograph of G1 (left) and G2 (right) hydrogels at 2.5 wt%. Insets show top-down view of the same gels, demonstrating their transparency.

To further evaluate the dendron hydrogels, a linear azide polymer was synthesized (see Supporting Info) to mimic the G2 system (Figure 4.2). Both polymers contain a 10 kDa PEG chain, with four azides at the ends. The gelation times for the linear system were determined using the same conditions as the G2 hydrogel: a 1:1 functional group ratio of strained cyclooctyne to azide, and the same overall hydrogel concentrations of 2.5 wt% and 5 wt%. However, there is a remarkable difference between the two systems. Other than the obvious disadvantage of batch-to-batch irreproducibility, the linear system exhibits much longer gelation times. We suspect that this is due to shorter spacing between azide groups on the linear chain. The PEG-G2-$(N_3)_8$ polymer has more room between azide moieties, allowing the bulky cyclooctyne to react more easily with adjacent azides, decreasing the gelation time. This further confirms the advantage of using the dendrimer hydrogel system over the linear counterpart.

Linear Azide

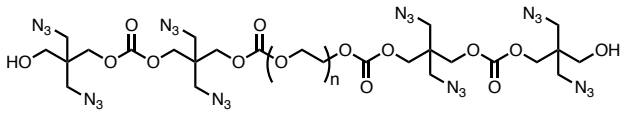

Dendritic Azide

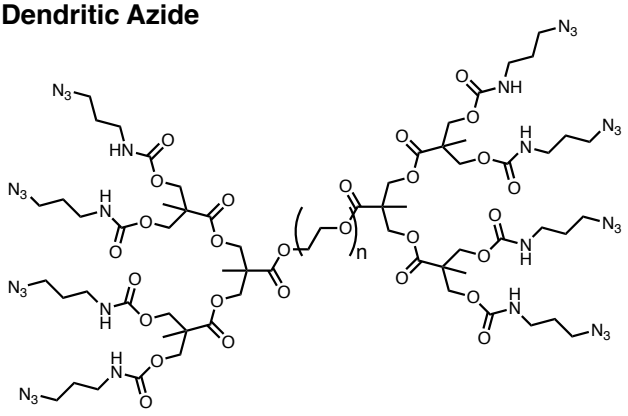

Figure 4.2. Structural comparison of the linear and corresponding dendritic azide-functionalized polymers.

The third generation azide-terminated dendron was also synthesized and esterified onto the ends of a 10 kDa PEG chain. This PEG-G3-$(N_3)_{16}$ polymer contains 16 azide groups, but, unfortunately, was not soluble in water or PBS buffer. Despite attempts at agitation, sonication, and dilution, we were unable to prepare an aqueous solution of this polymer, and therefore could not make G3 dendron hydrogels. This is likely due to the increased number of lipophilic azide species at either end of the polymer, making a greater proportion of the molecule hydrophobic. Attempts to use the G3 polymer to prepare crosslinked networks in organic solvent (organogels), followed by drying and reconstitution in water were made, but the resulting gels were physically different from the G1 and G2 hydrogels, making it difficult to draw comparisons in their properties.

4.3.3. Hydrogel Swelling

Swelling of the G1 and G2 dendron hydrogels at both 2.5 wt% and 5 wt% was measured by weighing the hydrogels at pre-determined time intervals as they swelled in 10 mM PBS at 37ºC. The mass-based swelling ratios over time were calculated and are plotted in Figure 4.3. From this image, it is clear that the overall swelling characteristics of the G1 and G2 hydrogels are very different. The mass-based swelling ratios of the 2.5 wt% and 5 wt% G1 dendrimer hydrogels increase over time. After 53.5 hours, both G1 hydrogels have the highest swelling ratios (i.e., ability to retain the most water), with values of 92.4 ± 4 and 45.8 ± 1 for the 2.5 wt% and 5 wt% gels, respectively. However, it is important to note that after this measurement, the 2.5 wt% G1 hydrogel degraded, most likely due to the low crosslink density. Measurements with the G2 dendrimer hydrogels at both 2.5 wt% and 5 wt% showed that these systems did not appreciably imbibe additional water over time, especially at the higher concentration. After 53.5 hours, the mass-based

swelling ratios for the 2.5 wt% and 5 wt% gels were 43 ± 1 and 25 ± 1, respectively. For certain biomedical applications, having a material that does not significantly swell could be advantageous because the physical and mechanical properties do not change over time and the total occupied volume does not increase.[41] For drug delivery and cell therapy, swelling can influence the release rate of the drug or therapeutic agent.[46]

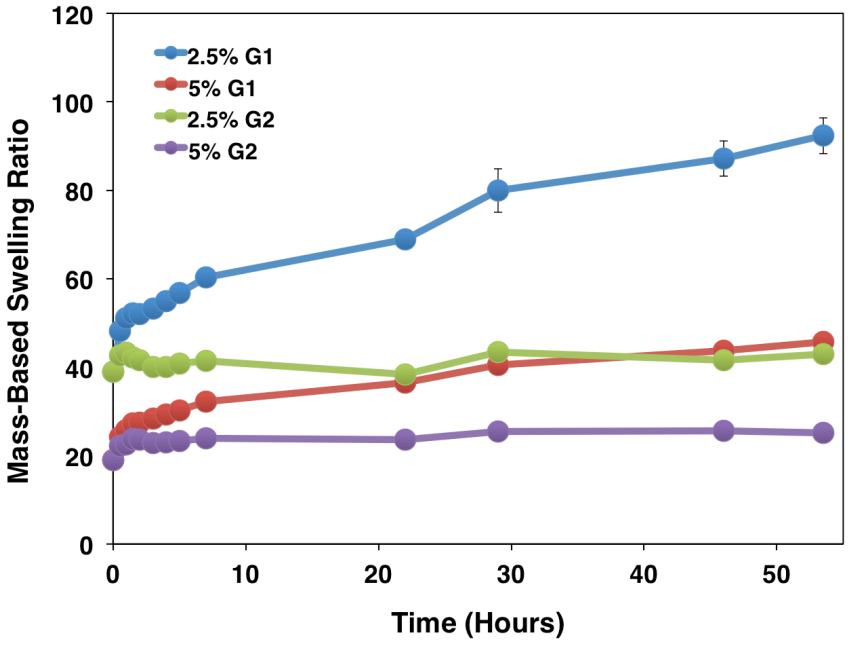

Figure 4.3. Graph of hydrogel swelling over time for 2.5 wt% and 5 wt% G1 and G2 dendrimer hydrogels at 37°C.

To further quantify the amount of swelling that occurred, the equilibrium swelling degree (ESD) was calculated for each system. ESD is defined as ESD (%) = $(W_{eq} - W_0)/W_0$ *100%, where W_{eq} is the weight of the gel at equilibrium swelling and W_0 is the weight of the gel prior to swelling. The ESD for the 2.5 wt% and 5 wt% G1 hydrogels was 133 ± 10 % and 180 ± 6 %, respectively. For the 2.5 wt% and 5 wt% G2 hydrogels, the ESD was 15 ± 2 % and 39 ± 2 %, respectively. Approximate ESD values of linear hydrogel systems were calculated from a previous swelling study.[40] The values

obtained from the linear system were much higher than the dendrimer-based hydrogel system, ranging from 177 to 540 %.

4.3.4. Hydrogel Rheology to Deduce Reproducibility

Two batches of each precursor azide-functionalized polymer (linear, G1 and G2) were synthesized to quantify the hydrogel mechanical properties and test the reproducibility in the hydrogel fabrication method. Small variations in the polymer functionality lead to changes in the hydrogel crosslinking density that are easy to quantify through mechanical measurements. Each azide polymer was reacted with PEG-$(DIBAC)_2$ and allowed to reach complete gelation. The concentration of the linear hydrogels was 5 wt% and the concentration of the dendritic hydrogels was 2.5 wt%. The linear azide polymer did not form an insoluble gels at 2.5 wt%, requiring the use of a 5 wt% gel. The mechanical properties of each gel were tested for reproducibility between batches. It is evident by ^1H NMR (Figures 4.6 - 4.8) that the linear azide polymers are not the same, based on their integration values. It is therefore unsurprising that the Young's modulus (YM) values for the two linear systems are very different, with values of 3.7 ± 0.6 kPa and 1.3 ± 0.2 kPa (Table 4.2). Since a polymerization reaction was used to incorporate azides onto the polymer, small batch-to-batch differences of 1-2 azides per polymer were unavoidable, resulting in large differences to the hydrogel properties. In contrast, the dendritic hydrogels appear nearly identical by ^1H NMR, and the resulting mechanical properties of the hydrogels are identical from one batch to the next (Table 4.2). We found that the G1 and G2 hydrogels exhibit YM values of 1.5 and 4.1 kPa, respectively.

Table 4.2. Young's Modulus Values for Two Batches (A and B) of the Linear, G1 and G2 Hydrogels.

	Linear (kPa)	G1 (kPa)	G2 (kPa)
A	3.7 ± 0.6	1.5 ± 0.05	4.1 ± 0.6
B	1.3 ± 0.2	1.5 ± 0.09	4.1 ± 0.3

4.3.5. Cell Viability with hMSCs

To assess the applicability of these hydrogels for cell encapsulation and primary cell culture, primary human mesenchymal stem cells (hMSCs) were encapsulated in 3 mm thick hydrogels with a diameter of 4.5 mm. For all of the cell culture experiments, the G2 hydrogel system was used, and an azide-functionalized RGD peptide was added to the formulation at 37 mM to allow for cell-matrix interactions. At time points of 4, 8 and 15 days, the viability of the hMSCs was measured using a Live/Dead cell assay (Table 4.3). Figure 4.4 shows the results of this test for three different concentrations of the G2 hydrogel: 9.6 wt%, 7.2 wt%, and 4.8 wt%. All three concentrations of hydrogel showed excellent viability after 4 days of culture. On day 8, the viability dropped slightly, but hMSC viability was still high overall, especially for the 9.6 wt% and 7.2 wt% gels. After 15 days, the 4.8 wt% gel degraded; however, the 9.6 wt% and 7.2 wt% gels remained intact, and the majority of the hMSCs survived. The fast degradation time of the 4.8 wt% hydrogel was attributed to the lower polymer concentration and therefore a lower crosslink density compared to the other two systems. A general trend in hMSC viability is observed among the three concentrations of hydrogel, where hMSCs show greater viability in the more concentrated, more crosslinked polymer microenvironments. From Figure 4.4, it is also apparent that the hMSCs are adhering to the hydrogel scaffold, particularly in the 9.6 wt% and 7.2 wt% hydrogels. These observations are indicative of local

changes occurring the hMSC pericellular regions. As there are hydrolytically labile ester groups within the hydrogel matrix, the decrease in crosslinking density is expected to permit hMSC spreading, proliferation, and even migration. However, hMSCs are also known to secrete many esterases, and this may further contribute to an accelerated and more local degradation of the hydrogel network. Although the specifics of cell migration are complex, involving many extracellular signals,[47] it is clear from these results that the dendrimer hydrogel system is a suitable matrix for studying stem cell growth and migration in highly controlled material environments.

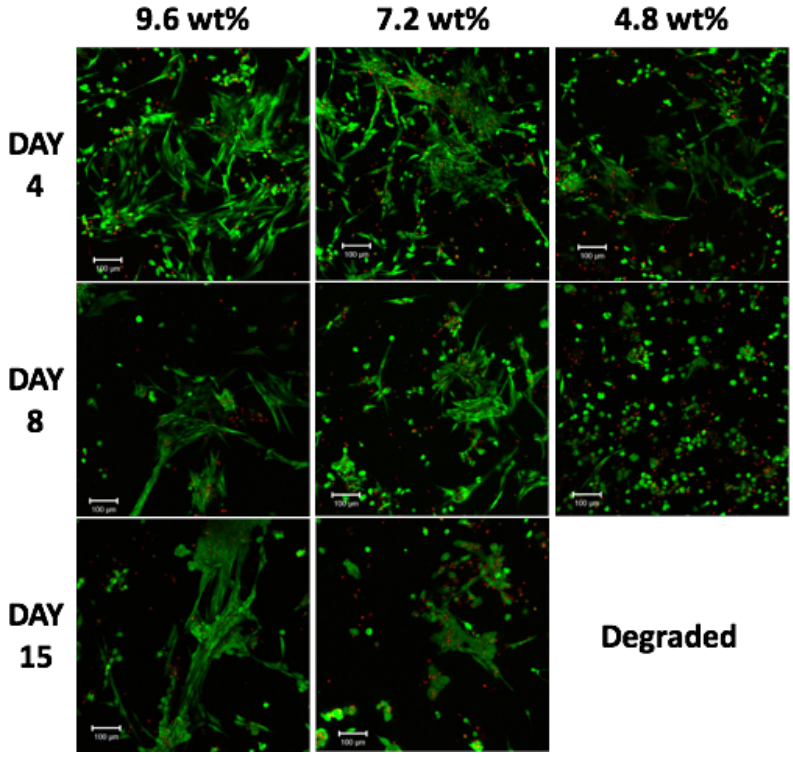

Figure 4.4. Representative projections of 3D confocal images of encapsulated hMSC cells, showing viability over time at different hydrogel concentrations: 9.6 wt% (left column), 7.2 wt% (middle column), 4.8 wt% (right column). Cells are stained with calcein AM (live – green) and ethidium homodimer (red – dead). Scale bar 100 μm.

Table 4.3. hMSC viability in G2 hydrogels after 4, 8, and 15 days. Three different concentrations of G2 hydrogel were assessed: 9.6 wt%, 7.2 wt% and 4.8 wt%.

Time (days)	% Viability		
	9.6 wt% gel	7.2 wt% gel	4.8 wt% gel
4	86 ± 5	73 ± 1	81 ± 4
8	82 ± 4	70 ± 3	64 ± 4
15	77 ± 2	63 ± 5	-

4.4. Conclusions

Novel, reproducible hydrogels were synthesized, utilizing first- and second-generation dendrons to incorporate multiple azide cross-linking groups on each end of a PEG polymer. These azide-functionalized polymers reacted with cyclooctyne-functionalized PEG chains to produce hydrogels at low polymer concentration with gelation times ranging from 10 seconds to 3.5 minutes. After 53.5 hours at 37ºC, the G1 hydrogels exhibited a small extent of swelling, while the G2 hydrogels swelled minimally. The reproducibility of these hydrogels was confirmed by comparing the Young's Modulus values of two different batches of each precursor polymer. Finally, hMSCs were encapsulated within the G2 hydrogel, and showed a high degree of viability over 15 days.

4.5. Supporting Information

4.5.1. Materials and Methods

4.5.1.1. General

All reagents and solvents were purchased from commercial sources and used as provided. NMR spectroscopy was performed on a Bruker AVANCE

AV600 spectrometer at 600 MHz or a Bruker AVANCE AV700 at 700 MHz. Both ^{1}H and ^{13}C spectra were referenced to a residual non-deuterated solvent signal. Polymer molecular weights and dispersities were evaluated using Gel Permeation Chromatography (GPC) using a Waters 2695 Separations Module equipped with a Waters 2414 Refractive Index Detector and a Jordi Fluorinated DVB mixed bed column. Polystyrene Standards were used for calibration, with THF as the eluent at a flow rate of 3.0 mL/min. High Resolution Electrospray Ionization Mass Spectrometry (HR-ESI) was performed on a Bruker MAXIS 4G or a Waters Micromass Quattro Ultima Global.

4.5.1.2. Synthesis

Synthesis of pTSe-G1(NO_2Ph)$_2$

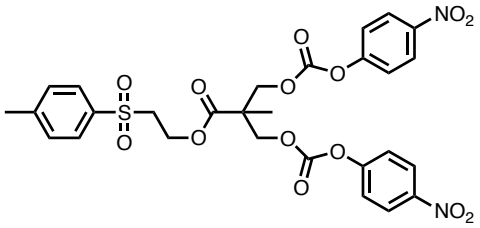

A flask equipped with a stir bar was charged with a solution of *p*TSe-G1-$(OH)_2$ (0.750 g, 2.371 mmol) in CH_2Cl_2 (20 mL) and pyridine (2 mL), and the reaction was cooled to 0˚C. *p*-Nitrophenyl chloroformate (1.911 g, 9.483 mmol) was dissolved in CH_2Cl_2 (5 mL) and transferred to the reaction mixture. The reaction was stirred at room temperature overnight. The reaction mixture was diluted with 25 mL of CH_2Cl_2 and washed with 1 M $NaHSO_4$ (3 × 30 mL), and brine (1 × 40 mL). The organic phase was dried over $MgSO_4$, filtered through a Buchner funnel, and the solvent removed *in vacuo*. The product was purified via column chromatography (100% dichloromethane until all nitrophenyl chloroformate eluted, then 5% EtOAc

in dichloromethane), to yield 1.423 g (93 %) of product as a white foam. ^{1}H NMR (700 MHz; C_6H_6): δ 1.12 (d, *J* = 5.6 Hz, 3H), 1.86 (s, 3H), 2.77-2.76 (m, 2H), 4.14-4.12 (m, 2H), 4.48 (dd, *J* = 71.1, 11.0 Hz, 4H), 6.75-6.74 (m, 2H), 6.80-6.77 (m, 4H), 7.65-7.63 (m, 6H). ^{13}C NMR (176 MHz; C6D6): δ 1.43, 17.29, 21.17, 46.69, 54.59, 58.46, 69.60, 121.69, 125.24, 128.33, 128.35, 130.05, 137.16, 144.82, 145.78, 152.53, 155.22, 171.48. MS Calcd for $C_{28}H_{26}N_2O_{14}S$ $[M]^+$ = 646.1105, $[M + NH_4]^+$ = 664.1448. Found HR ESI-MS $[M + NH_4]^+$ 664.1445.

Synthesis of pTSe-G2(NO_2Ph)$_4$

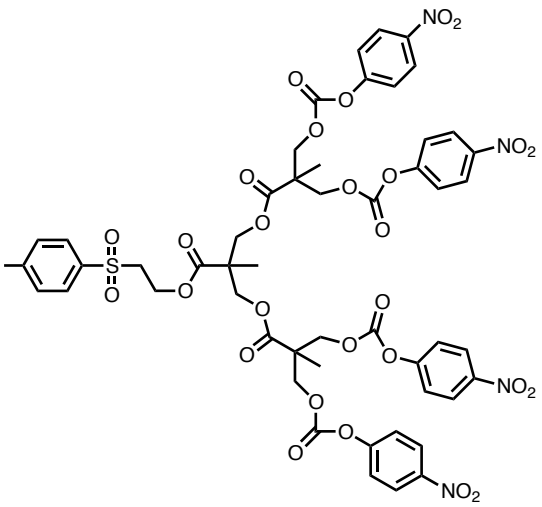

A flask equipped with a stir bar was charged with a solution of *p*TSe-G2-$(OH)_4$ (1.300 g, 2.370 mmol) in CH_2Cl_2 (20 mL) and pyridine (2 mL), and the reaction was cooled to 0˚C. *p*-Nitrophenyl chloroformate (3.821 g, 18.957 mmol) was dissolved in CH_2Cl_2 (5 mL), then transferred to the reaction mixture. The reaction was stirred at room temperature overnight. The reaction mixture was diluted with 25 mL of CH_2Cl_2, and washed with 1 M $NaHSO_4$ (3 × 30 mL), and brine (1 × 40 mL). The organic phase was dried over $MgSO_4$, filtered through a Buchner funnel, and the solvent removed *in vacuo*. The product was purified via column chromatography (100% dichloromethane until all nitrophenyl chloroformate eluted, then 10% EtOAc

in dichloromethane), to yield 2.385 g (83 %) of product as a white foam. ^{1}H-NMR (600 MHz; $CDCl_3$): δ 1.31 (s, 3H), 2.43 (s, 3H), 3.39 (t, *J* = 5.8 Hz, 2H), 4.39-4.35 (m, 4H), 4.45 (dd, *J* = 11.0, 2.2 Hz, 4H), 4.53-4.49 (m, 6H), 7.38-7.33 (m, 10H), 7.76 (d, *J* = 8.2 Hz, 2H), 8.25-8.23 (m, 8H). ^{13}C NMR (151 MHz; $CDCl_3$): δ 17.64, 17.79, 21.76, 46.76, 46.79, 54.78, 58.39, 65.85, 69.35, 76.95, 77.16, 77.37, 121.84, 121.86, 121.88, 121.92, 122.00, 125.38, 125.40, 125.44, 128.07, 130.26, 136.37, 145.49, 145.70, 152.23, 155.34, 171.19, 171.81. MS Calcd for $C_{52}H_{48}N_4O_{28}S$ $[M]^+$ = 1208.2176, $[M + NH_4]^+$ = 1226.2520. Found HR ESI-MS $[M + NH_4]^+$ 1226.2511.

Synthesis of 3-azidopropylamine[48]

In a flask equipped with a stir bar, 3-chloropropylamine hydrochloride (6.0 g, 46.147 mmol) and sodium azide (11.4 g, 175.358 mmol) were dissolved in distilled H_2O (20 mL), and the reaction was stirred at 80 ˚C for 6h. The reaction mixture was basified by adding saturated KOH (10 mL) drop-wise at 0 ˚C, then diluted with brine (20 mL). The aqueous layer was extracted with diethyl ether (4 x 25 mL). The collected organic layers were dried over K_2CO_3, then evaporated by rotary evaporation at room temperature. Two aliquots of pentane (5 mL) were added and evaporated to extract any remaining diethyl ether, to yield 4.538 g (72%) of product as a colourless oil. ^{1}H-NMR (600 MHz; DMSO-d_6): δ 3.37 (t, *J* = 6.8 Hz, 2H), 2.58 (t, *J* = 6.6 Hz, 2H), 1.59 (quintet, *J* = 6.7 Hz, 2H), 1.32 (s, 2H).

Synthesis of pTSe-G1-$(N_3)_2$

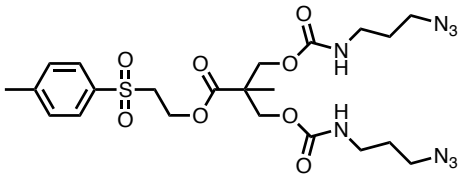

A flask equipped with a stir bar was charged with *p*TSe-G1-(*p*-N)$_2$ (1.072 g, 1.658 mmol) in CH_2Cl_2 (10 mL). 3-Azidopropylamine (0.664 g, 6.632 mmol) and diisopropylethylamine (DIPEA) (1.444 mL, 8.290 mmol) were added, and the reaction mixture was stirred at room temperature for 30 minutes. The reaction was diluted with 25 mL of CH_2Cl_2, and washed with 1 M $NaHSO_4$ (3 × 30 mL) and brine (1 × 40 mL). The organic phase was dried over $MgSO_4$, filtered through a Buchner funnel, and the solvent removed *in vacuo*. The crude product was purified using column chromatography (45% acetone in hexanes), to yield 0.839 g (89%) of product as a white waxy solid. ^{1}H-NMR (700 MHz; CD_2Cl_2): δ 1.09 (s, 3H), 1.73 (quintet, *J* = 6.5 Hz, 4H), 2.44 (s, 3H), 3.20 (q, *J* = 6.2 Hz, 4H), 3.34-3.30 (m, 4H), 3.42 (t, *J* = 5.9 Hz, 2H), 4.08-4.04 (m, 4H), 4.39 (t, *J* = 5.8 Hz, 2H), 5.06 (s, 2H), 7.40 (d, *J* = 8.3 Hz, 2H), 7.78 (d, *J* = 8.2 Hz, 2H). ^{13}C NMR (176 MHz; CD_2Cl_2): δ 17.29, 21.71, 29.45, 38.74, 47.19, 49.36, 55.40, 58.36, 66.06, 128.33, 130.47, 136.62, 145.76, 156.23, 173.03. MS Calcd for $C_{22}H_{32}N_8O_8S$ $[M]^+$ = 568.2064, $[M + H]^+$ = 569.2142. Found HR ESI-MS $[M + H]^+$ 569.2131.

Synthesis of pTSe-G2-(N_3)$_4$

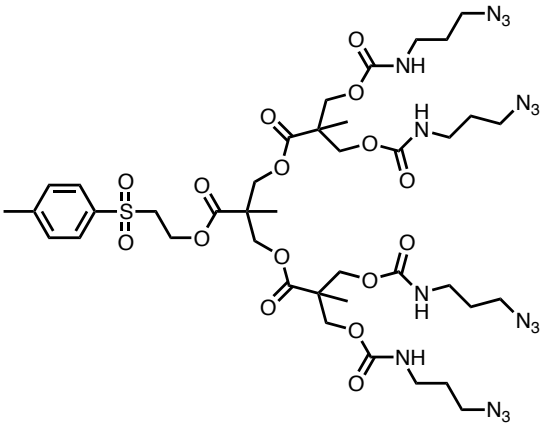

A flask equipped with a stir bar was charged with *p*TSe-G2-(*p*-N)$_4$ (2.350 g, 1.944 mmol) in CH_2Cl_2 (15 mL). 3-Azidopropylamine (1.168 g , 11.662 mmol) and DIPEA (2.370 mL, 13.606 mmol) were added, and the reaction mixture was stirred at room temperature for 1 hour. The reaction was diluted with 25 mL of CH_2Cl_2, and washed with 1 M $NaHSO_4$ (3 × 30 mL) and brine (1 × 40 mL). The organic phase was dried over $MgSO_4$, filtered through a Buchner funnel, and the solvent removed *in vacuo*. The crude product was purified using column chromatography (gradient of 10% to 100% acetone:hexanes over 13 column volumes). Fractions containing product were collected and solvent was removed *in* vacuo to yield 1.944 g (96%) of a clear, colourless oil. ^{1}H-NMR (700 MHz; $CDCl_3$): δ 1.28-1.16 (m, 9H), 1.80-1.73 (m, 8H), 2.45 (s, 3H), 3.26-3.20 (m, 8H), 3.37-3.34 (m, 8H), 3.45 (t, *J* = 5.8 Hz, 2H), 4.29-4.09 (m, 12H), 4.49 (dt, *J* = 6.8, 4.0 Hz, 2H), 5.56-5.35 (m, 4H), 7.39 (d, *J* = 8.0 Hz, 2H), 7.80 (d, *J* = 8.2 Hz, 2H). ^{13}C NMR (176 MHz; $CDCl_3$): δ 17.67, 17.80, 21.81, 29.17, 38.56, 46.48, 47.32, 49.07, 54.97, 58.30, 65.00, 66.17, 128.17, 130.33, 136.24, 145.52, 156.13, 172.22, 173.23. MS Calcd for $C_{40}H_{60}N_{16}O_{16}S$ $[M]^+$ = 1052.4094, $[M + NH_4]^+$ = 1070.4437. Found HR ESI-MS $[M + NH_4]^+$ 1070.4436.

Synthesis of COOH-G1-$(N_3)_2$

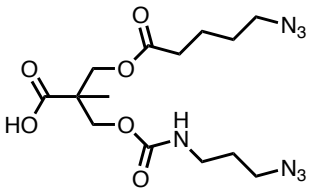

A flask equipped with a stir bar was charged with *p*TSe-G1-$(N_3)_2$ (0.700 g, 1.231 mmol) in CH_2Cl_2 (5 mL). 1,8-diazabicyclo[5.4.0]undex-7-ene (DBU) (1.105 mL, 7.387 mmol) was added to this, and the reaction mixture was stirred for 30 minutes. Diethylenetriamine (0.798 mL, 7.387 mmol) was then added and left to react for 30 minutes. The reaction was diluted with 40 mL of CH_2Cl_2, and washed with 1 M $NaHSO_4$ (3 × 30 mL) and brine (1 × 40 mL). The organic phase was dried over $MgSO_4$, filtered through a Buchner funnel, and the solvent removed *in vacuo* to give 0.462 g (97%) of a clear, colourless oil. ^{1}H-NMR (700 MHz; DMSO-d_6): δ 1.13-1.09 (m, 3H), 1.63 (quintet, *J* = 6.8 Hz, 4H), 3.01 (q, *J* = 6.3 Hz, 4H), 3.32 (t, *J* = 6.7 Hz, 5H), 4.08-4.02 (m, 4H), 7.22 (s, 2H).

Synthesis of COOH-G2-$(N_3)_4$

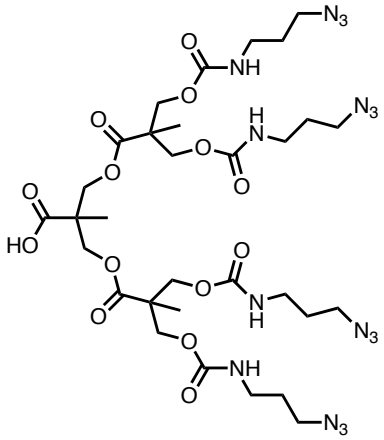

A flask equipped with a stir bar was charged with *p*TSe-G2-$(N_3)_4$ (1.000 g, 0.950 mmol) in CH_2Cl_2 (5 mL). DBU (0.852 mL, 5.698 mmol) was added to this, and the reaction mixture was stirred for 30 minutes. Diethylenetriamine

(0.616 mL, 5.698 mmol) was then added and left to react for 30 minutes. The reaction was diluted with 40 mL of CH_2Cl_2, and washed with 1 M $NaHSO_4$ (3 × 30 mL) and brine (1 × 40 mL). The organic phase was dried over $MgSO_4$, filtered through a Buchner funnel, and the solvent removed *in vacuo* to give 0.776 g (94%) of a clear, colourless oil. ^{1}H-NMR (700 MHz; DMSO-d_6): δ 1.17-1.11 (m, 9H), 1.63 (quintet, *J* = 6.6 Hz, 8H), 3.06-2.98 (m, 8H), 3.32 (d, *J* = 13.2 Hz, 8H), 4.13-3.99 (m, 12H), 7.16-6.92 (m, 4H).

Synthesis of PEG10k-G1(N_3)$_4$

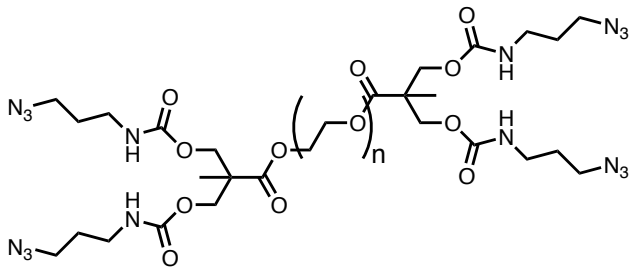

A flask equipped with a stir bar was charged with COOH-G1-(N_3)$_2$ (0.200 g, 0.518 mmol) and hydroxybenzotriazole hydrate (0.396 g, 2.588 mmol) dissolved in 1 mL of CH_2Cl_2. With rapid stirring, 1-ethyl-3-(3-dimethylaminopropyl)carbodiimide hydrochloride (EDC-HCl) (0.496 g, 2.588 mmol) was added to the reaction mixture. After 30 minutes, PEG-10k diol (0.400g, ~0.04 mmol) was added, followed by 4-dimethylaminopyridine (0.024 g, 0.200 mmol) and DIPEA (1.352 mL, 7.776 mmol). This was stirred overnight, then the reaction mixture was precipitated into 50 mL of rapidly stirring diethyl ether. The precipitate was filtered on a Hirsch funnel, then washed with ether (3 × 50 mL), ice cold ethanol (3 × 30 mL), and ether (1 × 30 mL). This was left to dry on the filter for 10 minutes, then dried in vacuo to give a white powder. (0.388 g, 91%). ^{1}H-NMR (600 MHz; DMSO-d_6): δ 1.18-1.14 (m, 6H), 1.63 (quintet, *J* = 6.7 Hz, 8H), 3.04-2.98 (m, 8H), 3.34 (q, *J* = 6.5 Hz, 8H), 3.65-3.37 (m, 963H), 4.16-4.05 (m, 12H), 7.24 (t, *J* = 5.4 Hz, 4H).

Synthesis of PEG10k-G2(N_3)$_8$

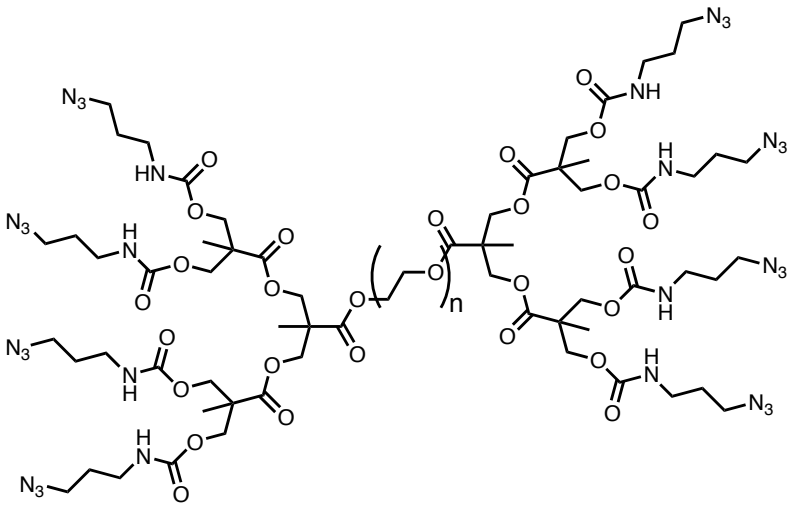

A flask equipped with a stir bar was charged with COOH-G2-(N_3)$_4$ (0.131 g, 0.150 mmol) and hydroxybenzotriazole hydrate (0.046 g, 0.30 mmol) dissolved in 1 mL of CH_2Cl_2. With rapid stirring, 1-ethyl-3-(3-dimethylaminopropyl)carbodiimide hydrochloride (EDC-HCl) (0.057 g, 0.3 mmol) was added to the reaction mixture. After 30 minutes, PEG-10k diol (0.300g, ~0.03 mmol) was added, followed by 4-dimethylaminopyridine (0.02 g, 0.015 mmol) and DIPEA (0.156 mL, 0.9 mmol). This was stirred overnight, then the reaction mixture was precipitated into 50 mL of rapidly stirring diethyl ether. The precipitate was filtered on a Hirsch funnel, then washed with ether (3 × 50 mL), ice cold ethanol (3 × 30 mL), and ether (1 × 30 mL). This was left to dry on the filter for 10 minutes, then dried in vacuo to give a white powder. (0.304 g, 87%). ^{1}H-NMR (600 MHz; DMSO-d_6): δ 1.24-1.12 (m, 21H), 1.63 (quintet, *J* = 6.7 Hz, 16H), 3.03-2.98 (m, 16H), 3.34 (t, *J* = 6.7 Hz, 16H), 3.63-3.38 (m, 1H), 4.18-4.02 (m, 29H), 7.19-7.18 (m, 8H).

Synthesis of PEG10k(N_3)$_8$[40]

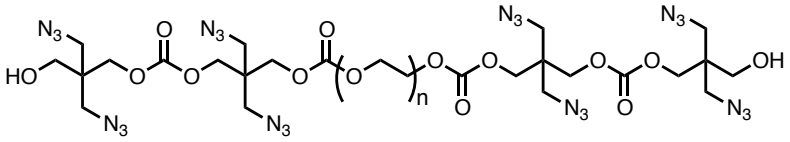

An oven-dried flask equipped with a magnetic stir bar was charged with 5,5- bis(azidomethyl)-1,3-dioxan-2-one (0.053 g, 0.23 mmol) and PEG-10k diol (0.5 g, 0.05 mmol). The flask was opened to argon atmosphere, and dry CH_2Cl_2 (10 mL) was added via syringe. Subsequently, DBU (0.003 mL, 0.02 mmol) was added to initiate the ring-opening oligomerization. After stirring for 4 h, benzoic acid (0.006 g, 0.05 mmol) was added to neutralize the DBU. After stirring for 10 min, the polymer was isolated by precipitation into diethyl ether to yield a white powder (0.499 g, 92%). ^{1}H NMR (600 MHz, $CDCl_3$) Batch 1: δ = 4.29– 4.27 (m, 4 H), 4.10 (s, 7 H), 4.08 (s, 4 H), 3.71–3.69 (m, 13 H), 3.67– 3.56 (m, 1160 H), 3.44 (s, 12 H), 3.41–3.38 (m, 16 H), Batch 2: δ = 4.29– 4.27 (m, 4 H), 4.10 (s, 5 H), 4.08 (s, 4 H), 3.71–3.69 (m, 12 H), 3.67– 3.56 (m, 1170 H), 3.44 (s, 11 H), 3.41–3.38 (m, 14 H).

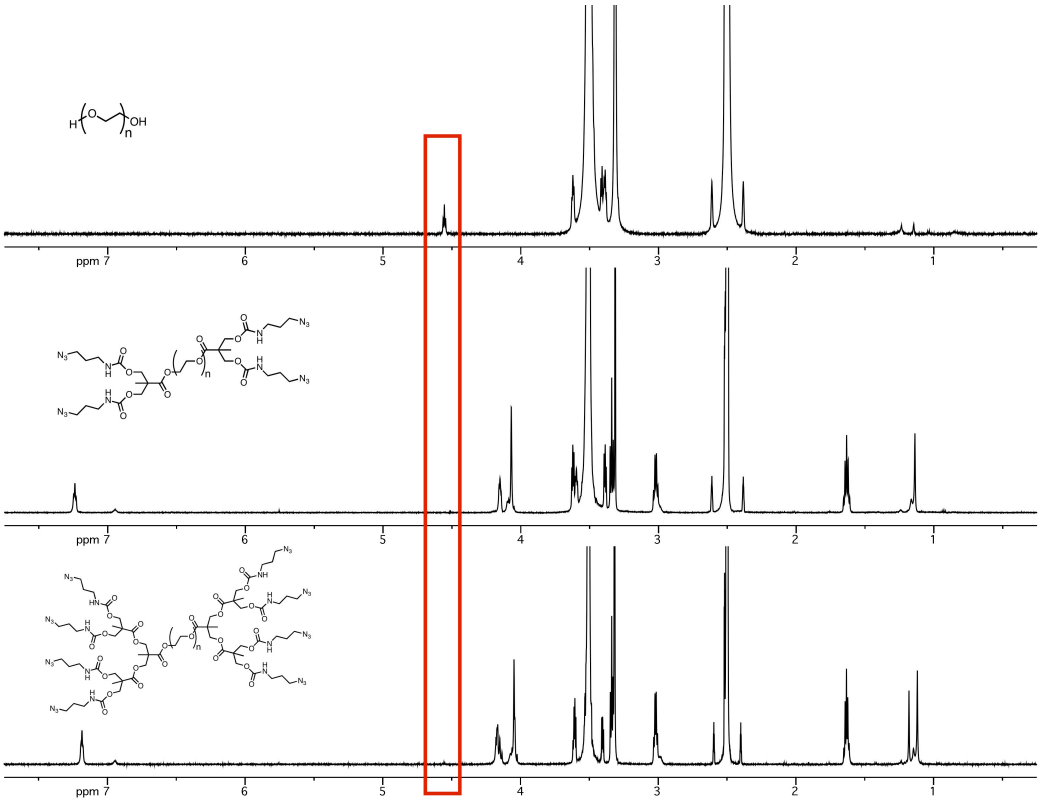

Figure 4.5. NMR spectra of poly(ethylene glycol) (top), PEG-G1$(N_3)_4$ (middle) and PEG-G2$(N_3)_8$ (bottom). Disappearance of the PEG-O<u>H</u> peak at 4.6 ppm in the spectra of PEG-G1$(N_3)_4$ and PEG-G2$(N_3)_8$ is evidence that the final step in the synthesis of the polymer was successful and that complete conversion was achieved.

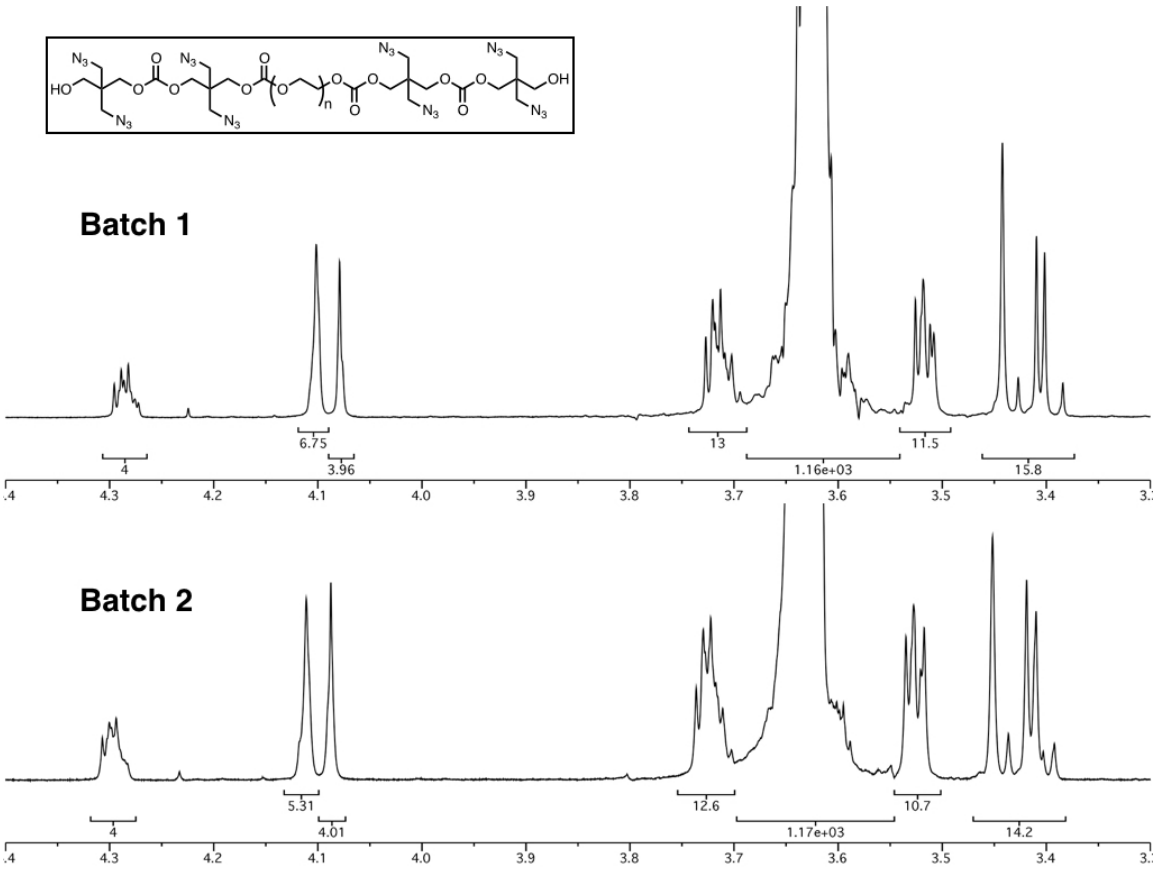

Figure 4.6. ^{1}H NMR spectra of two separately prepared batches of linear azide polymer.

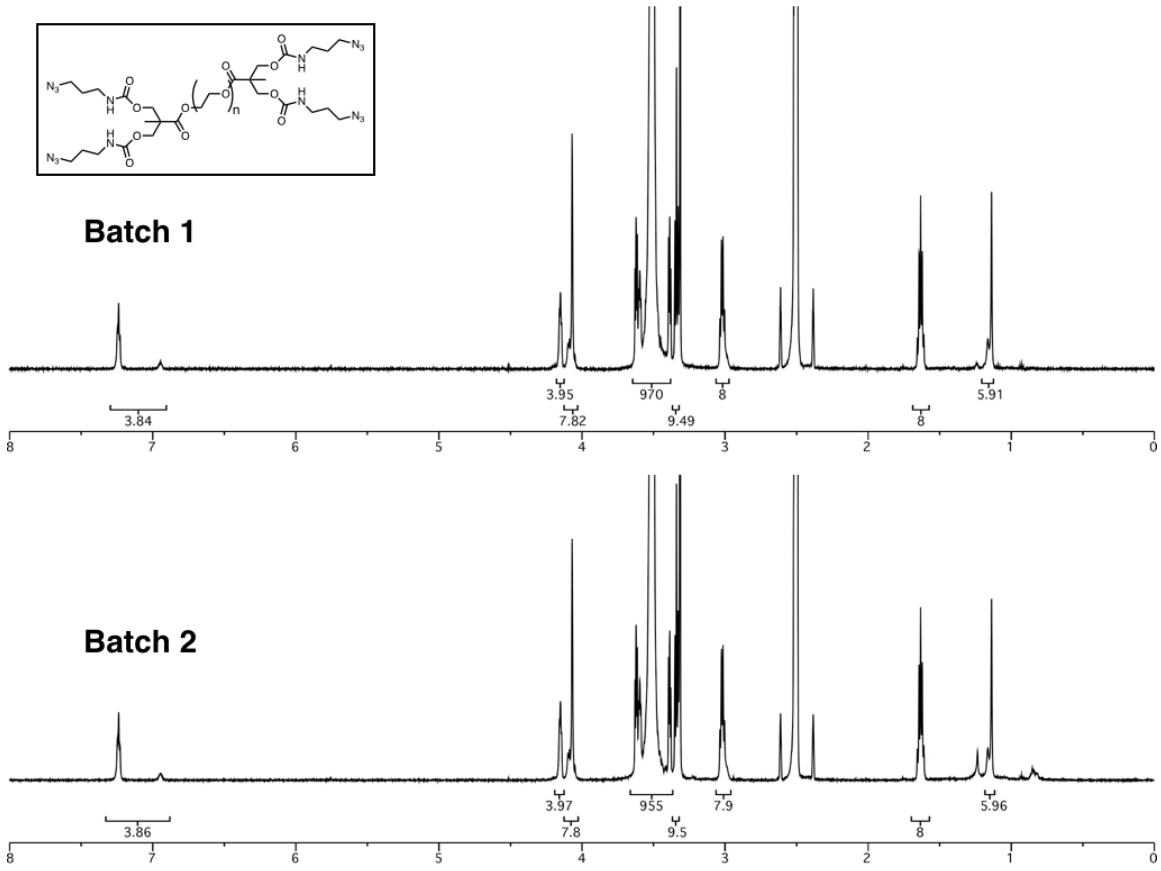

Figure 4.7. ^{1}H NMR spectra of two separately prepared batches of G1 azide polymer.

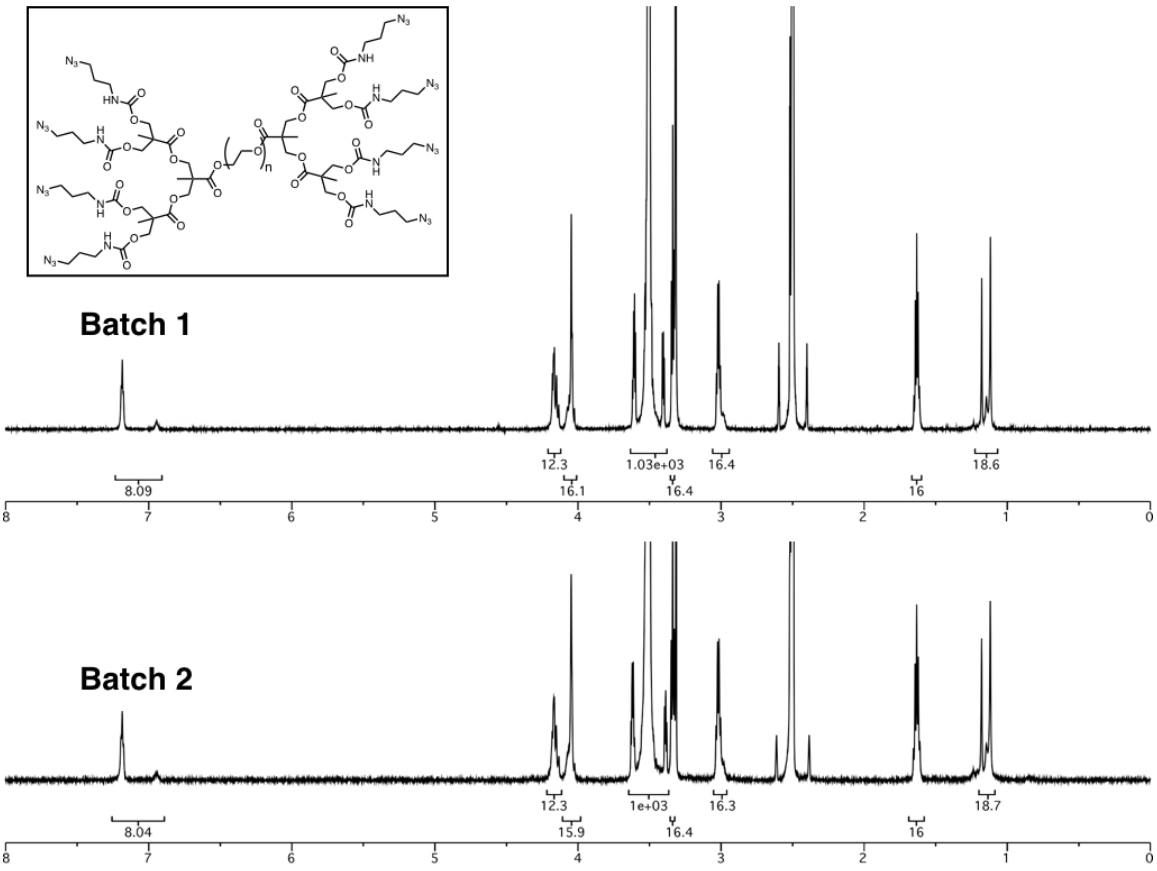

Figure 4.8. ^{1}H NMR spectra of two separately prepared batches of G2 azide polymer.

4.6. References

(1) Caliari, S. R.; Burdick, J. A. *Nat. Methods* **2016**, *13*, 405–414.

(2) Hennink, W. E.; van Nostrum, C. F. *Adv. Drug Deliv. Rev.* **2002**, *54*, 13–36.

(3) Mathur, A. M.; Moorjani, S. K.; Scranton, A. B. *J. Macromol. Sci. Part C* **1996**, *36*, 405–430.

(4) Truong, V. X.; Ablett, M. P.; Richardson, S. M.; Hoyland, J. a.; Dove, A. P. *J. Am. Chem. Soc.* **2015**, *137*, 1618–1622.

(5) Annabi, N.; Tamayol, A.; Uquillas, J. A.; Akbari, M.; Bertassoni, L. E.; Cha, C.; Camci-Unal, G.; Dokmeci, M. R.; Peppas, N. A.; Khademhosseini, A. *Adv. Mater.* **2014**, *26*, 85–124.

(6) Xu, J.; Filion, T. M.; Prifti, F.; Song, J. *Chem. Asian J.* **2011**, *6*, 2730–2737.

(7) Kaemmerer, E.; Melchels, F. P. W.; Holzapfel, B. M.; Meckel, T.; Hutmacher, D. W.; Loessner, D. *Acta Biomater.* **2014**, *10*, 2551–2562.

(8) Tibbitt, M. W.; Anseth, K. S. *Biotechnol. Bioeng.* **2009**, *103*, 655–663.

(9) Kaga, S.; Arslan, M.; Sanyal, R.; Sanyal, A. *Molecules* **2016**, *21* (497).

(10) Ghobril, C.; Rodriguez, E. K.; Nazarian, A.; Grinstaff, M. W. *Biomacromolecules* **2016**, *17*, 1235–1252.

(11) Mintzer, M. A.; Grinstaff, M. W. *Chem. Soc. Rev.* **2011**, *40*, 173–190.

(12) Holden, C. A.; Tyagi, P.; Thakur, A.; Kadam, R.; Jadhav, G.; Kompella, U. B.; Yang, H. *Nanomedicine Nanotechnology, Biol. Med.* **2012**, *8*, 776–783.

(13) Degoricija, L.; Bansal, P. N.; Sontjens, S. H. M.; Joshi, N. S.; Takahashi, M.; Snyder, B.; Grinstaff, M. W. *Biomacromolecules* **2008**, *9*, 2863–2872.

(14) Navath, R. S.; Menjoge, A. R.; Dai, H.; Romero, R.; Kannan, S.; Kannan, R. M. *Mol. Pharm.* **2011**, *8*, 1209–1223.

(15) Oelker, A. M.; Grinstaff, M. W. *IEEE Trans. Nanobioscience* **2012**, *11*, 37–45.

(16) Wu, X.-Y.; Huang, S.-W.; Zhang, J.-T.; Zhuo, R.-X. *Macromol. Biosci.* **2004**,

4, 71–75.

(17) Abou Taleb, M. F.; Elsigeny, S. M.; Ibrahim, M. M. *Radiat. Phys. Chem.* **2007**, *76*, 1612–1618.

(18) Unal, B.; Hedden, R. C. *Polymer* **2006**, *47*, 8173–8182.

(19) Desai, P. N.; Yuan, Q.; Yang, H. *Biomacromolecules* **2010**, *11*, 666–673.

(20) Wang, Y.; Zhao, Q.; Zhang, H.; Yang, S.; Jia, X. *Adv. Mater.* **2014**, *26*, 4163–4167.

(21) Yang, H.; Tyagi, P.; Kadam, R. S.; Holden, C. A.; Kompella, U. B. *ACS Nano* **2012**, *6*, 7595–7606.

(22) Lin, C.-C.; Anseth, K. S. *Pharm. Res.* **2009**, *26*, 631–643.

(23) Oelker, A. M.; Berlin, J. A.; Wathier, M.; Grinstaff, M. W. *Biomacromolecules* **2011**, *12*, 1658–1665.

(24) Konieczynska, M. D.; Villa-camacho, J. C.; Ghobril, C.; Perez-viloria, M.; Tevis, K. M.; Blessing, W. A.; Nazarian, A.; Rodriguez, E. K.; Grinstaff, M. W. *Angew. Chemie Int. Ed.* **2016**, *55*, 9984–9987.

(25) Carnahan, M. A.; Middleton, C.; Kim, J.; Kim, T.; Grinstaff, M. W. *J. Am. Chem. Soc.* **2002**, *124*, 5291–5293.

(26) Degortcija, L.; Johnson, C. S.; Wathier, M.; Kim, T.; Grinstaff, M. W. *Investig. Ophthalmol. Vis. Sci.* **2007**, *48*, 2037–2042.

(27) Grinstaff, M. W. *Biomaterials* **2007**, *28*, 5205–5214.

(28) Söntjens, S. H. M.; Nettles, D. L.; Carnahan, M. A.; Setton, L. A.; Grinstaff, M. W. *Biomacromolecules* **2006**, *7*, 310–316.

(29) Gitsov, I.; Zhu, C. *Macromolecules* **2002**, *35*, 8418–8427.

(30) Ghobril, C.; Charoen, K.; Rodriguez, E. K.; Nazarian, A.; Grinstaff, M. W. *Angew. Chemie Int. Ed.* **2013**, *52*, 14070–14074.

(31) Hed, Y.; Öberg, K.; Berg, S.; Nordberg, A.; von Holst, H.; Malkoch, M. *J. Mater. Chem. B* **2013**, *1*, 6015–6019.

(32) Altin, H.; Kosif, I.; Sanyal, R. *Macromolecules* **2010**, *43*, 3801–3808.

(33) Öberg, K.; Hed, Y.; Rahmn, I. J.; Kelly, J.; Löwenhielm, P.; Malkoch, M.

Chem. Commun. **2013**, *49*, 6938–6940.

(34) Wathier, M.; Jung, P. J.; Carnahan, M. A.; Kim, T.; Grinstaff, M. W. *J. Am. Chem. Soc.* **2004**, *126*, 12744–12745.

(35) Jewett, J. C.; Bertozzi, C. R. *Chem. Soc. Rev.* **2010**, *39* (4), 1272–1279.

(36) Nuttelman, C. R.; Tripodi, M. C.; Anseth, K. S. *Matrix Biol.* **2005**, *24*, 208–218.

(37) Kloxin, A. M.; Kasko, A. M.; Salinas, C. N.; Anseth, K. S. *Science* **2009**, *324*, 59–63.

(38) DeForest, C. A.; Anseth, K. S. *Nat. Chem.* **2011**, *3*, 925–931.

(39) Anderson, S. B.; Lin, C. C.; Kuntzler, D. V.; Anseth, K. S. *Biomaterials* **2011**, *32*, 3564–3574.

(40) Hodgson, S. M.; Bakaic, E.; Stewart, S. A.; Hoare, T.; Adronov, A. *Biomacromolecules* **2016**, *17*, 1093–1100.

(41) Anseth, K. S.; Bowman, C. N.; Brannon-Peppas, L. *Biomaterials* **1996**, *17*, 1647–1657.

(42) Long, R.; Hall, M. S.; Wu, M.; Hui, C.-Y. *Biophys. J.* **2011**, *101*, 643–650.

(43) Parrott, M. C.; Benhabbour, S. R.; Saab, C.; Lemon, J. A.; Parker, S.; Valliant, J. F.; Adronov, A. *J. Am. Chem. Soc.* **2009**, *131*, 2906–2916.

(44) Gillies, E. R.; Fréchet, J. M. J. *J. Am. Chem. Soc.* **2002**, *124*, 14137–14146.

(45) Chadwick, R. C.; Van Gyzen, S.; Liogier, S.; Adronov, A. *Synthesis* **2014**, *46*, 669–677.

(46) Peppas, N. A.; Franson, N. M. *J. Polym. Sci. Polym. Phys. Ed.* **1983**, *21*, 983–997.

(47) Kyburz, K. A.; Anseth, K. S. *Acta Biomater.* **2013**, *9*, 6381–6392.

(48) Jiang, X.; Zhang, J.; Zhou, Y.; Xu, J.; Liu, S. *J. Polym. Sci. Part A Polym. Chem.* **2008**, *46*, 860–871.

Chapter 5

Thesis Overall Conclusions and Recommendations for Future Work

5.1. General Conclusions

Hydrogels are crosslinked polymer networks that are swollen in water and have enormous potential in biomedical applications. The specific properties of the hydrogel vary based on the polymer material chosen, as well as the type of crosslinking that occurs between polymer chains. Polymer material can be categorized into two general types: natural or synthetic. Natural polymers are similar to native tissue and contain biomaterials that might be advantageous for incorporation into a host body. However, it is often impossible to completely elucidate their structure, which in turn makes the properties of resulting hydrogels difficult to control, or reproduce. The alternative is synthetic polymers, which allow for greater structural control, acting as a template that can be used to build a hydrogel with tunable properties. Many synthetic polymers have been investigated as hydrogel materials, with one of the most promising being poly(ethylene glycol) (PEG). PEG fits all the criteria for hydrogel material, and is also easily functionalized for crosslinking and incorporation of other factors necessary for certain applications. While there are many examples of PEG hydrogels, most use crosslinking chemistry that is either inefficient, requires cytotoxic catalysts, high temperatures, or other stimuli (e.g. UV light) that limits their application potential. One type of crosslinking that has proven extremely successful is strain-promoted alkyne-azide cycloaddition (SPAAC), a click reaction that occurs quickly under physiological conditions, does not require a catalyst or external stimuli, does not produce any byproducts, and is completely

bioorthogonal. The one disadvantage to this crosslinking method is the inefficient and tedious synthetic route required for the preparation of the cyclooctyne. Researchers often bypass this by purchasing the cyclooctyne, however, this is extremely costly.

In order to realistically be able to use SPAAC for hydrogel crosslinking, improving the synthesis of the cyclooctyne moiety is crucial. In Chapter 2 of this thesis, the optimization of the synthesis of the strained cyclooctyne, aza-dibenzocyclooctyne (DIBAC), was discussed and an enormous improvement from previous reports was presented. Modifications to the procedure, as well as reduction in the number of synthetic steps and purification procedures dramatically increased the overall yield from the literature reported value of 18% to 71%. These developments also allowed the procedure to be scaled up to multi-gram quantities, making this cyclooctyne a viable, affordable, and easy option for use in hydrogel preparation.

Having a successful, efficient and high-throughput method for synthesizing the strained cyclooctyne DIBAC was the first step in creating an ideal hydrogel system. In Chapter 3, this DIBAC molecule was incorporated onto either end of a PEG chain and reacted with a multi-azide functionalized linear PEG to form a series of hydrogels. By altering the PEG chain length between cyclooctyne groups on the alkyne precursor polymer, and varying the number of azide groups on the other PEG precursor polymer, the resulting hydrogel properties can be tuned. The series of hydrogels had gelation times under 60 seconds at room temperature, varied in the amount of swelling, and degraded within 1 to 35 days. Young's modulus values between 1 and 18 kPa were obtained, which directly compare to various tissues in the body, and can be adjusted based on the targeted application. Additionally, the hydrogels showed minimal protein adsorption with BSA and an MTT assay proved the precursor polymers, and therefore also the alkyne and azide groups, to be non-cytotoxic against 3T3 mouse fibroblasts.

The work in Chapter 4 involved a novel study that focused on creating reproducible hydrogels. Crosslinking between polymer chains is required for hydrogels to form; yet incorporating multiple crosslinks on one polymer chain is difficult to control. While maintaining PEG as the hydrogel material, and SPAAC as the crosslinking chemistry, adjustments were made to the previous system that put an end to batch-to-batch variations in hydrogel preparation. As an alternative to the previous study, which used polycarbonate azides on either end of PEG, this work took advantage of well-defined dendrons. Azide-terminated first- and second-generation dendrons were synthesized and attached to either end of a PEG chain and reacted with the same PEG-dicyclooctyne as in the previous study. The resulting hydrogels exhibited minimal to no swelling at 37°C, and proved reproducible based on identical Young's Modulus values from different batches. The hydrogels made from second-generation azides were seeded with human mesenchymal stem cells (hMSCs) and showed high viability and cell spreading over 15 days. For this test, the tripeptide RGD was covalently incorporated into the hydrogel to aid in cell adhesion to the matrix.

From this thesis work came two significant overall contributions to the field of hydrogels. The first is the fundamental work that was done to optimize the cyclooctyne synthesis. Without the improved method, the DIBAC synthesis was tedious and inefficient, which could have deterred researchers from utilizing otherwise perfect SPAAC crosslinking chemistry. Now with the optimized synthesis, DIBAC can be made easily in large quantities, opening up new possibilities for hydrogel formation, as well as many other bioconjugation applications.

The second significant contribution was the development of a reproducible, novel PEG hydrogel crosslinked via SPAAC. PEG-SPAAC hydrogels have tunable qualities that are ideal for biomedical applications; however, the one missing piece was reproducibility. By incorporating

dendrimers, each batch is guaranteed to be the same and produce identical hydrogels. Utilizing PEG as hydrogel material, SPAAC for crosslinking chemistry, and dendrimers for reproducibility, a completely controllable, hydrogel template was developed with great potential in biomedical applications.

5.2. Recommendations for Future Work

The work discussed in this thesis focused on the fundamental development of an easy to make hydrogel system that had reproducible and tunable properties. One of the properties of this system is that the hydrogels are degradable from hydrolysis of the ester bonds that are present in the PEG-cyclooctyne polymer backbone. This hydrolysis is amplified in the presence of cells, creating a hydrogel that degrades in as little as a couple weeks. One suggestion for future work on the degradable aspect of these hydrogels is to exchange the ester bonds for amides, which are less labile. Depending on the desired application, a non-degradable hydrogel might be favorable. It would be interesting to see the differences in degradation time between the hydrogel system containing only ester bonds versus only amide bonds, and if degradation time could be ultimately controlled under physiological conditions by varying the ratio of the ester and amide polymers.

The preliminary stem cell work presented in Chapter 4 of this thesis proves that this hydrogel system has great potential in the field of tissue engineering. Further study of hMSCs in this hydrogel could give insight into what types of differentiation are possible, and if there is one cell type that shows particular promise, for example, osteogenic differentiation into osteoblasts for bone repair. The results of that *in vitro* study could then be applied to a more detailed *in vivo* study for tissue regeneration. It would also be advantageous to test beforehand the incorporation of any necessary

biomaterials like growth factors or adhesion peptides that will aid in the proliferation of hMSCs in the hydrogel, as well as help the hydrogel matrix integrate well into the target site of the host.

There are many potential applications for the hydrogel systems described in this thesis aside from the previously mentioned tissue engineering. For applications involving controlled drug release, the hydrogel system can be adjusted to swell and degrade at a certain rate to allow for export of the small molecules. For applications in wound healing, the Young's Modulus and degradation of the gel can be adjusted to create an appropriate dressing. However, for applications in cell therapy, there are additional steps that are necessary for successful cell encapsulation. As an example, for Type 1 diabetes, islet cells can be encapsulated in the hydrogel and then transplanted into the host. The hydrogel creates a protective barrier for the foreign cells from the immune system, while allowing the islet cells to auto-regulate blood glucose levels and release insulin through the pores of the hydrogel, as necessary. For the cells to survive, oxygen and nutrients must be able to diffuse into the hydrogel matrix. This may be a problem for bulk hydrogels, where there could be a group of cells in the middle of the hydrogel that do not receive enough oxygen and ultimately asphyxiate. To solve this problem, microfluidics can be utilized to create hydrogel microcapsules that act in every way the same as the bulk hydrogel, except the total volume of gel is smaller, increasing the odds of survival of the encapsulated cells. Microfluidics can also control the number of cells per microgel, for those particular cell lines that require a solitary environment. For this work, the hydrogel system itself need not be altered, as it is already an ideal candidate for microfluidics due to the ease of formation of hydrogels from solutions of the two precursor polymers without requiring any other reagents or stimuli.